FIELD AND LABORATORY EVALUATION OF SIX INHALABLE AEROSOL SAMPLERS AND TWO IMPACTORS

By

SHOU-NAN LI

A DISSERTATION PRESENTED TO THE GRADUATE SCHOOL
OF THE UNIVERSITY OF FLORIDA IN PARTIAL FULFILLMENT
OF THE REQUIREMENTS FOR THE DEGREE OF
DOCTOR OF PHILOSOPHY

UNIVERSITY OF FLORIDA

1999

ACKNOWLEDGMENTS

First, I would like to thank Dr. Lundgren for his invaluable guidance, teaching, and support throughout my study in the University of Florida. He bears my mistakes, cares about my safety, and shares my joys. I would also like to thank Dr. Andino, Dr. Chadik, Dr. Moye, and Dr. Wu for their valuable input. I thank Dr. Allen and Dr. (Maxwell) Lee for their generous support and help, I thank Dr. (HungMin) Chein for his tutoring about aerosol research when I first arrived.

I thank my wife, Li-Hui Chen, for her encouragement and help in every aspect of my study here. Without her support, I would not have reached this far. I thank my parents for their support.

I would like to thank the National Council of the Paper Industry for Air and Stream Improvement Inc. (NCASI) for their financial support to perform this research project.

TABLE OF CONTENTS

page

ACKNOWLEDGMENTS ii

LIST OF TABLES v

LIST OF FIGURES vi

ABSTRACT x

CHAPTERS

1 INTRODUCTION 1

2 EQUIPMENT AND EXPERIMENTAL SETUP 8

- Inhalable Aerosol Samplers 8
- Impactors 13
- Vibrating Orifice Aerosol Generator 23
- Collison Atomizer 29
- Charge Neutralizer : Kr-85 31
- Fluorometer 31
- Hot-Wire Anemometer 32
- Wind Monitor 33
- Experimental Setup in the Field 33
- Experimental Setup in the Lab 36

3 RESULTS AND DISCUSSION 46

- Inhalable Aerosol Samplers 46
  - Weight Instability of the IOM and the CIS Plastic Filter Holders 46
  - Field Results for Inhalable Aerosol Samplers 53
  - Lab Results for Inhalable Aerosol Samplers 56
  - Lab Data Discussions for Inhalable Aerosol Samplers 68

Wood-Dust Size Distribution and Impactor Inlet Efficiency 72
    Field Results for Wood-Dust Size Distribution 72
    Lab Results for Impactor Inlet Efficiency Test 80
    Lab Results for Impactor Sizing Performance Test 95
Comparison Between the Calculated and Measured Inlet Efficiency 95
    Belyaev and Levin 99
    Vincent and his Colleague 102

4 CONCLUSIONS 107

APPENDICES

A LABORATORY RESULTS OF SIX INHALABLE AEROSOL SAMPLERS . . . 110
B PARTICLE SIZE DISTRIBUTION MEASURED IN THE WOODWORKING INDUSTRY 123
C LABORATORY RESULTS FOR TWO IMPACTOR INLET EFFICIENCY 151
D COMPARISON BETWEEN THE MEASURED AND THE CALCULATED INLET EFFICIENCY 164

REFERENCES 189

BIOGRAPHICAL SKETCH 193

LIST OF TABLES

Table page

2-1. Operating conditions of the VOAG for generating monodisperse particles. 26

3-1. Tare-weight variation (due to desiccation) of an IOM plastic cassette before and after a 3-day exposure to the ambient environment 52

3-2. Tare-weight variation (due to desiccation) of a 37-mm polyvinyl chloride filter before and after a 3-day exposure to the ambient environment 52

3-3. Particle concentration ratio between the closed-face 37-mm cassette and the other samplers at a plywood mill. 54

3-4. Particle concentration ratio between the closed-face 37-mm cassette and the other samplers at a particle-board mill. 55

3-5. Measured MMADs, GSDs, Mass/Volume, and wind speeds in woodworking industry. 77

3-6. Side-by-side measurement comparison of two Marple impactors (with a visor) with one University of Washington (UW) impactor in the wood-working industry 79

3-7. Comparison between the measured and calculated inlet efficiency using the equations developed by Belyaev and Levin (1974) for a thin-walled probe.. 100

LIST OF FIGURES

Figure page

1-1. Three human respiratory regions (a) nasal (b) tracheobronchial (C) pulmonary. . . . 2

1-2. Conventional curves for inhalable, thoracic, and respirable fractions. 4

2-1. A RespiCon sampler (a) outside appearance (b) inside schematic drawing. 9

2-2. Six inhalable aerosol samplers (a) IOM (b) CIS (C) 7-hole (d) Button (e) closed-face 37-mm cassette (f) open-face 37-mm cassette 12

2-3. Marple Personal Cascade impactors (a) with and (b) without a visor. 15

2-3c. A University of Washington impactor 16

2-4. A MOUDI impactor. 17

2-5. (a) Particle trajectory in an impactor stage (b) Collection efficiency of an impactor stage. 18

2-6. A schematic drawing of a cascade impactor 21

2-7. A schematic drawing of a Vibrating Orifice Aerosol Generator (VOAG) and a deflection test for droplet uniformity. 24

2-8. Scanning electron micrograph of ammonium fluorecein particles (a) particle diameter of 3.2 micrometer (b) particle diameter of 4.6 micrometer. 27

2-9. A Collison atomizer 30

2-10. A rotating-vane Wind Monitor used in the wood-working industry 34

2-11. Sampler arrangement in the wood-working industry (a) sampler arrangement (b) sampling height 35

2-12. A schematic diagram of the system setup for testing a MOUDI impactor, a UW impactor and two Marple Personal Cascade impactors 38

2-13. Schematic drawing of the testing wind tunnel 39

2-14. Sampler arrangement in the wind tunnel 42

2-15. A testing wind tunnel 45

3-1. An IOM sampler and its plastic filter cassette 47

3-2. A CIS sampler and its plastic filter holder. 48

3-3. Average tare-weight losses of six IOM plastic cassettes, six CIS plastic holders, and six IOM stainless-steel cassettes in a desiccator. 50

3-4. Measured efficiency and inside particle loss of a RespiCon sampler. 57

3-4e. Corrected efficiency of a RespiCon sampler 58

3-5. Measured efficiency of an IOM sampler at three different wind orientations 61

3-6. Measured efficiency and inside particle loss of a 7-hole sampler at three wind orientations and two wind speeds 63

3-7. Measured efficiency and inside particle loss of a closed-face 37-mm cassette at three wind orientations and two wind speeds 64

3-8. Measured efficiency and inside particle loss of a CIS sampler at three wind orientations and two wind speeds 66

3-9. Measured efficiency and inside particle loss of a Prototype Button sampler at three wind orientations and two wind speeds 67

3-10. Effects of velocity ratio, $R=V_{wind}/V_i$, on inlet efficiency of four aerosol samplers at 0^0 wind direction. 71

3-11. Effects of wind orientation on inlet efficiency of an IOM sampler. 73

3-12. Particle size distributions measured using a University of Washington impactor and a Marple Personal Cascade impactor at the trimming area of a particle-board mill . . 75

3-13. Inlet efficiency and particle loss on both the first stage and the cowl inlet of a Marple Personal Cascade impactor (with a visor) at a wind speed of 0.55 m/s and wind directions of (a) 0^0 and (b) 90^0. 82

3-13c.Inlet efficiency and particle loss on both the first stage and the cowl inlet of a Marple Personal Cascade impactor (with a visor) at a wind speed of 0.55 m/s and a wind direction of 180^0 83

3-14. Inlet efficiency and particle loss on both the first stage and the cowl inlet of a Marple Personal Cascade impactor (with a visor) at a wind speed of 1.1 m/s and wind directions of (a) 0^0 and (b) 90^0. 84

3-14c. Inlet efficiency and particle loss on both the first stage and the cowl inlet of Marple Personal Cascade impactor (with a visor) at a wind speed of 1.1 m/s and a wind direction of 180^0 85

3-15. Effect of wind direction on the inlet efficiency of a Marple Personal Cascade impactor (with a visor) at a wind speed of 1.1 m/s and particle aerodynamic diameter of 68 μm 87

3-16. Inlet efficiency and particle loss on both the first stage and the cowl inlet of a Marple Personal Cascade impactor (without a visor) at a wind speed of 0.55 m/s and wind directions of (a) 0^0 and (b) 90^0 89

3-16c Inlet efficiency and particle loss on both the first stage and the cowl inlet of a Marple Personal Cascade impactor (without a visor) at a wind speed of 0.55 m/s and a wind direction of 180^0 90

3-17. Effectiveness and particle loss on both the first stage and the cowl inlet of a Marple Personal Cascade impactor (without a visor) at a wind speed of 1.1 m/s and wind directions of (a) 0^0 and 90^0 91

3-17c. Effectiveness and particle loss on both the first stage and the cowl inlet of a Marple Personal Cascade impactor (without a visor) at a wind speed of 1.1 m/s and a wind direction of 180^0 92

3-18. Inlet efficiency of an upward circular tube (a) measured and calculated inlet efficiencies (b) inlet efficiency vs. $[(Stk)R]^{1/2}$ 93

3-19. Comparison of particle size distribution measurements using two Marple impactors with those using a MOUDI impactor and a University of Washington impactor 96

3-20. Inlet efficiency comparison between the experimental value and calculated value using the equations developed by Belyaev and Levin (1974) at 0^0 wind direction. 101

3-21. Inlet efficiency comparison between the experimental value and calculated value using the equations developed by Vincent (1995) at 0^0 wind direction. 103

3-22. Inlet efficiency comparison between the experimental value and calculated value using the equations developed by Vincent (1995) at 90^0 wind direction. 104

3-23. Inlet efficiency comparison between the experimental value and calculated value using the equations developed by Vincent (1995) at 180^0 wind direction. 105

Abstract of Dissertation Presented to the Graduate School
of the University of Florida in Partial Fulfillment of the
Requirements for the Degree of Doctor of Philosophy

FIELD AND LABORATORY EVALUATION OF SIX INHALABLE AEROSOL SAMPLERS AND TWO IMPACTORS

By

Shou-Nan Li

May 1999

Chairman: Dale A. Lundgren
Major Department: Environmental Engineering Sciences

Six inhalable aerosol samplers were experimentally evaluated as area samplers using monodisperse, solid particles with aerodynamic diameters ranging from 5 to 68 μm. Sampler performance and inside particle losses at two test wind speeds (0.55 and 1.1 m/s) and three wind orientations (0^0, 90^0, and 180^0) were investigated. The six inhalable aerosol samplers tested were a RespiCon, an IOM, a 7-hole, a CIS, a Prototype Button sampler, and a closed-face 37-mm cassette. It was found that the sampling performance of the RespiCon sampler matched the inhalable convention fairly well, while the sampling performances of the other five samplers depended on wind speed, wind direction, and particle size and they may not be appropriate for area sampling except for fine mode aerosols.

A Marple Personal Cascade (Marple) impactor and a MK III University of Washington (UW) impactor were experimentally evaluated in the laboratory to determine the reason for measurement difference observed in the woodworking environment when the impactors were used side-by-side to measure particle size distributions. In the laboratory, the inlet efficiencies of both impactors were experimentally determined using monodisperse, solid particles with aerodynamic diameters (D_a) ranging from 5 to 68 µm at wind speeds of 0.55 and 1.1 m/s. For particles with D_a greater than 20 µm, the aerosol sample obtained using the UW impactor was more representative because the Marple impactor inlet visor greatly restricted the sampling of large ($D_a > 20$ µm) particles at most wind directions.

CHAPTER 1
INTRODUCTION

Airborne particles (called aerosols) can cause respiratory system damage, such as nasal cancer, bronchitis, and pulmonary disease.[1] Each disease is related to a respiratory region where the particles deposit. For example, particles entering the nose and depositing in the nasal region can cause nasal cancer; particles depositing in the tracheobronchial region can cause bronchitis, and particles depositing in the pulmonary region can cause pulmonary disease. These three regions in the human respiratory system are shown schematically in Fig. 1-1.

Recent research studies found that the particle aerodynamic diameter, D_a, determines the probability for an airborne particle to enter the nose and the respiratory region to deposit.[3-4] To protect the health of workers and to prevent respiratory system damage due to workplace aerosols, the American Conference of Governmental Industrial Hygienists (ACGIH)[5], the International Organization for Standardization (ISO)[6], and the Comité Européen de Normalisation (CEN)[7] reached an agreement and defined three conventions for workplace aerosols that could enter and deposit on these three respiratory regions :

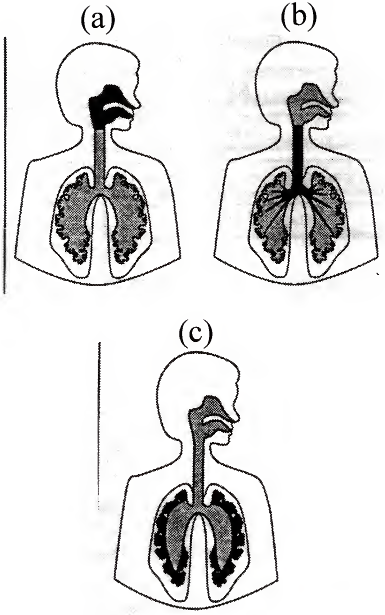

Fig. 1-1. Three human respiratory regions (dark shaded areas).
(a) nasal region, (b) tracheobronchial region, (c) pulmonary region.
Source : Jahnke[2].

Inhalable fraction : representing the aerosol fraction that enters the nose and/or mouth.

$$I(D_a) = 0.5[1+ \exp(-0.06\ D_a)] \qquad (1\text{-}1)$$

for $D_a \leq 100\ \mu m$

where

$I(D_a)$: inhalable fraction

D_a : particle aerodynamic diameter, μm

Thoracic fraction : representing the sub-fraction of the inhalable aerosol that penetrates the respiratory tract below the larynx.

$$T(D_a) = I(D_a) \{ 1 - F_T(D_a) \} \qquad (1\text{-}2)$$

where

$T(D_a)$: thoracic fraction

$F_T(D_a)$ is specified as a cumulative log-normal function with its median at $D_a = 11.64\ \mu m$ and having a geometric standard deviation (σ_g) of 1.5.

Respirable fraction : representing the sub-fraction of the inhalable aerosol that penetrates the alveolar region of the lung.

$$R(D_a) = I(D_a) \{ 1 - F_R(D_a) \} \qquad (1\text{-}3)$$

where

$R(D_a)$: respirable fraction

$F_R(D_a)$ is a cumulative log-normal function with its median at $D_a = 4.25\ \mu m$ and having a geometric standard deviation (σ_g) of 1.5. The complex mathematical functions for $F_T(D_a)$ and $F_R(D_a)$ are described elsewhere.[8] These three defined conventions are graphically shown in Fig. 1-2.

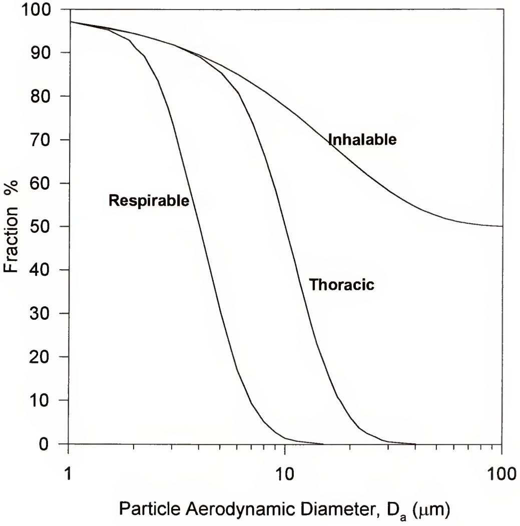

Fig. 1-2. Conventional curves for inhalable, thoracic, and respirable fractions.

In addition to the particle aerodynamic diameter, the particle composition and concentration is an important factor of health concerns. Workplace aerosol concentration standards, called threshold limit values (TLVs), are listed in the TLVs and BEIs (Biological Exposure Indices) booklet[5] (published by the ACGIH) to assist in the control of health hazards. For some aerosols not listed, the ACGIH committee recommends an 8-hour time-weighted average (TWA) concentration of 10 mg/m^3 for inhalable aerosols and an 8-hour TWA concentration of 3 mg/m^3 for respirable aerosols.

To measure the concentration of the aerosols in each defined convention, the sampler performance should match the ACGIH, ISO and CEN common convention. For example, if a sampler is intended to collect inhalable aerosols, the performance of this sampler should match equation 1-1. Workplace aerosol samplers are used as area or personal samplers. Area samplers are used as free-standing collection devices, while samplers mounted on the body of the worker are called personal samplers. Because personal samplers collect aerosols more representative of worker exposure, most lab studies and field measurements have been conducted using personal sampling.

Traditionally, workplace aerosol concentration measurements were obtained using a closed-face 37-mm cassette. The former published TLVs (by the ACGIH) were based on the epidemiologic studies using the concentration measurements using closed-face 37-mm cassette. However, Kenny et al.[9] evaluated eight different personal inhalable aerosol samplers and found that the closed-face 37-mm cassette did not match the inhalable convention. On the other hand, an inhalable aerosol sampler from the Institute of Occupational Medicine (IOM) matched the inhalable convention well. Therefore, the IOM sampler is recommended by the AIHA[10] as the appropriate personal inhalable aerosol sampler. The IOM sampler was developed and tested by Mark and Vincent.[11]

To revise the former TLVs, which were based on the aerosol concentration measurements using the closed-face 37-mm cassette, Tsai et al.[12] conducted a side-by-side measurement using the closed-face 37-mm cassette and the IOM sampler in a nickel alloy plant. They found that the aerosol concentration measurements using the IOM sampler were 1.3 to 2.4 times higher than those using the closed-face 37-mm cassette. Wilsey et al.[13] conducted similar tests in a metal machining shop and found that the aerosol concentration measurements using the IOM sampler were about 3 times higher than those using the closed-face 37-mm cassette. In a lead smelter plant, Spear et al.[14] found that the aerosol concentration measurements using the IOM sampler were about 1.29 to 2.14 times higher than those using the closed-face 37-mm cassette. Werner et al.[15] summarized a conversion factor varying from 1.0 to 2.5 between the IOM and the closed-face 37-mm cassette. Their conversion factor was mainly based on the particle diameter. For small particles, such as smokes and fumes, the conversion factor was 1.0, while for large dust, the conversion factor was 2.5.

Although the personal sampler collects a more representative workplace aerosol, personal sampling requires more labor, instruments, and worker involvement than area sampling.[8] The difficulty of having workers involved often makes personal sampling impractical. In addition, particles collected on the filter of a personal sampler may be knocked off by the worker's body movement, thus resulting in a significant sampling error.

For area sampling, there are very few commercially available samplers having known particle sampling performances that fit the inhalable convention. The use of personal samplers as area samplers is strongly discouraged by the American Industrial Hygiene Association (AIHA)[10] because of the unknown performances.

In this study, six personal inhalable aerosol samplers were evaluated in both the laboratory and the woodworking environment as area samplers. In the laboratory, aerosol samplers were tested in a wind tunnel using monodisperse, solid particles. Measured efficiencies and inside losses of the six samplers were obtained. In the field, all six samplers were mounted on a cart, at the human breathing zone height, to simultaneously collect wood dusts.

In addition to the inhalable aerosol samplers, a University of Washington (UW) impactor and a Marple Personal Cascade (Marple) impactor were evaluated in both the laboratory and the woodworking environment. In the woodworking environment, the UW and the Marple impactor were also mounted on the cart with the six inhalable samplers to measure wood-dust size distributions. The measured wood-dust size distributions can be used for the understanding of human health effects and for the development of wood-dust control techniques. In the laboratory, these two impactors were tested in the wind tunnel to determine their inlet efficiencies at different wind speeds, wind directions, and particle sizes. The impactor inlet-efficiency results were used to find the reason for the large difference of wood-dust size distributions measured using these two impactors.

CHAPTER 2
EQUIPMENT AND EXPERIMENTAL SETUP

Inhalable Aerosol Samplers

The inhalable aerosol samplers tested in the woodworking industry and/or in the laboratory are described below.

RespiCon Sampler. As shown in Fig. 2-1a, the RespiCon sampler (Model 8522, TSI Inc., St. Paul, MN, U.S.A.) has a circular inlet around the inlet-head perimeter. Aerosol is aspirated into the circular inlet at a flow rate of 3.10 l/min. The aerosol is then separated into three fractions by two virtual impactors. Inside the RespiCon, as shown in Fig. 2-1b, particles with aerodynamic diameters (D_a) less than 4 µm are separated in Stage 1 and collected onto the top filter. Particles with D_a greater than 4 µm pass straight through Stage 1 and flow downwards to Stage 2. In Stage 2, particles with D_a between 4 µm and 10 µm are collected onto the filter in Stage 2. Those particles with D_a greater than 10 µm pass straight through the Stage 2 and are collected onto the bottom filter. Particles on these three filters allow the determination of particle concentration for the inhalable, thoracic, and respirable fractions :

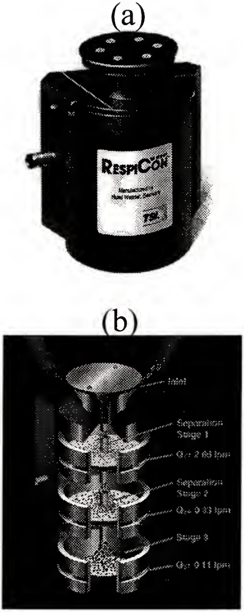

Fig. 2-1. A RespiCon sampler.
(a) Outside appearance (b) inside schematic drawing.
Source : manufacturer (TSI inc.) catalog.

$$C_R = \frac{Mass_1}{Q_1\ t} \tag{2-1}$$

$$C_T = \frac{Mass_1 + Mass_2}{(Q_1 + Q_2)\ t} \tag{2-2}$$

$$C_I = \frac{Mass_1 + Mass_2 + Mass_3}{(Q_1 + Q_2 + Q_3)\ t} \tag{2-3}$$

where

C_R : particle concentration in the respirable fraction

$Mass_1$: particle mass on top filter (stage 1)

Q_1 : sampling flow rate for Stage 1 (= 2.66 l/min)

t : sampling time

C_T : particle concentration in the thoracic fraction

$Mass_2$: particle mass on middle filter (stage 2)

Q_2 : sampling flow rate for Stage 2 (= 0.33 l/min)

C_I : particle concentration in the inhalable fraction

$Mass_3$: particle mass on bottom filter (stage 3)

Q_3 : sampling flow rate for Stage 3 (= 0.11 l/min)

Particles depositing on the inner surfaces of the RespiCon sampler are considered as inside losses. The RespiCon sampler is the only sampler tested that separates the aerosols into the three defined fractions. The other samplers are intended to collect the inhalable aerosols only.

Institute of Occupational Medicine (IOM) Sampler. Aerosol is aspirated into the IOM sampler (Cat. No. : 225-70, SKC Inc., Eighty Four, PA, U.S.A.) through a 15-mm diameter inlet orifice at a flow rate of 2.0 l/min. Particles aspirated into the inlet are either collected by a 25-mm filter or depositing on the inside surfaces of an internal two-piece cassette. Since particles on both the filter and the cassette are analyzed as the particulate matter sampled, there is no inside particle loss in the IOM sampler. A picture of the IOM sampler is shown in Fig. 2-2a.

Conical Inhalable Sampler (CIS). As shown in Fig. 2-2b, the CIS sampler (BGI Inc., Waltham, MA, U.S.A.) has a conical inlet section. Aerosol is aspirated into the CIS sampler through an 8-mm diameter inlet orifice at a flow rate of 3.5 l/min. In normal use, both the particles collected onto a 37-mm filter and those depositing on the filter holder are analyzed as the particle sample, while those depositing on the conical inlet section are considered as inside losses.

7-hole Sampler. Aerosol is aspirated into a 7-hole (SKC Inc., Eighty Four, PA, U.S.A.) sampler through seven 4-mm diameter inlet orifices at a flow rate of 2.0 l/min. In normal use, particles collected onto a 25-mm filter are analyzed as the particles sampled, while those depositing on the inner surfaces are considered as inside losses. A picture of the 7-hole sampler is shown in Fig. 2-2c.

Prototype Button Sampler. As shown in Fig. 2-2d, the Prototype Button sampler (SKC Inc., Eighty Four, PA, U.S.A.) has a hemispherical, metal-screen inlet, which contains many 381-µm diameter openings. The screen has a total open area of 21%. Aerosol is aspirated through the inlet at a flow rate of 2.0 l/min and collected onto a 25-mm diameter

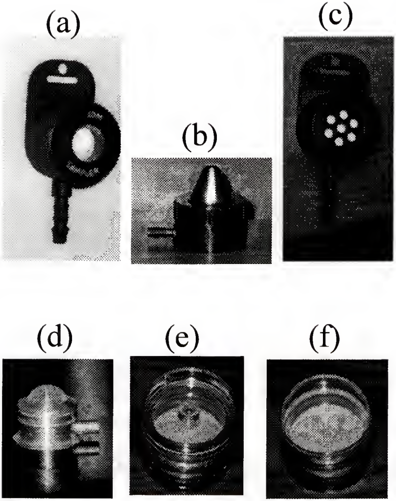

Fig. 2-2. Six inhalable aerosol samplers.
(a) IOM (b) CIS (c) 7-hole (d) Button (e) closed-face 37-mm cassette (f) open-face 37-mm cassette.

filter. Only those particles depositing on the front filter gasket were quantified as inside losses.

Closed-face 37-mm Filter Cassette. Aerosol is aspirated into a closed-face 37-mm filter cassette (Millipore Inc., Bedford, MA, U.S.A.) through a 4-mm diameter inlet orifice at a flow rate of 2.0 l/min. In normal use, particles collected onto a 37-mm diameter filter are analyzed as the particle catch, while those depositing on the inner surfaces are considered as inside losses. A picture of the closed-face 37-mm filter cassette is shown in Fig. 2-2e.

Open-face 37-mm Filter Cassette. Aerosol is aspirated into an open-face 37-mm filter cassette (Millipore Inc., Bedford, MA, U.S.A.) through a 38-mm diameter inlet at a flow rate of 2.0 l/min. Particles collected onto a 37-mm diameter filter are analyzed as the particle catch, while those depositing on the inner surfaces are considered as inside losses. The open-face cassette has the same sampler body as the closed-face cassette. The difference between these two cassettes is that the front piece (with a 4-mm inlet orifice) of the closed-face cassette is removed in the open-face cassette. The open-face cassette is shown in Fig. 2-2f. The open-face cassette was tested only in the woodworking industry.

Impactors

Three impactors were used in this study. The Marple impactor (Model 298, Andersen Samplers Inc., Atlanta, GA, U.S.A.) and the UW impactor (Model D, Pollution Control Systems Corp., Seattle, WA, U.S.A.) were used in both the field and lab tests. A MOUDI impactor (Model 100, MSP Inc., Minneapolis, MN, U.S.A.), developed and calibrated by Marple et al.[16], was used in the lab only as a reference impactor to compare the measured particle size distributions with those measured using the UW and the Marple impactor. These three impactors are shown in Figs. 2-3 and 2-4.

As shown in Fig. 2-3a, the Marple impactor inlet consists of a cowl and a front plate (called a visor). To investigate the effect of the visor, the Marple impactors with the visor and without the visor, as shown in Fig. 2-3b, were tested in the wind tunnel. The UW impactor inlet was fitted with a circular, metal tube with an inside diameter of 20 mm and an outside diameter of 27 mm. The length of this inlet tube was 60 mm, with the bottom 10 mm threaded into the UW impactor body. The MOUDI impactor inlet is a built-in metal tube with an inside diameter of 17 mm and an outside diameter of 25.5 mm. The length of the built-in tube is 42 mm. Inlet efficiencies of the Marple impactor and the UW impactor were determined using different particle sizes at different wind speeds and wind directions.

When the particles pass the inlet and reach the first impaction stage, the particles are fractionated by their inertial difference. As shown in Fig. 2-5a, particles of high inertia which do not follow the air streamline well, hit the impaction plate and are collected onto the plate; while particles of low inertia follow the air streamline very well and pass by the impaction plate. Generally, particles of large diameter have high inertia and are more easily collected. The particle diameter which has a 50% probability of being collected by an impaction plate is called the cut-point diameter, or D_{50}. The D_{50} for an impactor stage (consisting of a nozzle and a following impaction plate) is governed by the Stokes number

:

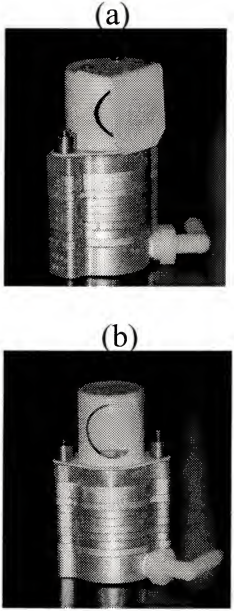

Fig. 2-3. A Marple Personal Cascade impactor. (a) with a visor (b) without a visor.

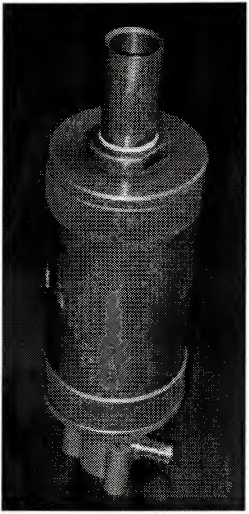

Fig. 2-3c. A University of Washington impactor.

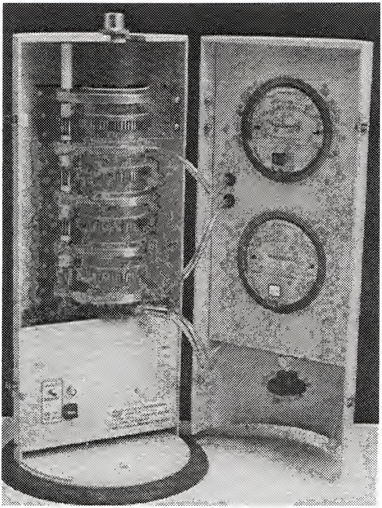

Fig. 2-4. A MOUDI impactor.
Source : Marple et al.[16]

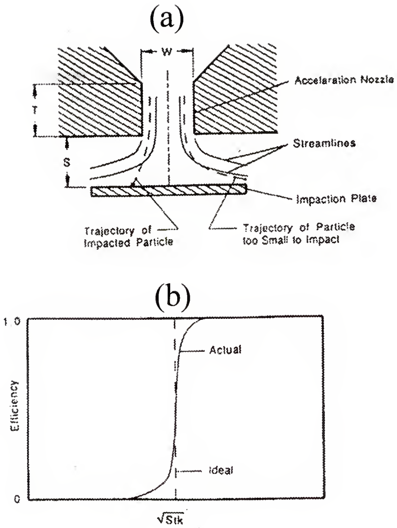

Fig. 2-5. (a) Particle trajectory in an impactor stage.
(b) Collection efficiency of an impactor stage.
Source : Willeke and Baron.[17]

$$Stk_{50} = \frac{\tau U}{W/2} = \frac{\rho_p D_{50}^{\ 2} U C_c}{9 \mu W} \tag{2-4}$$

or

$$D_{50}\sqrt{C_c} = \sqrt{\frac{9 \mu W (Stk_{50})}{U \rho_p}} \tag{2-5}$$

where

Stk_{50} : Stokes number corresponding to D_{50}, (no unit)

τ : particle relaxation time, or the particle response time, (sec)

U : average air velocity at the nozzle outlet

ρ_p : particle density, (g/cm^3)

C_c : Cunningham slip correction factor, (no unit)

μ : air viscosity, (g/cm.sec)

W : nozzle diameter, (cm)

Ideally, the collection efficiency curve should be a step function, i.e., all particles with diameters larger than D_{50} are collected by the impaction plate, while all particles with diameter less than D_{50} are not collected. A typical collection efficiency curve for an impaction stage is like the "S" shape shown in Fig. 2-5b. Although some of the mass percentage of larger particles ($> D_{50}$) is not collected and some of the mass of smaller particles ($< D_{50}$) is collected, the particle mass collected onto a specific stage is assumed to be all from the larger particles.

Impactors are usually constructed with several impaction stages in series and the nozzle diameters in every stage are in decreasing order. This is called a cascade impactor, as shown in Fig. 2-6.

Because the air flow rate into an impactor is fixed, when the nozzle diameter (W) is decreased the air velocity (U) is increased. From Equation 2-5, we know that D_{50} can be decreased by increasing U or by decreasing W. Since the nozzle diameters of a cascade impactor are in decreasing order, the D_{50} of every impaction stage is also in decreasing order. When the particle-laden air is directed through the cascade impactor, larger particles will be collected by the first stages and smaller particles by the latter stages. Particles passing the last impaction stage are all collected by a follow-up filter. Particle size distribution is obtained by plotting the weight gains of the impaction plates and the filter vs. the D_{50} values of the impaction stages.

For certain particle sampling, impactors with lower D_{50} are required. By greatly reducing the nozzle diameter to 52 μm, Marple et al.[15] designed a MOUDI impactor with D_{50} as low as 0.056 μm. By examining Equation 2-5, D_{50} can also be reduced by increasing C_c value. The C_c value is increased when the impactor is operated at low pressure, because

$$C_c = 1 + \frac{2}{PD_p}[6.32 + 2.01\exp(-0.1095PD_p)] \tag{2-6}$$

where

P : absolute pressure, (cm-Hg)

D_p : particle diameter, (μm)

Vanderpool and Lundgren (1990)[18] designed an impactor with D_{50} as low as 0.047 μm, which operated at a pressure of about 160 mm-Hg and is called a low-pressure impactor.

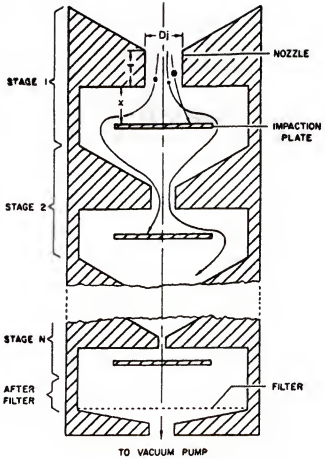

Fig. 2-6. A schematic drawing of a cascade impactor.
Source : Lundgren et al.[19]

To have a fixed and predictable collection efficiency curve, Marple (1970)[20] found that the ratio between plate-to-nozzle distance and nozzle diameter, S / W, should be from 1 to 5 and the Reynolds number in the nozzle from 500 to 10,000. When an impactor is designed following these guidelines, the Stk_{50} is approximately equal to 0.24 and 0.59 for round and rectangular nozzles, respectively.[20]

Particle bounce, collection surface overload, and interstage particle loss can be major problems when operating an impactor. Particle bounce can be greatly reduced by applying a thin layer of sticky material, such as Apiezon or Vaseline, on the surface of the impaction plates. To weight-stabilize the collection surface, the greased impaction plates are baked in an oven at about 90° C for 1 hour and then cooled in the desiccator overnight. Particle overload on the impaction plate is avoided by reducing the sampling time or by slowly rotating the impaction surface, such as a Lundgren impactor[21] or a MOUDI[16] impactor. Interstage particle loss is mainly reduced by using a well designed impactor.

Although the particle separation characteristic inside the impactor have been theoretically and experimentally investigated, the impactor inlet efficiency is not well known. Different impactors may have significantly different inlet efficiencies due to different inlet geometries. Different inlet efficiencies would result in different measured particle size distributions. The inlet efficiencies of the UW impactor and the Marple impactor were measured in the lab to help explain the large difference in particle size distributions measured in the wood-working industry by the different impactors.

Vibrating Orifice Aerosol Generator (VOAG)

A VOAG (Model 3050, TSI Inc., St. Paul, MN, U.S.A.), developed by Berglund and Liu[22], was used to generate monodisperse test aerosols for use in the lab studies and is shown in Fig. 2-7. Uniform droplets are produced by pushing the liquid solution, supplied by a syringe pump, through a small orifice (5 - 41 μm) to form a liquid cylinder. This liquid cylinder is evenly broken up along its length by a disturbance from a function generator. The generated uniform droplets are first dispersed using a dispersion air (~ 1.5 L / min) to prevent singlet droplets from forming doublets and triplets, and then completely dried using additional dilution air in the drying column. To prevent the plugging of the VOAG orifice, a membrane filter with a fine pore size is used to remove insoluble material in the liquid solution.

One main advantage of the VOAG is that the generated particle size can be easily calculated using Equation 2-7 :

$$D_d = (6\, Q_l / \pi\, f)^{1/3}$$

$$D_p = D_d\, (C)^{1/3} \qquad (2\text{-}7)$$

where

D_d = droplet size, cm

Q_l = liquid flow rate, cm^3 / sec

f = frequency of the function generator, Hz

D_p = dry particle diameter, cm

C = volumetric concentration of the solution, dimensionless

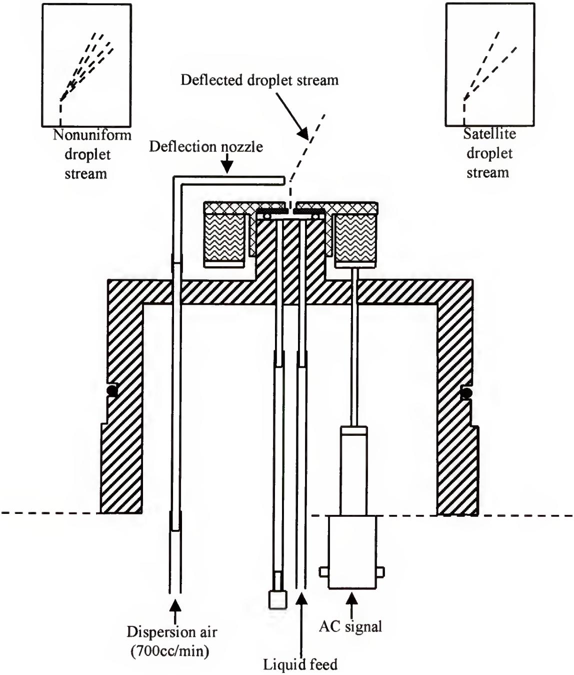

Fig. 2-7. A schematic drawing of a Vibrating Orifice Aerosol Generator (VOAG) and a deflection test for droplet uniformity.

Li and Lundgren[23] found that the difference between the calculated and the measured particle diameters was less than 5%. The main difficulty in operating the VOAG is that the small orifice is easily clogged. Therefore, a lot of patience and time are required.

The orifice diameter and the syringe pump liquid flow rate of the VOAG were determined by the desired particle diameter. The detailed working ranges of these two parameters were described by Berglund and Liu.[22]

The frequency of the function generator for each orifice diameter was determined by a deflection test, as shown in Fig. 2-7. When the frequency was out of tune, the droplet stream was deflected into several minor streams, as shown in the upper left-hand corner of Fig. 2-7. When the frequency was close to that required, the droplet stream was deflected into two streams, as shown in the upper right-hand corner of Fig. 2-7. By slowly adjusting the function generator, the frequency was tuned and the droplet stream was deflected into single stream, as shown in the center of Fig. 2-7. The operating conditions for the orifice diameter, the syringe pump flow rate and the frequency of the function generator are listed in Table 2-1.

In this study, the VOAG generated monodisperse particles were made of ammonium fluorescein shown in Fig. 2-8. The reason for choosing ammonium fluorescein particles as the test aerosol was that ammonium fluorescein particles could be easily recovered using a 0.1 N sodium hydroxide (NaOH) solution and then be accurately quantified using a fluorometer. To generate spherical particles, the dilution-air flow rate should be carefully controlled.[23] A liquid particle solution of 28% volume concentration was initially produced and other concentrations of particle solution were generated by

Table 2-1. Operating conditions of the VOAG for generating monodisperse particles.

Calculated D_a (μm)	5	10	21	41	68
Orifice Diameter (μm)	15	15	30	41	41
Frequency (KHz)	47	47	39	23.5	21.5
Particle Solution Conc., (%)	0.1	0.8	3	8	28
Syringe Pump Flow Rate (cm^3/min)	0.11	0.11	0.25	0.42	0.48

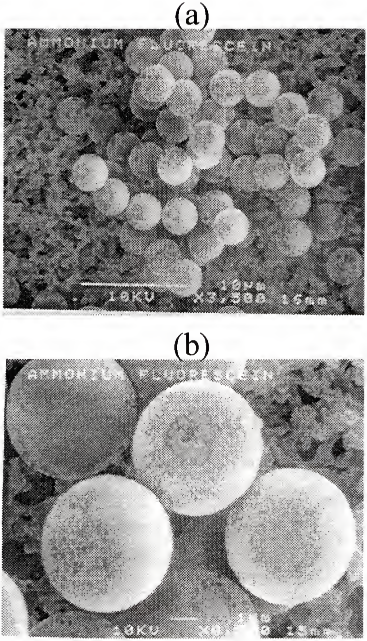

Fig. 2-8. Scanning electron micrograph of ammonium fluorescein particles. (a) Particle diameter of 3.2 micrometer. (b) Particle diameter of 4.6 micrometer.

diluting this 28% solution with deionized (DI) water. Production of the 28% ammonium fluorescein solution is shown as the following :

MW (Molecular Weight) of fluorescein ($C_{20}H_{12}O_5$) = 332 (g/g-mole)

MW of ammonium hydroxide (NH_4OH) = 35 (g/g-mole)

$$C_{20}H_{12}O_5 + NH_4OH \rightarrow C_{20}H_{11}O_5NH_4 \text{ (MW = 349)} + H_2O \qquad (2\text{-}8)$$

Density of the ammonium fluorescein ($C_{20}H_{11}O_5NH_4$), $\rho_p = 1.35$ (g/cm^3), (Stöber and Flachsbart[24])

28% concentration by volume = 280 ml of ammonium fluorescein / 1000 ml of solution

= 378 g of ammonium fluorescein / 1 liter of solution

The quantity of fluorescein needed = 378 (332 / 349) g / 1 liter of solution

= 360 g / 1 liter of solution

To ensure that all of the solid fluorescein reacted with ammonium hydroxide, the amount of ammonium hydroxide added was twice as much as that requested by Equation 2-8.

Moles of NH_4OH = (360 / 332) 2 = 1.08 (g-mole)

The NH_4OH solution available was 14.8 N (g-mole/liter).

The volume of NH_4OH solution = 1.08 / 14.8 = 0.073(liter) = 73 (ml)

Therefore an ammonium fluorescein solution of 28% volume concentration was produced by adding 360 g of solid fluorescein to 73 ml of 14.8-N NH_4OH solution and making this solution up to 1 liter with DI water.

The diameters of the particles generated by the VOAG were calculated using Eq. 2-7. The following example is presented for $D_a = 68$ µm :

$D_d = (6Q_l / \pi f)^{1/3}$

$Q_l = 0.485\ (\text{cm}^3/\text{min}) = 8.08*10^{-3}\ (\text{cm}^3/\text{sec})$; $f = 21.5\ \text{KHz} = 2.15*10^4\ \text{Hz}$

$D_d = [6*8.08*10^{-3}/\pi*2.15*10^4]^{1/3} = 89.6\ (\mu\text{m})$

$D_p = D_d*(C)^{1/3}$, Conc. = 28%, $D_p = 89.6*(0.28)^{1/3} = 58.6\ (\mu\text{m})$

$D_a = D_p*(\rho_p)^{1/2}$, (Hinds [25]), $D_a = 58.6*(1.35)^{1/2} = 68\ (\mu\text{m})$

Other calculated particle aerodynamic diameters are listed in Table 2-1.

To generate the 68 μm particles, the particle solution (28%) had to be prefiltered to prevent the plug-up of the membrane filter located before the orifice disk. Because of the high pressure drop through the membrane filter, a 25 cm^3 syringe was used to supply the prefiltered particle solution. When a 50 cm^3 syringe was used the syringe pump slipped, which resulted in the non-uniformity of the test particles. To reduce the pressure drop, a membrane filter of 5 μm pore size was used to remove insoluble particles from clogging the 41-μm orifice.

Attempts were made to generate particles with D_a greater than 80 μm using higher particle concentration (greater than 28%) or larger orifice diameter (greater than 41 μm), but both attempts were not successful. It was found that when the concentration of the ammonium fluorescein solution was greater than 30%, the solution was saturated and some solid fluorescein was not dissolved. When the orifice diameter was greater than 50 μm, the generated particles were too large to reach the sampler testing area due to gravity and impaction losses.

Collison Atomizer

A Collison atomizer, as shown in Fig. 2-9, was applied to generate polydisperse uranine test particles with mass median aerodynamic diameter (MMAD) smaller than 2

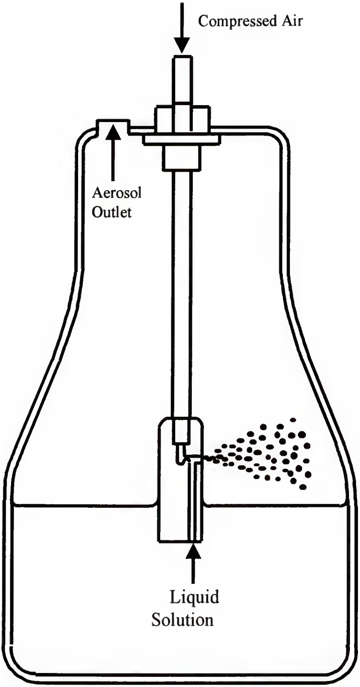

Fig. 2-9. A Collison atomizer.

μm. Droplets of wide size range are formed by using compressed (267 kPa, Pa=N/m^2) air to nebulize a uranine solution. Larger droplet (with higher inertia) are removed when they hit the wall and trickle back to the solution reservoir, while the smaller droplets (with lower inertia) follow the air stream and exit.

Charge Neutralizer : Kr-85 (Krypton-85)

The radioactive source, Kr-85, was used to charge neutralize the small particles generated using the Collison atomizer. When the electrically charged particles pass through the Kr-85 chamber, these charged particles attract oppositely charged air molecules, generated by the Kr-85 source. The charged particles eventually reach a Boltzmann charge equilibrium, the charge distribution of a particle in charge equilibrium with bipolar ions.

Fluorometer

A fluorometer (Model 112, Turner Assoc., Palo Alto, CA, U.S.A.) was used to determine the quantity of the ammonium fluorescein and uranine particles, which deposit on the glass-fiber filters or on the inner surfaces of the aerosol samplers. By applying a UV (ultraviolet) light to excite fluorescein in the solution, the solution concentration is determined. After multiplying the solution concentration by its volume, the particle mass is obtained.

To dissolve the ammonium fluorescein particles and the uranine particles, sodium hydroxide (NaOH) solution of 0.1 N and 0.01 N were used, respectively. About 30 ml of the NaOH solution was added to dissolve the particles on the filter. To ensure complete dissolution of the particles, this solution was sonicated in a water bath for about 10 minutes. The particle loss on the inside surfaces was fully recovered using the same NaOH solution (in a squeeze bottle). Three readings were obtained and averaged for each particle sample. The background measurements of the glass fiber filters used were near the fluorometer detection limit.

Hot-Wire Anemometer

A hot-wire anemometer (Model 8330, TSI Inc., St. Paul, MN, U.S.A.) was used to measure the air velocity inside the lab wind tunnel. The hot-wire anemometer has an air-velocity sensor which is maintained at a fixed temperature. When the air stream passes the heated sensor, the sensor is cooled down. To heat up the sensor to the fixed temperature, an electrical current was supplied by a battery. The amount of electrical current supplied is proportional to the air velocity.

The hot-wire anemometer was calibrated at 21° C and 1 atm by the manufacturer. When the hot-wire anemometer is used at other temperature and pressure, it should be corrected by the following equation :

$$V_{act}=V_m[\frac{273+T_m}{273+21}][\frac{101.4}{P_m}] \tag{2-9}$$

where

V_{act} = actual air velocity

V_m = measured air velocity

T_m = measured temperature, °C

P_m = measured pressure, kPa

Wind Monitor

A rotating-vane Wind Monitor (Model 05305, R.M. Young Company, Traverse City, MI, U.S.A.), as shown in Fig. 2-10, was used to measure the wind velocity and wind direction inside the wood-working plants. The Wind Monitor used has a detection limit of 0.2 m/s. When the measured wind speed was less than 0.2 m/s, the displayed readout is 0.

Experimental Setup in the Field

As shown in Fig. 2-11a, field samples of airborne wood-dusts were obtained using five different inhalable aerosol samplers and two different impactors. For each kind of the sampler, duplicates were used in each run except for the IOM and the UW impactor. Three IOMs were simultaneously used to measure the wood-dust concentration difference in the sampling zone. Only one UW impactor was used in each run.

As shown in Fig. 2-11b, all samplers were mounted side-by-side on a cart at human breathing zone height. The flow rates of the Marple impactor, IOM, 7-hole, closed-face and open-face cassette were controlled at 2.0 l/min. The flow rate of the UW impactor and that of the CIS were controlled at 15 l/min and 3.5 l/min, respectively. Each flow rate was controlled using a critical orifice and monitored using a rotameter except for the UW impactor. The flow rate of the UW impactor was only monitored using a rotameter. Each flow rate was calibrated using a Gilibrator (an electronic standard bubble meter)(Gilian Instrument Corp., Wayne, NJ, U.S.A.) at the sampler inlet. The Gilibrator was checked using a manual standard bubble meter with an one-liter column. The measured flow rate difference between the Gilibrator and the manual standard bubble meter was less than 2%.

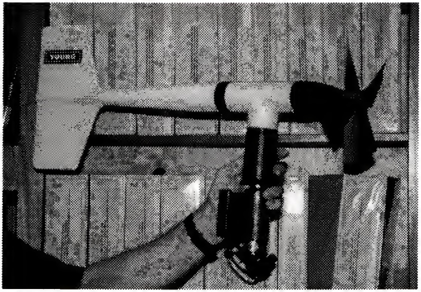

Fig. 2-10. A rotating-vane Wind Monitor used in the wood-working industry.

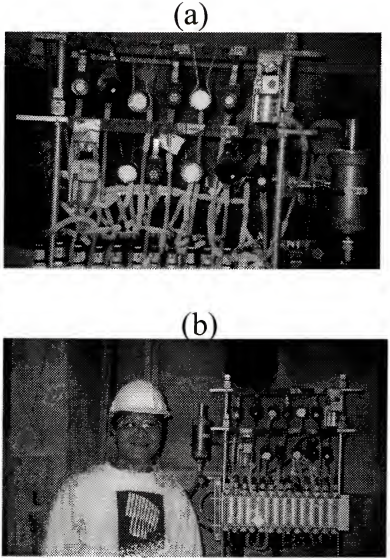

Fig. 2-11. Sampler arrangement in the wood-working industry. (a) Sampler arrangement (b) sampling height.

The collected particle-sample weights were determined by weighing the filters and the impaction plates before and after the test using a Cahn microbalance (Model C-31, Cahn Instrument Inc., Cerritos, CA, U.S.A.) or using a Mettler balance (Model HK 60, Mettler-Toledo Inc., Hightstown, NJ, U.S.A.). The Cahn microbalance used has a readability of 0.001 mg (1μg) and the Mettler balance has a readability of 0.01 mg. For the IOM and the CIS sampler, the filter and the filter holder were weighed together. Because of the heavy tare weights (greater than 3 g) of these filter holders, the particle samples collected using the IOM and the CIS were weighed using the Mettler balance. The other samples were weighed using the Cahn microbalance.

The impaction plates, made of stainless-steel, were coated with Apeizon-H grease to prevent particle bounce. A 5-μm (pore-size) polyvinyl chloride (PVC) filter was put behind the last impaction stage to collect the particles with aerodynamic diameters smaller than the last-stage cut-point diameter (D_{50}). Before the weighting, the impaction plates and the PVC filter were desiccated for 2 days.

Before the field sampling, the Mylar (thin plastic film) impaction plates for the Marple impactor were tested in the lab using sodium chloride (NaCl) particles, generated by the Collison atomizer. It was found that when the particle loading on the Mylar substrate was high, the collected particles could fall off due to the wrinkle of the Mylar substrate, which stuck tightly to the O-ring inside the impactor stage. Therefore, only the impaction plates made of stainless-steel were used in this study.

Experimental Setup in the Lab

To compare the particle sizing performances of three impactors, as shown in Fig.

2-12, the test aerosol was generated by atomizing a solution of sodium chloride (NaCl) and uranine using a Collison atomizer operated at a pressure of 200 kPa. This aerosol was charge-neutralized using Kr-85 (radioactive material) and mixed with 100 l/min of dilution air. There were a circular mixing plate inside the tubing (150-mm diameter) to help the test aerosol uniformly mix with the dilution air. A flow laminator was used to evenly distribute the diluted aerosol. The end of the tubing was expanded to 200 mm diameter to accommodate the four impactors (one MOUDI, one UW impactor, and two Marple impactors). These four impactors were evenly located inside the 200 mm diameter circular space.

To determine the inlet efficiencies of the aerosol samplers, solid, monodisperse, ammonium-fluorescein test particles with aerodynamic diameters ranging from 5 to 68 μm were generated using a Vibrating Orifice Aerosol Generator (VOAG). To effectively transport large VOAG generated particles, the drying air system supplied to the VOAG was modified as shown in Fig. 2-13. Liquid particles from the VOAG were lifted upwards, dried, and directed into a wind tunnel using an air flow rate of 425 l/min. In the vertical wind tunnel section, the test aerosol was mixed with a dilution air using a mixing plate, it was then transported horizontally to the sampler testing zone. To reduce large-scale turbulence at the sampler testing zone, a laminator with 20 rectangular openings of 25 mm by 100 mm was used.

At the beginning of this study, it was found that the original VOAG drying column was too small and the drying air flow rate was too low to effectively transport particles with D_a greater than 40 μm. It was found that using the original drying air system, more

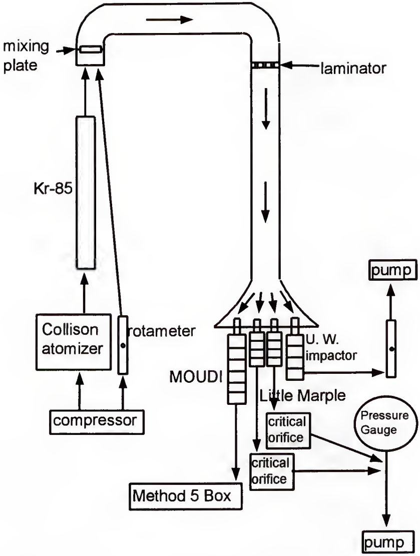

Fig. 2-12. A schematic diagram of the system set-up for testing a MOUDI impactor, a UW impactor and two Marple Personal Cascade impactors.

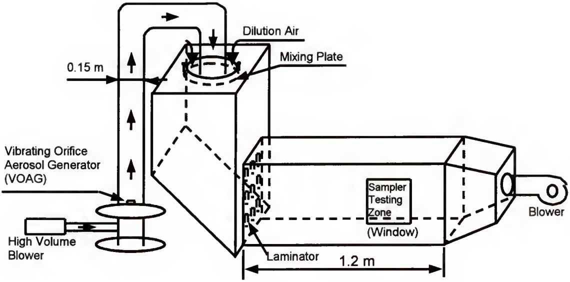

Fig. 2-13. Schematic drawing of the testing wind tunnel..

than 95% of the large particles (D_a greater than 40 µm) were lost before they reached the test wind tunnel. This low particle generation rate resulted in an undetectable particle concentration at the sampler testing zone of the wind tunnel. Therefore, the drying column was increased from 100 mm to 150 mm and the drying air flow rate increased from 100 l/min to 425 l/min, which resulted in abundant large test particles available at the sampler testing zone.

For the 68 µm particles, the mixing plate was removed to reduce the observed high particle losses. Because of the high settling velocity (14 cm/s) of the 68-µm particles, when testing the samplers using this particle size, the samplers were located at the bottom half of the sampler testing zone to overcome the high particle concentration difference at the top half due to the gravity settling.

To assure the test particle quality, during each syringe run of the VOAG, particles were collected at the sampler testing zone using an open-face 37-mm cassette with the sampler inlet air velocity similar to the test section air velocity. Diameter of the collected particles was measured using a light microscope. Particles collected on the filters of the aerosol samplers were also checked using the light microscope.

The VOAG particle mass output was unacceptably low for small particles. Therefore, polydisperse, uranine test particles with a mass median diameter (MMD) of 1.6 µm and geometric standard deviation (GSD) of 2.7 were generated using a Collison atomizer. The MMD and GSD values were measured at the sampler testing zone using an 8-stage Marple Personal Cascade impactor (without a visor).

Two wind speeds, 0.55 m/s and 1.1 m/s, were used in this study. The wind speeds were measured using a hot-wire anemometer. For each test condition, three sampling positions with particle concentration difference less than 10% were located in the sampler testing zone by simultaneous measurement using three isokinetic sharp-edge probes.

For the inhalable aerosol sampler test, as shown in Fig. 2-14, one isokinetic probe and two inhalable aerosol samplers were simultaneously put at the same positions as those located by the three isokinetic probes and then the samplers' positions were sequentially changed. The measured efficiency and the inside loss of the inhalable aerosol sampler are determined by Equations (2-10) and (2-11), respectively :

$$\text{Measured Efficiency} = \frac{C_{inh}}{C_{isok}} = \frac{Mass_{inh}/Q_{inh}}{Mass_{isok}/Q_{isok}} \tag{2-10}$$

$$\text{Inside Loss} = \frac{Mass_{loss}/Q_{inh}}{Mass_{isok}/Q_{isok}} \tag{2-11}$$

Where

C_{inh} = particle concentration measured by the inhalable aerosol sampler,

C_{isok} = particle concentration measured by the isokinetic probe,

$Mass_{inh}$ = mass of particle sample collected by the inhalable aerosol sampler,

$Mass_{isok}$ = mass of particles collected by the isokinetic probe,

$Mass_{loss}$ = mass of particles depositing on the inner surfaces of the inhalable aerosol sampler,

Q_{inh} = air flow rate through the inhalable aerosol sampler,

Q_{isok} = air flow rate through the isokinetic probe.

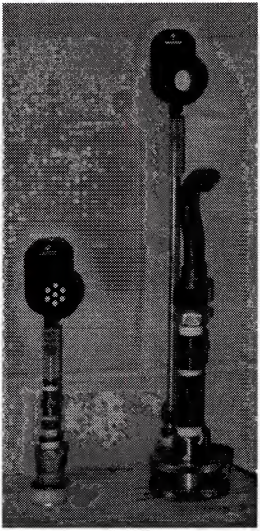

Fig. 2-14. Sampler arrangement in the wind tunnel.
Front - an isokinetic probe, right - an IOM, left - a 7-hole.

For the impactor test, two sampling locations were found with nearly equal particle concentration (difference less than 10%). Concentration differences were determined from simultaneous measurement using two isokinetic sharp-edge probes. In each test, one isokinetic probe and one impactor were located at the previously determined test positions. In a second test, the isokinetic probe and the impactor positions were reversed. For the Marple impactor, the first-stage outlet efficiency and the losses on both the cowl inlet and the first-stage surfaces are determined by Equations (2-12) and (2-13), respectively :

$$First\text{-}stage\ outlet\ efficiency = \frac{C_{imp}}{C_{isok}} = \frac{Mass_{imp}/Q_{imp}}{Mass_{isok}/Q_{isok}} \tag{2-12}$$

$$Inside\ Loss = \frac{Mass_{loss}/Q_{imp}}{Mass_{isok}/Q_{isok}} \tag{2-13}$$

Where

C_{imp} = measured particle concentration at the first-stage outlet of the Marple impactor,

C_{isok} = measured particle concentration using the isokinetic probe,

$Mass_{imp}$ = mass of particles collected at the first-stage outlet of the Marple impactor,

$Mass_{isok}$ = mass of particles collected using the isokinetic probe,

$Mass_{loss}$ = mass of particles depositing on the cowl inlet or on the first-stage surfaces,

Q_{imp} = air flow rate through the Marple impactor,

Q_{isok} = air flow rate through the isokinetic probe.

The inlet efficiency of the Marple impactor is determined by summing the first-stage outlet efficiency and the inside losses on both the cowl inlet and the first-stage surfaces. For the UW impactor inlet, all particles entering the inlet were quantified together using similar method. The air flow rate through each impactor (including the isokinetic probe) was monitored using a rotameter, which was calibrated using a Gilibrator. The testing wind tunnel is shown in Fig. 2-15.

To recover the particle losses inside the samplers, different procedures were used. For example, to recover the inside losses on the inlet head of the RespiCon sampler, the outside surfaces of the inlet head were first cleaned using a NaOH-soaked Q-tip. Particles depositing inside various sampler sections were then dissolved and washed out using the NaOH solution. Particle losses inside the 7-hole sampler were recovered using a NaOH-soaked Q-tip, and then sonicating the Q-tip for 5 minutes in a NaOH solution. Particle losses inside the CIS conical inlet and the closed-face 37-mm cassette were recovered by carefully rinsing the inside surfaces using a NaOH-containing squeeze bottle. Before rinsing the inside surfaces, the outside surfaces around the inlets were carefully cleaned to prevent the particles on the outside surfaces from being included.

The air flow rate through each sampler (including the isokinetic probe) was monitored using a rotameter and controlled using a critical orifice. The rotameters and the orifices were calibrated using a calibrated Gilibrator. To minimize the effect of filter pressure drop on flow rate variation, glass fiber filers (A/E type) were used for particle collection in lab study. The sampling flow rate difference due to filter loading was found to be less than 1%.

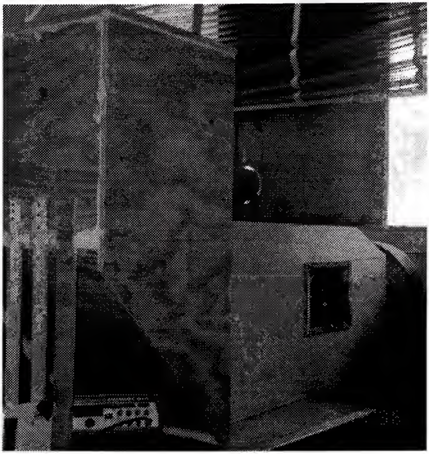

Fig. 2-15. A testing wind tunnel.

CHAPTER 3
RESULTS AND DISCUSSION

Inhalable Aerosol Samplers

Weight Instability of the IOM and the CIS Plastic Filter Holders

At the beginning of field sampling in the woodworking mills, many particle samples collected using the IOM and the CIS samplers had "negative" weight gains. For the IOM and the CIS samplers, aerosols were aspirated into the inlet orifice and collected onto a filter, which was supported by a filter holder made of a plastic material. The filter and the filter holder for the IOM and the CIS sampler were weighed together before and after the sampling to determine the net weight of the collected particles. For the 7-hole, closed-face and open-face 37-mm cassettes, only the filter was weighed before and after the sampling to determine the net weight of the collected particles. This gravimetric analysis technique has been widely used and recommended by many researchers.[9-13, 26]

To determine the source of error in the sampling procedures, three consecutive tests were conducted. The first test measured the tare-weight variations during desiccation of six IOM plastic (filter) cassettes, six IOM stainless-steel cassettes, six CIS plastic holders, six 25-mm Polyvinyl Chloride (PVC) filters and six 37-mm PVC filters. The second test measured the tare-weight changes of the PVC filters and the plastic cassettes/holders shown in Figs. 3-1 and 3-2 after they were exposed to the ambient environment for 3 days. The third test measured the tare-weight variations of the plastic

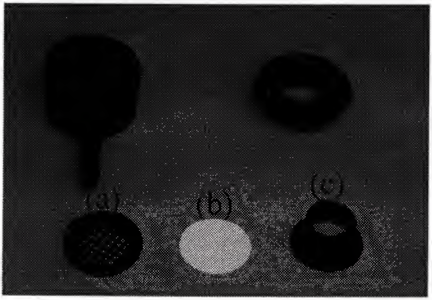

Fig. 3-1. An IOM sampler and its plastic cassette.
Note : (a), (b) and © were weighed together.

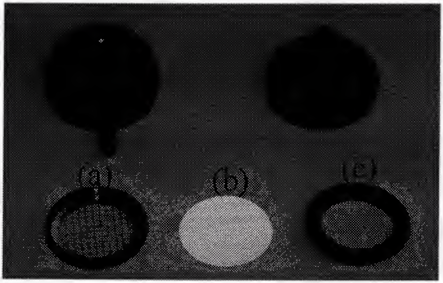

Fig. 3-2. A CIS sampler and its plastic holder.
Note : (a), (b) and © were weighed together.

cassettes/holders in the weighing room conditions.

In the first test series, IOM plastic and stainless-steel cassettes and CIS plastic holders were cleaned with distilled water, dried in the weighing room for seven days, and then desiccated for 10 days. The relative humidity (RH) and temperature (T) in the weighing room were in the range of 75% ± 5% and 21 °C ± 1 °C, respectively. The desiccant used was silica gel. When one sample was weighed, the others were kept in the desiccator. The IOM plastic cassettes and the PVC filters were weighed using a Cahn C-31 microbalance (1 μg readability). The CIS plastic holders and the IOM stainless-steel cassettes were weighed using a Mettler HK-60 balance (10 μg readability).

In the second test series, plastic cassettes and holders were put on a metal screen, covered with Petri dishes, and then placed in an outside sheltered housing for three days. During those three days, the housing RH varied between 50% and 98% and the temperatures varied between 21 and 33 °C. The samples were then desiccated and reweighed every 24 hours over a 12-day period. At the beginning of the test, fresh silica gel was put into the desiccator and used (without change) for 12 days.

At the beginning of the third test series, the same plastic cassettes and holders were washed with distilled water and wiped dry. The plastic cassettes and holders were then exposed to the weighing room conditions and reweighed daily for 14 days.

The average tare-weight losses of six IOM stainless-steel cassettes, six IOM plastic cassettes and six CIS plastic holders in the desiccator are plotted in Fig. 3-3. For 10 consecutive days, the average tare-weights of the IOM plastic cassette and the CIS plastic holder continuously decreased. Weight losses for the CIS plastic holders were typically

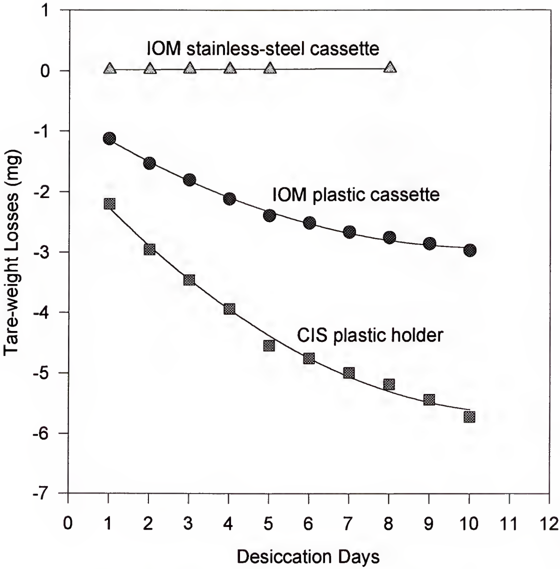

Fig. 3-3. Average tare-weight losses of six IOM plastic cassettes, six CIS plastic holders, and six IOM stainless-steel cassettes in a desiccator.

greater than those for the IOM plastic cassettes. On the other hand, tare-weights of the IOM stainless-steel cassettes were stable.

After a 3-day exposure to the ambient environment, the average tare-weight losses (due to desiccation) of six IOM plastic cassettes and six CIS plastic holders were very similar to Fig. 3-3. However, it was found that tare-weights, for all plastic cassettes or holders, would not return to the initial values even though the desiccation time was the same. This means that the tare-weights of plastic cassettes and holders vary with exposure conditions prior to desiccation. Typical tare-weight variations of an IOM plastic cassette before and after a 3-day ambient exposure is shown in Table 3-1. This tare-weight variation will bias the estimated weight of collected particle samples. For example, if the IOM plastic cassette is desiccated for only three days before and after sampling, the weight difference is 0.48 mg (802.903 - 802.423). This 0.48-mg variation would introduce a 48% error to a 1 mg sample. Sample weights typically range from 0.1 mg to 2 mg.[27]

For the PVC filters alone, it was found that the weight variations were no more than 0.006 mg (6 μg) after two days desiccation time. Typical tare-weight variations of a 37-mm Polyvinyl Chloride (PVC) filter before and after a 3-day ambient environment exposure is shown in Table 3-2. Following the previous test series, six IOM plastic cassettes and six CIS plastic holders were placed in the weighing room and reweighed daily for 14 days. It was found that the tare-weights of all plastic filter holders (or cassettes) continuously increased for 14 days.

It appeared that these commercially available plastic cassettes or holders were hygroscopic and should not be weighed together with the particle samples. In the

Table 3-1. Tare-weight variation (due to desiccation) of an IOM plastic cassette before and after a 3-day exposure to the ambient environment.

Desiccation Days	0	1	2	3	4	5	6
Before (mg)	**804.666**	**803.530**	**803.161**	**802.903**	**802.614**	**802.309**	**802.223**
After (mg)	**804.070**	**803.065**	**802.645**	**802.423**	**802.129**	**801.852**	**801.718**

Table 3-2. Tare-weight variation (due to desiccation) of a 37-mm Polyvinyl Chloride (PVC) filter before and after a 3-day exposure to the ambient environment.

Desiccation Days	0	1	2	3	4	5	6
Before (mg)	**12.941**	**12.935**	**12.937**	**12.933**	**12.934**	**12.935**	**12.934**
After (mg)	**12.935**	**12.936**	**12.933**	**12.935**	**12.931**	**12.932**	**12.933**

following field sampling, for the IOM sampler, the stainless-steel filter cassettes were used. For the CIS sampler, only the filter was weighed before and after a field test. A commercially available stainless-steel filter holder was not available. After each field test, particles depositing on the CIS plastic filter holder were carefully recovered and deposited onto the filter using a small paint brush.

Field Results for Inhalable Aerosol Samplers

For the particle mass concentration measurements in the wood-working mills, only the normalized data are presented in this study due to the business confidentiality and contract agreement with the project sponsor. For each test, the average value of two or three simultaneous measurements from each type of sampler was divided by the average value of two simultaneous measurements made using the closed-face 37-mm filter cassette. The normalized results are shown in Tables 3-3 and 3-4.

As shown in Tables 3-3 and 3-4, the particle concentration measurement made using the IOM sampler had the highest average ratio value (IOM/closed-face) ranging from 117% to 217%. The range of this ratio is close to the conversion factor (100% to 250%) summarized by Werner et al.[15] although their conversion factor is mainly for personal sampling. This ratio value (open-face/closed-face) between the open-face cassette and the closed-face cassette ranged from 49% to 122%. The concentration measurements using the 7-hole and the CIS sampler were greater than those using the closed-face cassette.

To measure the particle concentration difference within the sampler array at a given sampling location, three IOM samplers (as shown in Fig. 2-11) were simultaneously

Table 3-3. Particle concentration ratio between the 37-mm closed-face cassette and the other samplers at a plywood mill.

	Test 1	Test 2	Test 3	Test 4
Closed-face	97%, 103% Avg.= 100%	100%, 100% Avg.= 100%	93%, 107% Avg.= 100%	105%, 95% Avg. = 100%
CIS	140%, 152% Avg.= 146%	130%, 120% Avg. = 125%	128%, 135% Avg.= 132%	180%, 155% Avg.= 168%
IOM	81%, 184% 144% Avg.= 136%	120%, 220% 190% Avg.= 180%	140%, 205%, 146% Avg.= 164%	158%, 145%, 160% Avg.= 154%
Open-face	102%, 77% Avg.= 90%	130%, 110% Avg.= 120%	104%, 138% Avg.= 121%	*NA
7-hole	125%, 112% Avg.= 119%	140%, 140% Avg.= 140%	135%, 128% Avg.= 132%	130%, 110% Avg.= 120%

* Samples were dropped during the transportation from the field to the lab.

Table 3-3(cont.). Particle concentration ratio between the 37-mm closed-face cassette and the other samplers at a plywood mill.

	Test 5	Test 6	Average
Closed-face	103%, 97% Avg.= 100%	107%, 93% Avg.= 100%	**100%**
CIS	104%, 117% Avg.= 111%	184%, 180% Avg.= 182%	**143%**
IOM	92%, 147%, 113% Avg.= 117%	116%, 201% 185% Avg.= 168%	**153%**
Open-face	100%, 100% Avg.= 100%	111%, 88% Avg.= 99%	**106%**
7-hole	100%, 110% Avg.= 105%	125%, 121% Avg.= 123%	**123%**

Table 3-4. Particle concentration ratio between the 37-mm closed-face cassette and the other samplers at a particle-board mill.

	Test 1	Test 2	Test 3	Test 4	**Avg.**
Closed-face	103%, 97% Avg.= 100%	108%, 92% Avg.= 100%	114%, 86% Avg.=100%	110%, 90% Avg.=100%	**100%**
IOM	244%, 189% Avg.= 217%	279%, 142% Avg.= 210%	166%, 121% Avg.= 143%	147%, 112% Avg.= 129%	**175%**
Open-face	54%, 129% Avg.= 92%	42%, 77% Avg.= 59%	88%, 61% Avg.= 75%	48%, 50% Avg.= 49%	**69%**
7-hole	146%, 151% Avg.= 149%	137%, 30% Avg.= 84%	112%, 84% Avg.= 98%	92%, 88% Avg.= 90%	**105%**

used. Table 3-3 shows that the concentration difference is greater than 50% for most tests and occasionally the concentration difference is greater than 100%. It shows that particle concentration in the workplace is highly variable.

To obtain a better estimate of particle concentration in the workplace, simultaneous measurements using at least three samplers of the same type together with multiple sampling tests at the same location are recommended. Before choosing a specific sampling location, a thorough survey of the plant (or mill) was essential. In our field sampling, the sampling locations were chosen based on the number of workers present and the apparent dustiness of the location. To further understand the measured particle concentration difference for each type of the sampler, a series of laboratory wind tunnel tests were conducted. The tests are described below.

Lab Results for Inhalable Aerosol Samplers

RespiCon sampler. Fig. 3-4a shows the average measured efficiency vs. particle size for the RespiCon sampler at a wind speed of 0.55 m/s. The differences between the measured efficiencies and the inhalable convention are less than 10%. The measured efficiency was determined by comparing the particle mass concentration measured using the RespiCon sampler with that measured using an isokinetic probe. Theoretically, the isokinetic probe has a 100% inlet efficiency for particle sampling. For each data point, an average value of two or three measurements was plotted. The detailed results are shown in Appendix A.

At wind speed of 1.1 m/s, as shown in Fig. 3-4b, the performances of the RespiCon sampler fit the inhalable convention fairly well except at the 68-μm particle size. The RespiCon sampler over-samples 68-μm particles by 25%. A recent study by Baldwin

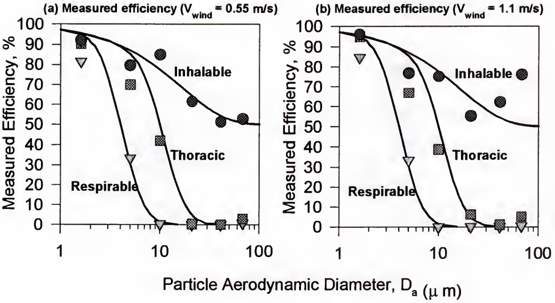

(a) Measured efficiency (V_{wind} = 0.55 m/s)

(b) Measured efficiency (V_{wind} = 1.1 m/s)

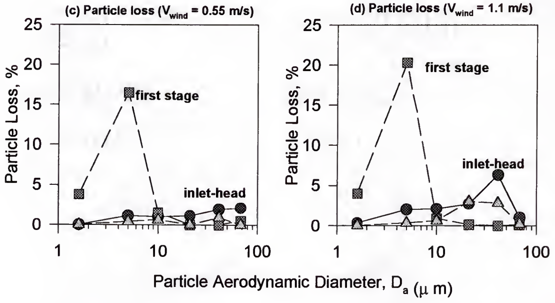

(c) Particle loss (V_{wind} = 0.55 m/s)

(d) Particle loss (V_{wind} = 1.1 m/s)

Fig. 3-4. Measured efficiency and inside particle loss of a RespiCon sampler.
(a) and (b) : measured efficiency.
Circle symbols : inhalable; square symbols : thoracic; triangle symbols : respirable.
(c) and (d) : inside particle loss. Triangle symbols : loss on second stage.
Note : the 1.6 micrometer test aerosol was not of a uniform size and those data points need a correction factor.

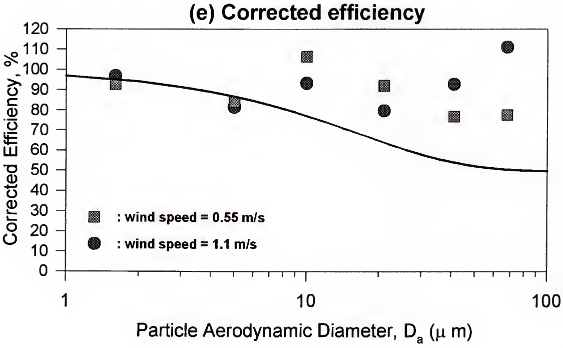

Fig. 3-4e. Corrected efficiency of a RespiCon sampler.
Solid line : inhalable convention.

and Maynard[28] shows that the average wind speed in indoor workplaces is 0.3 m/s. The test wind speed of 0.55 m/s is close to this reported average workplace wind speed. Wind speed less than 0.55 m/s was not used in this study due to the difficulty in transporting large particles at lower wind speed.

Inside particle losses of the RespiCon sampler are shown in Figs. 3-4c and 3-4d. For 5 µm particles, the RespiCon sampler has particle losses of about 18% associated with the first stage nozzle, which has a cutpoint diameter of 4 µm (particle loss at 4 µm may even be higher). Most inside losses of the 5-µm particles were found on the tip of the first receiving tube. The high particle losses on the first receiving tube could result from the low ratio value between the diameter of the first receiving tube and that of the (first) nozzle from the inlet head. According to the study of Loo and Cork[29], to minimize the inside particle losses of a virtual impactor, this diameter ratio should be between 1.35 and 1.40. The ratio for the first stage of the RespiCon is only 1.1 (3.2/2.9). These high particle losses could result in partial plugging of the receiving tube and performance change of the RespiCon sampler. Particle losses inside the inlet head and on the second nozzle are generally low.

The measured efficiencies for the respirable and the thoracic fraction are also shown in Figs. 3-4a and 3-4b. For the thoracic fraction, the performances of the RespiCon sampler match the thoracic convention very well except for the 5-µm particles. The under-sampling of the 5-µm particles probably results from the high inner particle losses. With the addition of the 5-µm particle losses to the measured thoracic efficiency, the difference between the measured value and the thoracic convention would be less than 10%.

The measured respirable efficiencies fit the respirable convention very well except for the 1.6-μm particles. Under-sampling of the 1.6-μm particles results from the non-uniformity of the test particles. The 1.6-μm test aerosol has 17% of the particles with aerodynamic diameters greater than the cutpoint diameter (4 μm) of the respirable fraction.

In the operational manual of the RespiCon sampler, a correction factor of 1.5 is applied to the inhalable fraction. When the correction factor is used, as shown in Fig. 3-4e, the corrected efficiencies are much higher than the inhalable convention for particles with aerodynamic diameters greater than 10 μm. Based on the results of this study, the 1.5 correction factor for the RespiCon sampler appears unnecessary for area sampling.

IOM sampler. The aerosol measurement efficiencies of the IOM sampler, at three wind orientations (0^0, 90^0, and 180^0) and two wind speeds (0.55 and 1.1 m/s), are shown in Figs. 3-5a and 3-5b. For 0^0 orientation (wind toward the sampler inlet), the measured efficiencies continuously increase from 100% as the particle aerodynamic diameter increases from 10 to 68 μm. For 90^0 and 180^0 orientations, the measured efficiencies continuously decrease from about 100% to nearly 0% as the particle aerodynamic diameter increases. Because the filter and the filter cassette are analyzed together in the IOM sampler, there was no separate measurement for particle loss.

For the sampling of inhalable aerosols, the IOM sampler significantly over-sampled large particles (D_a greater than 20 μm) when the wind orientation was about 0^0 and under-sampled large particles when the wind orientation was 90^0 and 180^0, as shown in Figs. 3-5a and 3-5b. As the particle diameter increases, the difference between the inhalable convention and the measured efficiency of the IOM sampler increases. Because the wind

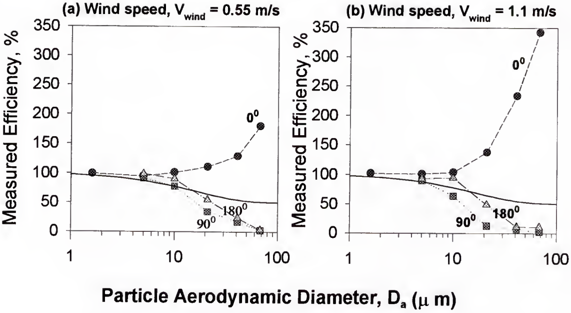

Fig. 3-5. Measured efficiency of an IOM sampler at three different wind orientations. Solid line : inhalable convention.
(a) Wind speed = 0.55 m/s; (b) wind speed = 1.1 m/s.

condition inside the indoor working environment varies, the IOM sampler would not normally have an appropriate sampling efficiency for the inhalable aerosols when it is used as an area sampler.

7-hole sampler. The measured efficiencies, as shown in Figs. 3-6a and 3-6b, are similar to those of the IOM sampler except for the test condition of 0.55 m/s wind speed and 0^0 wind orientation, which has measured efficiencies gradually decreasing from 100% as the particle diameter increases. This measured efficiency decrease resulted mainly from the particle loss increase, as shown in Fig. 3-6c. As will be discussed in the following section, when large particles were collected onto the filter, some particles bounced off. Although the inlet efficiency increased as the particle diameter increased, particle bounce resulted in a measured efficiency decrease (based on particle mass on the filter only) and a measured particle loss increase.

Similar to the IOM sampling performance, the 7-hole sampler over-sampled the large inhalable particles ($D_a > 20$ μm) when the wind orientation was about 0^0 and under-sampled the large inhalable particles when the wind orientation was 90^0 and 180^0. The inside particle losses, as shown in Figs. 3-6c and 3-6d, are nearly 0% for 90^0 and 180^0 orientations. For 0^0 orientation, the inside losses increase as the particle diameter increases.

Closed-face 37-mm cassette. Generally, the measured efficiencies (based on particle mass on the filter only), as shown in Figs. 3-7a and 3-7b, decrease from 100% as the particle diameter increases for all test wind conditions. For the sampling of particles with D_a greater than 30 μm, the closed-face 37-mm cassette has a measured efficiency lower than the inhalable convention in all three wind directions (0^0, 90^0 and 180^0). As the particle

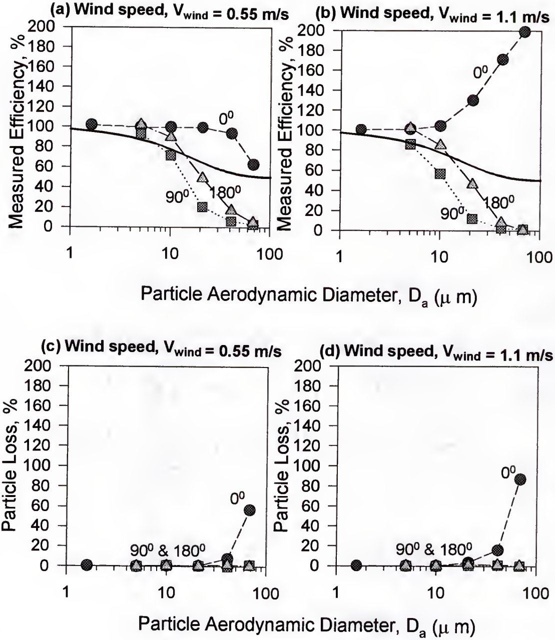

Fig. 3-6. Measured efficiency and inside particle loss of a 7-hole sampler at three different wind orientations and two wind speeds.
(a) and (b) : measured efficiency, (c) and (d) : particle loss.
Solid lines in (a) and (b) : inhalable convention.

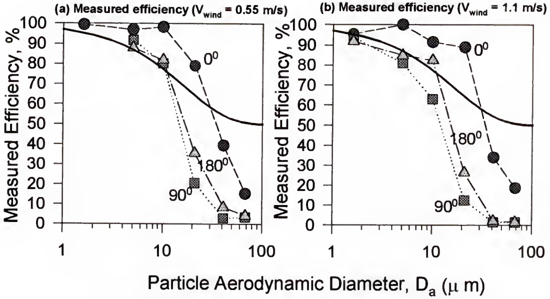

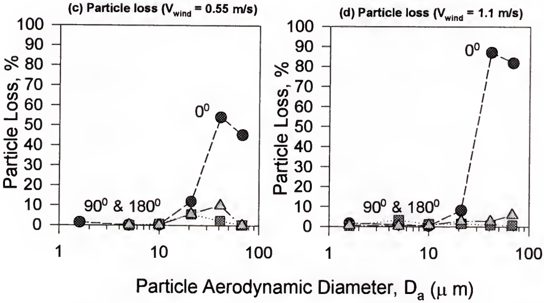

Fig. 3-7. Measured efficiency and inside particle loss of a closed- face 37-mm cassette at three different wind orientations and two wind speeds.
(a) and (b) : measured efficiency, (c) and (d) : particle loss.

Solid lines in (a) and (b) : inhalable convention.

diameter increases, the difference between the inhalable convention and the measured efficiency of the closed-face cassette increases.

The inside particle losses, as shown in Figs. 3-7c and 3-7d, are low for 90^0 and 180^0 orientations. For 0^0 orientation, the inside losses have a steep increase and reach a maximum measured value at the particle test diameter of 41 µm. At a particle test diameter of 68 µm, the losses were lower. The maximum inside loss is 87% for a wind speed of 1.1 m/s, and 54% for a wind speed of 0.55 m/s. Losses may be higher at other non-tested particle sizes.

CIS sampler. The measured efficiencies (based on particle mass on both the filter and the filter holder), as shown in Figs. 3-8a and 3-8b, decrease from 100% as the particle diameter increases for all test wind conditions. For the sampling of particles with D_a greater than about 50 µm, the CIS sampler under-sampled the inhalable aerosols for all test wind conditions. The inside particle losses on the conical inlet section, as shown in Figs. 3-8c and 3-8d, are insignificant for 90^0 and 180^0 orientations. For 0^0 orientation, the inside losses increase as the particle diameter increases.

Prototype Button sampler. For 0^0 wind orientation, the measured efficiencies (based on particle mass on the filter only), as shown in Figs. 3-9a and 3-9b, have the maximum measured value at 41 µm. When the particle diameters are less than 10 µm, the measured efficiencies are fairly stable (from 87% to 98%). When the tested particle diameter increases from 41 to 68 µm, the measured efficiencies decrease. The low measured efficiency for the 21 µm particles at 0.55 m/s wind speed could result from experimental errors.

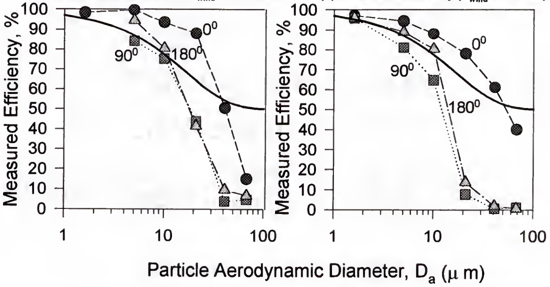

(a) Measured efficiency (V_{wind} = 0.55 m/s)

(b) Measured efficiency (V_{wind} = 1.1 m/s)

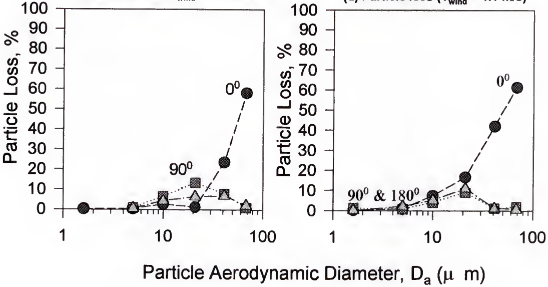

(c) Particle loss (V_{wind} = 0.55 m/s)

(d) Particle loss (V_{wind} = 1.1 m/s)

Fig. 3-8. Measured efficiency and inside particle loss of a CIS sampler at three different wind orientations and two wind speeds.
(a) and (b) : measured efficiency, (c) and (d) : particle loss.
Solid lines in (a) and (b) : inhalable convention.

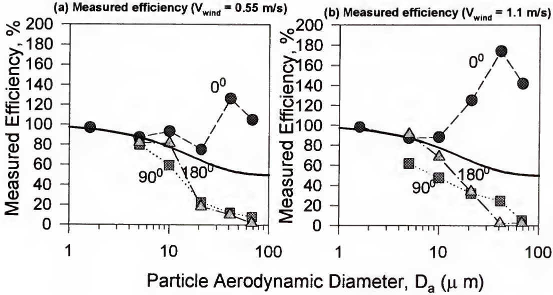
(a) Measured efficiency (V_{wind} = 0.55 m/s)

(b) Measured efficiency (V_{wind} = 1.1 m/s)

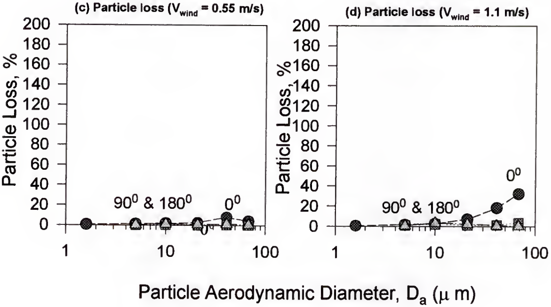
(c) Particle loss (V_{wind} = 0.55 m/s)

(d) Particle loss (V_{wind} = 1.1 m/s)

Fig. 3-9. Measured efficiency and inside particle loss of a Prototype Button sampler at three different wind orientations and two wind speeds.
(a) and (b) : measured efficiency, (c) and (d) : particle loss.

Solid lines in (a) and (b) : inhalable convention.

For 90^0 and 180^0 orientations, the measured efficiencies decrease from about 80% to nearly 0% as the particle diameter increases from 1.6 to 68 µm. Similar to the IOM and the 7-hole sampler, the Prototype Button sampler over-sampled the large inhalable aerosols (D_a greater than 20 µm) when the wind direction was about 0^0 and under-sampled the large inhalable aerosols when the wind direction was greater than 90^0. The particle losses, as shown in Figs. 3-9c and 3-9d, on the front gasket are insignificant except for large particles at the test condition of 1.1 m/s wind speed, 0^0 wind orientation. The detailed lab results for each of the inhalable aerosol samplers are shown in Appendix A.

Lab Data Discussion for Inhalable Aerosol Samplers

Among the six aerosol samplers tested as area samplers at wind speeds of 0.55 and 1.1 m/s, only the RespiCon sampler has a sampling performance which reasonably matches the inhalable convention. For the other five samplers, sampling performance is highly dependent on wind direction. For example, when sampling 68 µm particles at a wind speed of 0.55 m/s, the IOM sampler has a measured efficiency of 180% for a 0^0 wind orientation and about a 3% sampling efficiency for 90^0 and 180^0 wind orientations. Generally, for a given particle diameter, the measured efficiency at 0^0 resulted in the highest value, and the measured efficiency at 180^0 was generally somewhat greater than that at 90^0. In the workplace, the wind condition varies. When a sampler is used as an area sampler in the workplace, its position is fixed. This could result in an over-sampling or an under-sampling of the workplace aerosols depending on sampler inlet orientation relative to the air movement. For large particles ($D_a > 50$ µm) in moderate air velocity (~ 1 m/s), concentration measurements could vary by a factor of 2 to 10 because of sampler orientation to the wind direction.

In this study, it was found that the closed-face 37-mm cassette, CIS sampler, and 7-hole sampler had high inside particle losses for large particles. To obtain some insight into this problem, only the central area (~ 20 mm) of the 37-mm filters in the closed-face cassette and the CIS sampler were coated with Vaseline to collect and prevent bouncing off the 41-μm particles at the test condition of 1.1 m/s wind speed, 0^0 wind orientation. With the greased filters, the inside particle losses of the 37-mm cassette decreased from 87% to 1% and the inside losses of the CIS sampler decreased from 42% to 15%. This means that most of the large, solid particles entering the closed-face 37-mm cassette hit the filter and bounce off, which results in the low measured efficiency. High inner particle losses of the closed-face 37-mm cassette were also found by Moore et al.[30] in the wood-dust sampling. For the CIS sampler, about two-thirds of the inside large-particle losses are due to the particle bounce-off and one-third of the losses are due to gravity settling. Therefore, when these three samplers were used as personal or area samplers, their sampling performances (based on particle mass on the filter) will depend on the stickiness of the sampled particles. For example, for the same particle diameter, the measured efficiency of solid particles will be less than that of liquid particles (approximately equal to the measured efficiency plus measured particle loss for the solid particles).

To have a better understanding of the sampler inlet performances (noted as the inlet efficiency), a plot of the measured efficiency plus the inside loss of four aerosol samplers operating at 0^0 wind orientation are shown in Figs. 3-10a and 3-10b. Generally, at 0^0 wind orientation, the inlet efficiency increases with the velocity ratio R ($R = V_{wind} / V_i$ where V_{wind} = wind velocity, V_i = inlet velocity). When R is greater than one, the inlet efficiency increases from 100% as the particle diameter increases; on the other hand, when R is less than one, the inlet efficiency decreases from 100% as the particle diameter increases. When R is close to 1, as shown in the CIS curve of Fig. 3-10b, the inlet efficiency is almost constant at 100%. However, for large particles, the inlet efficiency of the closed-face 37-mm cassette is slightly greater than 100% even though R is less than 1. That could result from the re-entrainment or bounce of large particles from the outside surfaces of the closed-face cassette. Theoretically, for particles of infinite inertia, the inlet efficiency will asymptotically approach the R value. For example, at wind speed of 0.55 m/s, the IOM sampler has the R value of 2.9; therefore, the maximum inlet efficiency of the IOM could be 290% for very large particles. For 90^0 and 180^0 wind orientations, since the inside losses are low, the inlet efficiency will be close to the measured efficiency; the measured efficiency (~ inlet efficiency), as shown in Figs. 3-4 to 3-8, decreases as the particle diameter increases.

Inlet efficiency error bars, equal to ± one sample standard deviation (SSD), at 0^0 wind orientation are shown in Figs. 3-10a and 3-10b. Generally, the SSD values are less than 10% for particles less than 41 μm. For 68-μm particles, the SSD values are relatively high. This probably resulted from the non-uniform mixing of large particles due to the mixing plate removal and the gravity settling. To decrease the effect of gravity settling on the particle concentration uniformity, the samplers were located at the bottom half of the

(a) Wind speed, V_{wind} = 0.55 m/s

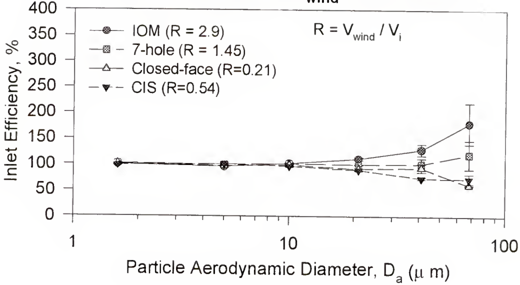

(b) Wind speed, V_{wind} = 1.1 m/s

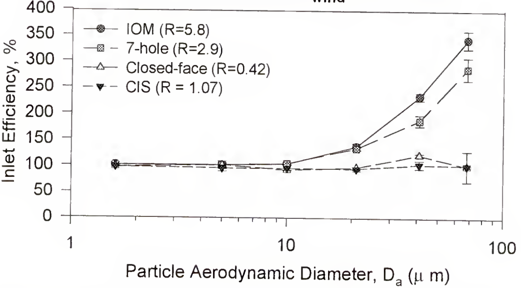

Fig. 3-10. Effects of velocity ratio, R = V_{wind} / V_i (inlet velocity), on inlet efficiency of four aerosol samplers at 0^0 wind orientation.
(a) Wind speed = 0.55 m/s, (b) wind speed = 1.1 m/s.
Note : error bars shown equal to plus-minus one (sample) standard deviation.

wind tunnel for the 68-µm particle testing. The SSD values for other samplers and wind orientations are similar to those of Figs 3-10a and 3-10b. Two to six replica tests were run at every data point. Errors due to the background (fluorocein) particles, particle recovery, uniformity of particle size, and sampling flow rate variations were found to be insignificant. Measurement variability was probably due to aerosol concentration variability.

To further understand the effect of wind orientation on the inlet efficiency, an IOM sampler was tested at 30^0 intervals from 0^0 to 180^0 using monodisperse, solid particles of 21 µm at wind speed of 1.1 m/s. As shown in Fig. 3-11, the inlet efficiency (based on particle mass on both the filter and the filter cassette) continuously decreases from 0^0 to 90^0 and stays fairly constant from 90^0 to 120^0. From 120^0 to 180^0, the inlet efficiency slowly and continuously increases. As the sampler is rotated from 0^0 to 90^0, the effective inlet area continuously decreases, which decreases the inlet efficiency. When the sampler is further rotated from 90^0 to 180^0, at a certain angle greater than 120^0, the sampler body will induce a particle-trapping turbulence around the sampler inlet, which results in the inlet efficiency increase.

Wood-Dust Size Distribution and Impactor Inlet Efficiency

Field Results for Wood-Dust Size Distribution

Cascade impactors are used to measure particle size distributions for the understanding of human health effects and for the development of particle control techniques.[31] To obtain an accurate particle size distribution, the aerosol sampled by the impactor should be the same as that present in the environment. Although most cascade

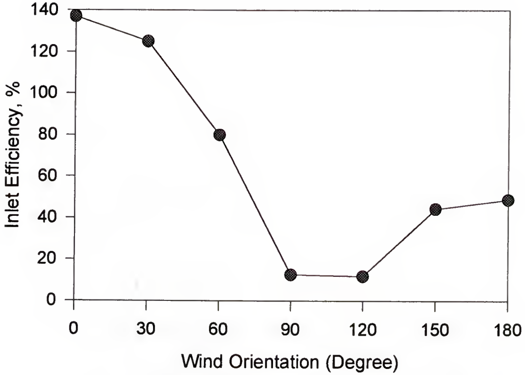

Fig. 3-11. Effect of wind orientation on inlet efficiency of an IOM sampler. Wind speed = 1.1 m/s, particle aerodynamic diameter = 21 micrometer.

impactors have similar particle separation characteristics, they may have significantly different inlet efficiencies due to different inlet geometries. Different inlet efficiencies would result in different measured particle size distributions.

Typical side-by-side particle size distribution measurements in the woodworking industry using a UW impactor and a Marple impactor are shown in Figs. 3-12a to 3-12d. As shown in Figs. 3-12a and 3-12b, particles in the woodworking industry appear to have a bimodal size distribution. The coarse mode is for the particles with aerodynamic diameter (D_a) greater than about 1 μm, and the fine mode is for the particles with D_a less than about 1 μm. After the field measurements, it was observed that particles depositing on the impactor stages with D_{50} greater than 1 μm have a light brown color, while those particles on the impactor stages with D_{50} less than 1 μm and on the after-filter have a dark black color. It assumes that most "wood" particles have their aerodynamic diameters greater than 1 μm.

The cumulative plots for wood particles only ($D_a > 1$ μm) are shown in Figs. 3-12c and 3-12d. The wood particles appear to have a log-normal size distribution. The mass median aerodynamic diameter (MMAD) and the geometric standard deviation (GSD) measured using the UW impactor (Fig. 3-12c) are 110 μm and 4.2, respectively. The MMAD and the GSD are defined as the following :

$$\mathrm{MMAD} = d_{50\%} \qquad (3\text{-}1)$$

$$GSD=\frac{d_{84\%}}{d_{50\%}}=\frac{d_{50\%}}{d_{16\%}} \qquad (3\text{-}2)$$

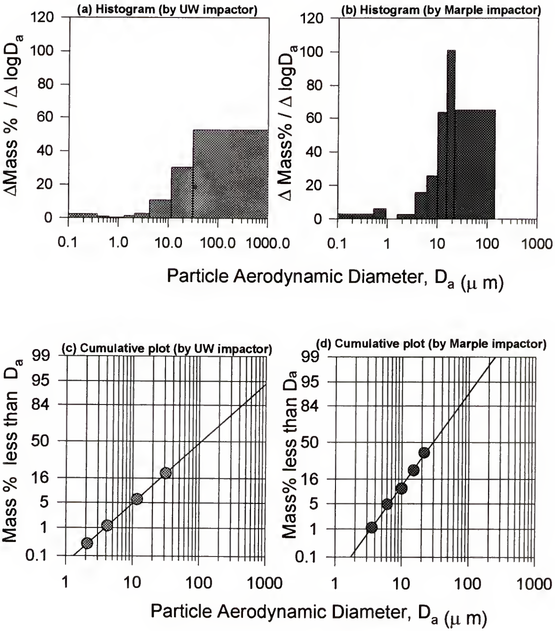

Fig. 3-12. Particle size distributions measured using a University of Washington impactor and a Marple Personal Cascade impactor at the trimming area of a particle-board mill.

(a) and (b) : histogram for all measured particles.

(c) and (d) : cumulative plot for wood particles only (D_a > 1 μ m) where

$d_{16\%}$, $d_{50\%}$, $d_{84\%}$= particle aerodynamic diameter corresponding to 16%, 50%, and 84% mass percentage in the cumulative plot, respectively.

However, the MMAD and the GSD measured using the Marple impactor (Fig. 3-12d) are 30 μm and 2.3, respectively. The coarse mode MMADs, GSDs, total mass / sampling flow rate, and wind speeds measured at other locations in the wood products mills are summarized in Table 3-5. The detailed particle size distribution plots are shown in Appendix B.

The maximum particle diameters in the histograms, Figs. 3-12a and 3-12b, were chosen as the particle diameters at the 95% mass limit on the cumulative plots, Figs. 3-12c and 3-12d. For example, the upper-limit of Fig. 3-12b is 140 μm, which corresponds to the particle diameter at 95% in Fig. 3-12d. The chosen maximum particle diameter was checked by observing the particles collected on the first impaction plate using a light microscope. The lower-limit particle diameter of 0.1 μm was arbitrarily chosen for easy plotting, which is the same as the low-limit particle diameter used by Burkhart et al.[31]

As shown in Table 3-5, the GSD values measured by the UW impactor are greater than those measured by the Marple impactor. For large particles (e.g. MMAD ≥ 50 μm) the MMAD values measured by the UW impactor are much greater than those measured by the Marple impactor. As the MMAD value (as measured by the UW impactor) increases, the difference between the MMAD measured by these two impactors increases. For smaller particles (e.g. MMAD ≤ ~ 20 μm), the MMAD values measured by these two impactors are very close. The MMADs measured by the UW impactor vary from 6.2 μm to 250 μm and the GSDs from 2.6 to 6.3, while the MMADs measured by the Marple

Table 3-5. Measured MMADs, GSDs, Mass / Volume, and wind speeds in woodworking industry.

I.D. No.	MMAD (μm) (Coarse Mode)		GSD (Coarse Mode)		Mass / Volume (Total)		Mass / Volume for $D_a < \sim 10$ μm		Wind Speed (m/s)
	UW	Marple	UW	Marple	UW	Marple	UW	Marple	
1	46	30	4.3	2.7	1.6	1.3	0.30	0.17	0.3
2	16	17	2.8	1.8	0.72	0.80	0.30	0.22	0.3
3	6.5	6.0	3.8	3.0	0.68	0.77	0.52	0.54	< 0.2
4	120	31	5.8	2.9	1.82	0.84	0.18	0.13	< 0.2
5	250	40	6.2	3.9	3.94	1.35	0.26	0.22	0.2
6	150	40	5.0	3.1	3.09	2.74	0.21	0.42	< 0.2
7	68	22	3.8	2.8	0.87	0.85	0.11	0.23	< 0.2
8	50	19	3.8	2.7	0.82	0.83	0.18	0.25	0.3
9	250	45	6.3	2.6	5.88	4.70	0.35	0.44	< 0.2
*10	110	28	4.2	2.2	2.34	2.22	0.18	0.29	< 0.2
11	21	18	2.6	2.1	1.03	1.37	0.35	0.34	< 0.2
12	160	30	5.0	2.1	3.47	1.49	0.27	0.19	< 0.2
Avg.	104	27	4.5	2.7	2.19	1.60	0.27	0.29	---

* For Marple impactor, average value of two simultaneous measurements shown in Table 3-6 was used.

impactor vary from 6.4 µm to 45 µm and the GSDs from 1.8 to 3.8.

Table 3-5 also shows a particle concentration measurement, calculated from the ratio of total collected particle mass and sampled volume, for the Marple impactor and the UW impactor. Generally, when the measured MMAD (using the UW impactor data) was less than 100 µm, the relative concentrations calculated for these two impactors were similar. However, when the measured MMAD from the UW impactor was greater than 200 µm, the particle concentration obtained using the UW impactor could be up to three times as high as that obtained from the Marple impactor. For particles with D_a less than about 10 µm, the average concentration measurements from these two impactors are almost the same. The cutpoint diameters used for the UW impactor and the Marple impactor comparison were 11.6 µm and 9.8 µm, respectively.

Table 3-6 shows a side-by-side measurement comparison between two Marple impactors and a UW impactor. The measured MMAD, GSD, and concentration values between these two Marple impactors were close. As expected, the measured MMAD and GSD values using the UW impactor were greater than those using the Marple impactors. However, the total concentration measurement using the UW impactor was within the two values determined by the Marple impactors. For particles with D_a less than about 10 µm, the concentration measurement using the UW impactor was less than the two measured values using the Marple impactors. This measured concentration difference could result from actual concentration difference at the sampling location or from the weighing error due to the low weight gain on the impaction stages with D_{50} less than 10 µm.

The maximum measured wind speed, shown in Table 3-5, is 0.3 m/s. These results

Table 3-6. Side-by-side measurement comparison of two Marple impactors (with a visor) and one University of Washington (UW) impactor in the woodworking industry.

	MMAD (μm) (Coarse Mode)	GSD (Coarse Mode)	Mass / Volume (Total)	Mass / Volume for $D_a < \sim 10$ μm
Marple-1	30	2.3	2.42	0.33
Marple-2	27	2.1	2.02	0.25
UW impactor	110	4.2	2.34	0.18

are similar to what was reported by Baldwin and Maynard.[28] They measured an average indoor workplace wind speed of 0.3 m/s with about 85% of the measured values less than 0.3 m/s.

The wood-dust size distribution measurements in this study were similar to those found in former studies. For example, Whitehead et al.[32] used a Sierra cascade impactor (Model No. : 216, Andersen Samplers Inc., Atlanta, Ga., U.S.A.), having an upward circular inlet, to measure wood-dust size distributions. They found that more than 70% of the wood-dust aerosol (by mass) had aerodynamic diameters greater than 22.5 μm. The inlet geometry and the measured wood-dust size distributions using the Sierra impactor were close to those using the UW impactor.

On the other hand, Bullock and Laird[33] used a Marple Personal Cascade (Marple) impactor (Model No. : 298), having a plate (called a visor) in front of a forward-facing cowl inlet, to measure wood-dust size distributions in two particle-board mills. They found that most of the airborne wood-dust (by mass) have their aerodynamic diameters less than 20 μm, which was close to the results found in this study using the same (Marple) impactor.

Lab Results for Impactor Inlet Efficiency Test

To further investigate the large difference of measured wood-dust size distributions, wind tunnel tests of the Marple and the UW impactor inlets were conducted using monodisperse aerosols with D_a ranging from 5 to 68 μm. The effect of impactor inlet efficiencies on the measured wood-dust size distributions are discussed. In addition to the inlet efficiency test, a simultaneous size distribution measurement using a Marple impactor, a UW impactor and a MOUDI impactor was also conducted. The objective of this test was to compare the (inner) sizing performances of the impactors. Small, polydisperse uranine aerosols were used to assure that all aerosols enter the inlets of the tested impactors.

The Marple impactor, designed specifically for personal sampling by Rubow et al.[34], has a net weight of 250 grams and an overall height of 86 mm. The UW impactor, designed specifically for stack sampling, has a net weight of 2670 grams and a body height of 170 mm plus 50 mm inlet tube. In this study, both impactors were used as area samplers due to the availability.

The inlet efficiency, or sum of the first-stage outlet efficiency and particle losses (on both the cowl inlet and the first-stage surfaces), of the Marple impactor (with a visor) at wind speed of 0.55 m/s and wind directions (θ) of 0^0, 90^0, and 180^0 as a function of particle size is shown in Figs. 3-13a to 3-13c. Generally, the inlet efficiency (solid line) decreases as the particle aerodynamic diameter (D_a) increases. When D_a is less than 5 µm, the inlet efficiency is near 100%. When D_a is equal to 68 µm, the inlet efficiency is less than. Particle losses on both the cowl inlet and the first-stage surfaces were insignificant. The maximum measured loss is 12% when $D_a = 21$ µm and $\theta = 180^0$.

The inlet efficiency of the Marple impactor (with a visor) at wind speed of 1.1 m/s and wind directions (θ) of 0^0, 90^0, and 180^0 is shown in Figs. 3-14a to 3-14c. Similarly, the inlet efficiency (solid line) decreases as the particle aerodynamic diameter (D_a) increases. When D_a is less than 5 µm, the inlet efficiency is near 100%. For large particles (D_a greater than 40 µm), at $\theta = 90^0$, the inlet efficiency at 1.1 m/s wind speed is greater

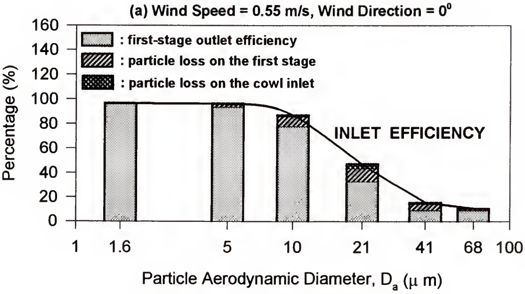

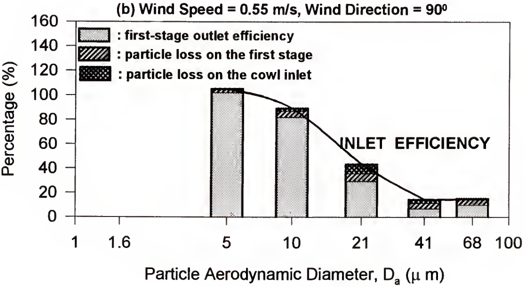

Fig. 3-13. Inlet efficiency and particle loss on both the first stage and the cowl inlet of a Marple Personal Cascade impactor **(with a visor)** at a wind speed of 0.55 m/s and wind directions of (a) 0^0 and (b) 90^0.

Note : Sum of the first-stage outlet efficiency and the loss on both the first stage and the cowl inlet are equal to the inlet efficiency.

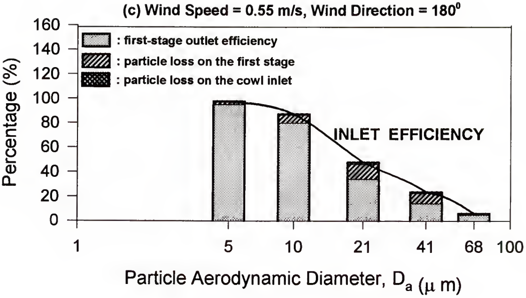

Fig. 3-13c. Inlet efficiency and particle loss on both the first stage and the cowl inlet of a Marple Personal Cascade impactor **(with a visor)** at a wind speed of 0.55 m/s and a wind direction of 180^0.

Note : Sum of the first-stage outlet efficiency and the loss on both the cowl inlet and the first stage are equal to the inlet efficiency.

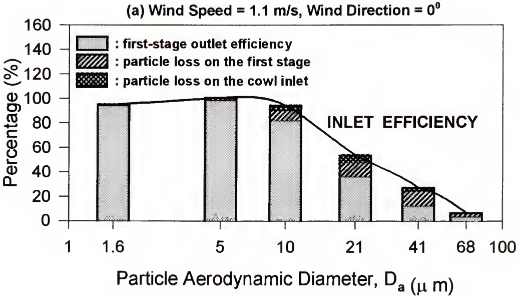

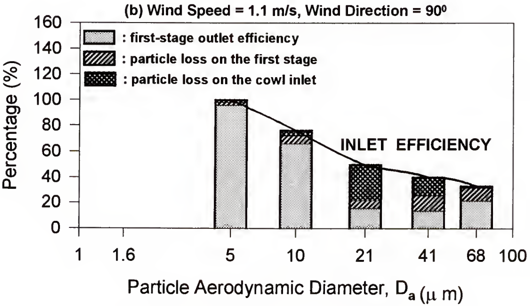

Fig. 3-14. Inlet efficiency and particle loss on both the first stage and the cow inlet of a Marple Personal Cascade impactor **(with a visor)** at a wind speed of 1.1 m/s and wind directions of (a) 0^0 and (b) 90^0.

Note : Sum of the first-stage outlet efficiency and the loss on both the first stage and the cowl inlet are equal to the inlet efficiency

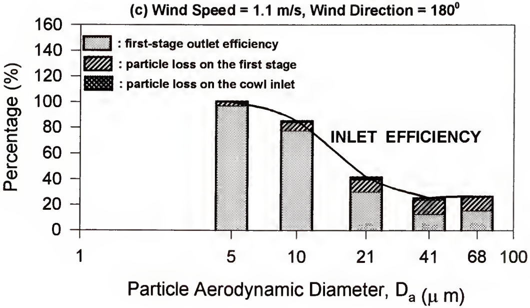

Fig. 3-14c. Inlet efficiency and particle loss on both the first stage and the cowl inlet of a Marple Personal Cascade impactor **(with a visor)** at a wind speed of 1.1 m/s and a wind direction of 180^0.

Note : Sum of the first-stage outlet efficiency and the loss on both the first stage and the cowl inlet are equal to the inlet efficiency.

than that at 0.55 m/s wind speed. This inlet efficiency increase could result from the larger scale turbulence generated in the space between the visor and the inlet cowl when the wind speed increased.

Fig. 3-15 shows the effect of wind direction on the inlet efficiency of a Marple impactor (with a visor) at wind speed of 1.1 m/s and particle diameter of 68 µm. At wind directions of 0^0, 90^0, and 180^0, the inlet efficiency is less than 33%. But at wind directions of 45^0 and 135^0, the inlet efficiency greatly increases to more than 100%. It was found that at 45^0 wind direction, some particles were able to directly enter the cowl inlet without being blocked by the visor, which resulted in the higher inlet efficiency. At wind direction of 135^0, the wind directly moved toward the inner surface of the visor and a turbulence could be generated at the space between the visor and the cowl inlet, which would increase the inlet efficiency. When the visor was removed, the inlet efficiency at 135^0 wind direction decreased to 5.5%. Particle losses at wind directions of 45^0 and 135^0 also greatly increased, which was due to the increase of the inlet efficiency.

In the Marple impactor operational manual, a correction factor for each particle diameter was applied to account for the difference between the effectiveness and 100% efficiency. The effectiveness was defined as the difference between the inlet efficiency and the overall inside particle losses.[34] For example, the correction factor is 1.92 for the first impaction stage ($D_{50} = 21.3$ µm) and approximate 1.0 for the impactor stages with D_{50} less than 1 µm. This correction factor was obtained when the Marple impactor was tested in a calm air condition. Data from this study (Fig. 3-15) show that the effectiveness also depends on the wind direction and speed.

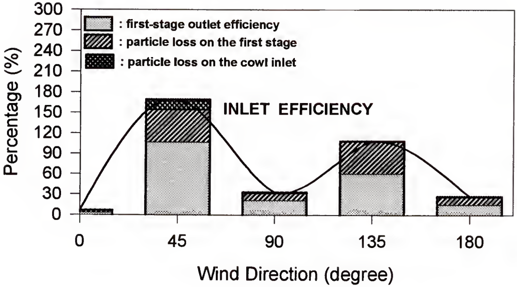

Fig. 3-15. Effect of wind direction on the inlet efficiency of a Marple Personal Cascade impactor **(with a visor)** at a wind speed of 1.1 m/s and particle aerodynamic diameter of 68 μm.

Note : Sum of the first-stage outlet efficiency and the loss on both the first stage and the cowl inlet are equal to the inlet efficiency.

To further understand the effect of the visor on the particle inlet efficiency, a Marple impactor without a visor was tested in the wind tunnel at wind speeds of 0.55 and 1.1 m/s and the results are shown in Figs. 3-16 and 3-17. At 0^0 wind direction, for both wind speeds, the inlet efficiency increases from 100% as the particle diameter increases. While at 90^0 and 180^0 wind directions, the inlet efficiency decreases from 100% as the particle diameter increases. At wind speed of 1.1 m/s, for the 68-µm particles, the inlet efficiency is 750% at 0^0 and about 15% at 90^0 and 180^0. Particle losses (without a visor) on the first-stage surfaces, at 0^0 wind direction, increase as the particle diameter increases. At 90^0 and 180^0, the losses are negligible. Particle losses on the cowl inlet are insignificant.

The inlet efficiencies for the 20-mm diameter vertical tube, with a sampling flow rate of 15 l/min, are shown in Fig. 3-18a. At both wind speeds ($V_{wind} = 0.55$ and 1.1 m/s), the inlet efficiencies decrease from 100% as the particle diameter increases. For the same particle diameter, the inlet efficiency at wind speed of 0.55 m/s is greater than that at wind speed of 1.1 m/s as would be expected from theory. The detailed results for impactor inlet efficiencies are shown in Appendix C.

Inlet efficiency at lower wind speed (~ 0.2 m/s) was not measured because of the difficulty in transporting and uniformly mixing large particles ($D_a > 50$ µm) in the wind tunnel. In an attempt to predict the inlet efficiency at lower wind speed, the inlet efficiency is plotted vs. $[(Stk)R]^{1/2}$ in Fig. 3-18b. The Stk and the R values are defined as :

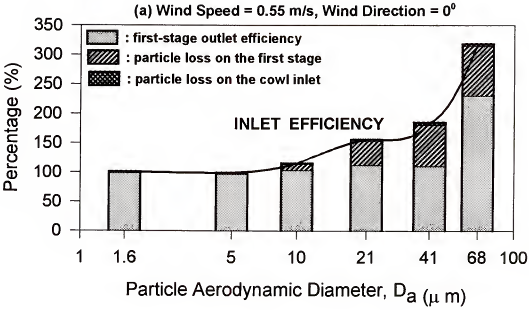

(a) Wind Speed = 0.55 m/s, Wind Direction = 0°

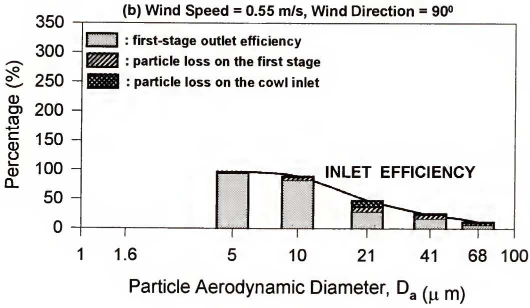

(b) Wind Speed = 0.55 m/s, Wind Direction = 90°

Fig. 3-16. Inlet efficiency and particle loss on both the cowl inlet and the first stage of a Marple Personal Cascade impacor **(without a visor)** at a wind speed of 0.55 m/s and wind directions of (a) 0^0 and (b) 90^0.

Note : Sum of the first-stage outlet efficiency and the loss on both the cowl inlet and the first stage are equal to the inlet efficiency.

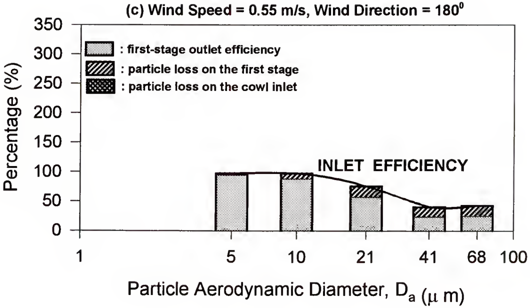

Fig. 3-16c. Inlet efficiency and particle loss on both the first stage and the cowl inlet of a Marple Personal Cascade impactor **(without a visor)** at a wind speed of 0.55 m/s and a wind direction of 180^0.

Note : Sum of the first-stage outlet efficiency and the loss on both the first stage and the cowl inlet are equal to the inlet efficiency.

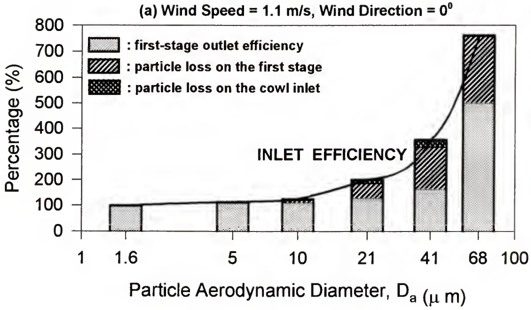

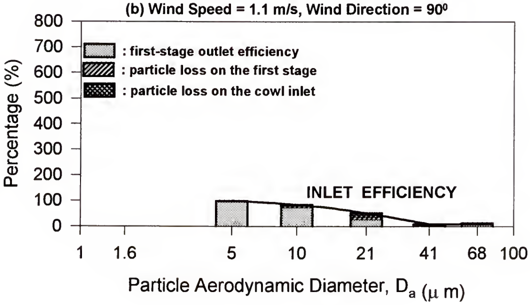

Fig. 3-17. Inlet efficiency and particle loss on both the first stage and the cowl inlet of a Marple Personal Cascade impactor **(without a visor)** at a wind speed of 1.1 m/s and wind directions of (a) 0^0 and (b) 90^0.

Note : Sum of the first-stage outlet efficiency and the loss on both the first stage and the cowl inlet are equal to the inlet efficiency.

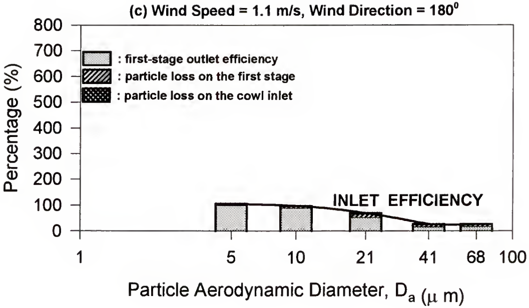

Fig. 3-17c. Inlet efficiency and particle loss on both the first stage and the cowl inlet of a Marple Personal Cascade impactor **(without a visor)** at a wind speed of 1.1 m/s and a wind direction of 180^0.

Note : Sum of the first-stage outlet efficiency and the loss on both the first stage and the cowl inlet are equal to the inlet efficiency.

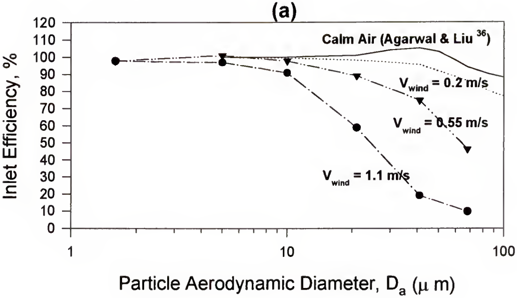

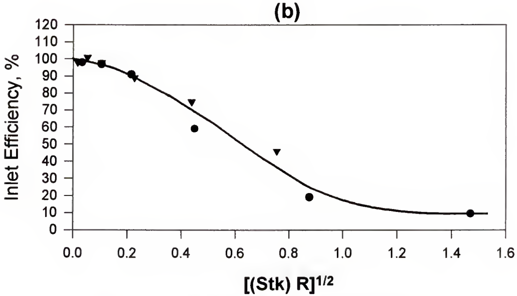

Fig. 3-18. Inlet efficiency of an upward circular tube.
(a) measured and calculated inlet efficiencies
(b) inlet efficiency vs. $[(Stk)\ R]^{1/2}$.
Tube inside diameter = 20 mm, outside diameter = 27 mm, sampling flow rate = 15 l/min.

$$Stk = \frac{D_a^2 V_{wind}\, \rho_w\, C}{9\eta D_i} \tag{3-3}$$

$$R = \frac{V_{wind}}{V_i} \tag{3-4}$$

Where

D_a = particle aerodynamic diameter

C = Cunningham correction factor

V_{wind} = wind speed

ρ_w = density of water

η = air viscosity

V_i = inlet velocity

To predict the inlet efficiency of an upward circular tube, Okazaki et al.[35] proposed that the inlet efficiency was related to the product of Stk and $R^{1/2}$. Experimental data in this study suggested that using $[(Stk)R]^{1/2}$ gave a better correlation for the inlet efficiency.

The calculated inlet sampling efficiency of the inlet tube at a wind speed of 0.2 m/s is shown in Fig. 3-18a as the dotted line. In addition to the Stk and the R value, the inlet efficiency may also depend on the inlet diameter (D_i) and sampling flow rate (Q_i). The effects of D_i and Q_i on the inlet efficiency were not investigated in this study. Therefore, the regression line in Fig. 3-18b can only be applied to an inlet geometry and sampling flow rate close to those used in this study. The inlet efficiency at calm air condition, based on the study of Agarwal and Liu[36], is shown in Fig. 3-18a as a solid line. For an upward (vertical) inlet tube , the inlet efficiency for calm air condition represents a maximum value.

Measured wind speeds in the field study were no greater than 0.3 m/s. At wind speed of 0.2 m/s, the inlet efficiency of the vertical inlet tube could be as high as 80% for 100-µm particles. While the inlet efficiency of the Marple impactor (with a visor) at low wind speed, for most wind directions, may be less than 10% for 100-µm particles. Therefore, for the measurements of large wood-dusts, the size distributions obtained using a vertical inlet tube should be more representative than using the visor inlet of the Marple impactor.

Lab Results for Impactor Sizing Performance Test

As shown in Fig. 3-19, the particle size distribution measurements using the Marple Personal Cascade impactors (with and without a visor) agree very well with those using the UW impactor and the MOUDI impactor for the mass percentage less than 99% or the particle aerodynamic diameters (D_a) less than 10 µm. The MMD and GSD of the test uranine aerosol were 1.8 µm and 2.2, respectively. These data show that the particle characterization of the Marple impactor, the UW impactor, and the MOUDI impactor are equivalent in the 1-10 µm size range. The large difference of measured wood-dust size distributions was due to the different inlet efficiencies of the Marple impactor and the UW impactor. Experimental set-up for this test is shown in Fig. 2-12.

Comparison Between the Calculated and Measured Inlet Efficiency

To predict the inlet efficiency of a thin-walled probe at 0^0 wind direction ($\theta = 0^0$), which is similar to the isokinetic probe shown in Fig. 2-14, Belyaev and Levin (1974)[37]

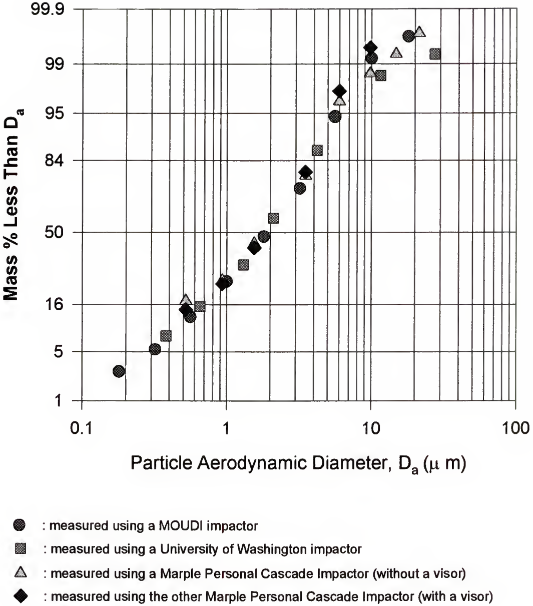

Fig. 3-19. Comparison of particle size distribution measurements using two Marple impactors with those using a MOUDI impactor and a University of Washington impactor.

developed an empirical equation :

$$A = 1 + (R-1)\beta(St, R) \qquad (3\text{-}5)$$

$$\beta(St,\ R) = 1 - \frac{1}{1 + (2 + 0.617/R)St} \qquad (3\text{-}6)$$

$$R = V_{wind} / V_i \qquad (3\text{-}7)$$

$$St = \frac{D_a^{\,2}\ V_{wind}\ C\ \rho_w}{18\mu D_i} \qquad (3\text{-}8)$$

where A : inlet efficiency

V_{wind} = wind velocity

V_i = inlet velocity

D_a = particle aerodynamic diameter

C = Cunningham correction factor

μ = air viscosity

D_i = inlet diameter

ρ_w = density of water

The inlet efficiency equation proposed by Belyaev and Levin (1974)[37] can only be applied to a thin-walled probe aerosol sampler at 0^0 wind direction. For other types of aerosol samplers, this equation would need to be modified.

To describe the inlet efficiency for most aerosol samplers at different wind directions, Vincent and his colleague [8, 38-40] developed a series of equations to be applied to both a thin-walled probe and a blunt sampler. A blunt sampler, unlike a thin-walled probe, does not have a sharp and thin-walled inlet. Most aerosol samplers are blunt samplers, such as an IOM and a 7-hole. The equations developed by Vincent and his colleague are shown below :

For $\theta < 90^0$:

$$A = A_1 A_2 \quad (3\text{-}9)$$

$$A_1 = 1 + \alpha_1[\phi^{-1/3} - 1] \quad (3\text{-}10)$$

$$A_2 = 1 + \alpha_2[(D_i / D_b\phi^{1/3})^2 - 1] \quad (3\text{-}11)$$

$$\alpha_1 = 1 - [1/(1+0.25St_1)] \quad (3\text{-}12)$$

$$\alpha_2 = 1 - [1/(1+6St_2)] \quad (3\text{-}13)$$

$$\phi = r^2 / R \quad (3\text{-}14)$$

$$St_1 = St(r)\phi^{-1/3} \quad (3\text{-}15)$$

$$St_2 = St\ \phi^{1/3} \quad (3\text{-}16)$$

$$r = D_i / D_b \quad (3\text{-}17)$$

where D_b : sampler body diameter

For $\theta = 90^0$:

$$A = 1 / [1+4(2.21St)(r / \phi)^{1/2}] \quad (3\text{-}18)$$

For $\theta = 180^0$:

$$A = 1 / [1+4(4.5St)\phi^{1/3}\ r^{-0.29}] \quad (3\text{-}19)$$

During the development of the equation for $\theta < 90^0$, Vincent and his colleague[38] incorporated the data obtained using aerosol samplers of different inlet geometries, such as a model human head, a thin-walled probe, a disc-shaped probe, and a cylindrical sampler with circular orifice. Most data points used had inlet efficiencies less than 200%. For $\theta =$

90^0 and 180^0, Vincent and his colleague[39] incorporated the data obtained using a model human head and a thin-walled probe. Most data points used had inlet efficiencies less than 100%.

In this study, the measured inlet efficiencies of six aerosol samplers were used to compare with those calculated using the equations developed by Belyaev and Levin for $\theta = 0^0$ and by Vincent and his colleague for $\theta = 0^0$, 90^0, and 180^0. These six aerosol samplers included four inhalable aerosol samplers (IOM, CIS, 7-hole, and closed-face 37-mm cassette), one Marple impactor (without a visor), and a thin-walled probe. The thin-walled probe had an inlet diameter of 6.8 mm and a sampling flow rate of 2.0 l/min. The measured inlet efficiency of the RespiCon, the Prototype Button, and the Marple impactor with a visor was not used due to their complex inlet geometries.

Belyaev and Levin. Tables 3-7a and 3-7b show the calculated and measured inlet efficiency for the thin-walled probe at wind direction, $\theta = 0^0$ and wind speed, $V_{wind} = 0.55$ and 1.1 m/s. The calculated and the measured values agree very well with the difference less than 9%. To apply these equations to a blunt sampler at $\theta = 0^0$, the inlet diameter, D_i, in Equation 3-8 was replaced by the sampler body diameter, D_b. The calculated and measured inlet efficiency for these six aerosol samplers are listed in Appendix D and plotted in Fig. 3-20.

As shown in Fig. 3-20, the calculated and measured inlet efficiencies agree quite well. The difference between the best-fitting regression line (middle dotted line) and the one-to-one ratio line (solid line) is less than 5%. The 95% confident interval lines (dotted lines) for all data points are in the range of ± 20%. The correlation coefficient, R^2_{corr}, for

Table 3-7a. Comparison between the measured inlet efficiency and the calculated one using the equations developed by Belyaev and Levin (1974) for a thin-walled probe ($D_i = 6.8$ mm, $Q_i = 2.0$ l/min).
Wind speed, V_w = 0.55 m/s, wind direction, $\theta = 0^0$.

D_a (µm)	68	41	21	10	5	1.6
Calculated value	69%	78%	90%	97%	99%	100%
Measured value	67%	78%	99%	97%	101%	100%

Table 3-7b. Comparison between the measured inlet efficiency and the calculated one using the equations developed by Belyaev and Levin (1974) for a thin-walled probe ($D_i = 6.8$ mm, $Q_i = 2.0$ l/min).
Wind speed, V_w = 1.1 m/s, wind direction, $\theta = 0^0$.

D_a (µm)	68	41	21	10	5	1.6
Calculated value	117%	114%	107%	102%	101%	100%
Experimental value	108%	105%	105%	102%	101%	100%

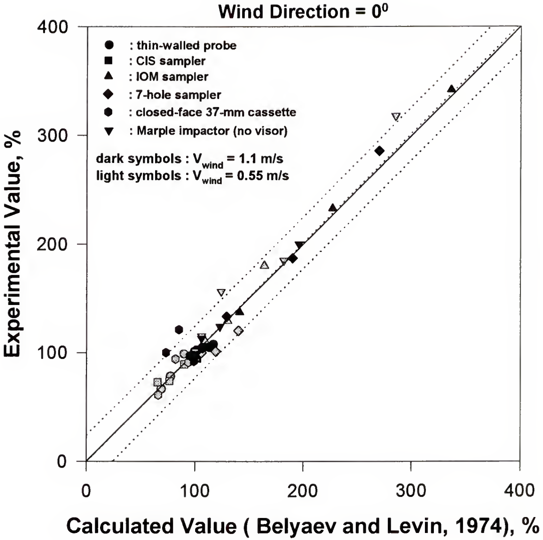

Fig. 3-20. Inlet efficiency comparison between the experimental value and calculated value using the equations developed by Belyaev and and Levin (1974) at 0^0 wind direction.
Solid line : one-to-one ratio line.
Dotted lines : regression and 95% confidence interval lines.

the regression line is equal to 0.98, which indicates that the line accounts for 98% of the data variation and a strong linear correlation for the data points. Data was not obtained at low (< 60%) efficiency values for $\theta = 0^0$. For the 7-hole sampler, an effective inlet diameter of 13 mm was chosen to represent the seven 4-mm orifices located on an indented circular surface with a diameter of 21.5 mm. The effective inlet area for this 13-mm inlet is slightly greater than the total area of those seven 4-mm orifices to account for the inlet efficiency increase due to the particle bounce-off and reentrainment occurring on the indented circular surfaces. For the Marple impactor (without a visor) shown in Fig. 2-3b, a sampler body diameter of 45 mm was chosen, which is greater than the cowl diameter of 32 mm, to account for the effect of the impactor body on the inlet efficiency.

Vincent and his Colleague. The comparison between the measured and calculated inlet efficiency, using the equations developed by Vincent and his colleague, at wind directions of 0^0, 90^0, and 180^0 and wind speeds of 0.55 and 1.1 m/s is listed in Appendix D and plotted in Figs. 3-21 to 3-23. Fig. 3-21 shows that at $\theta = 0^0$, the calculated inlet efficiency is less than the measured value. As the inlet efficiency increases above 100%, the difference between the calculated and the measured value increases. The underestimation by these equations could result from the large ratio value between the inlet diameter (D_i) and the sampler body diameter (D_b) used in this study. In developing the equations for the inlet efficiency, Vincent and his colleague used the samplers with the inlet diameter much less than the sampler body diameter. The R^2_{corr} value for the regression line is 0.96.

Fig. 3-22 shows the comparison between the measured and calculated inlet efficiency using the equations developed by Vincent and his colleague for $\theta = 90^0$. The

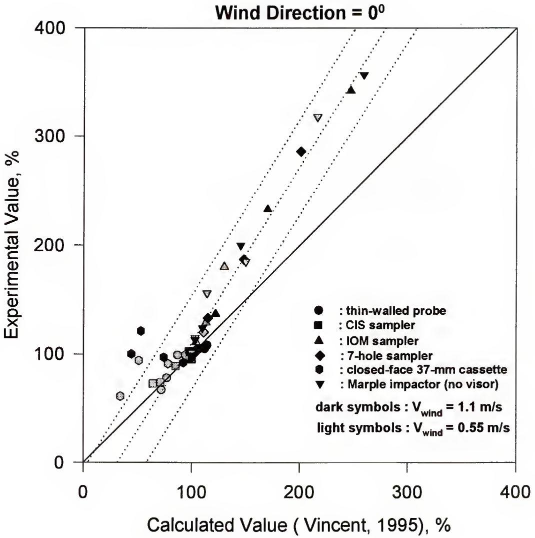

Fig. 3-21. Inlet efficiency comparison between the experimental value and calculated value using the equations developed by Vincent (1995) at 0^0 wind direction. Solid line : one-to-one ratio line.
Dotted lines : regression and 95% confidence interval lines.

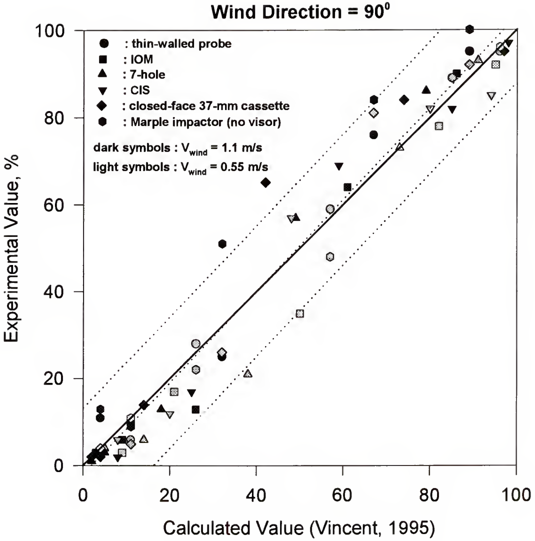

Fig. 3-22. Inlet efficiency comparison between the experimental value and calculated value using the equations developed by Vincent (1995) at 90⁰ wind direction. Solid line : one-to-one ratio line. Dotted lines : regression and 95% confidence interval lines.

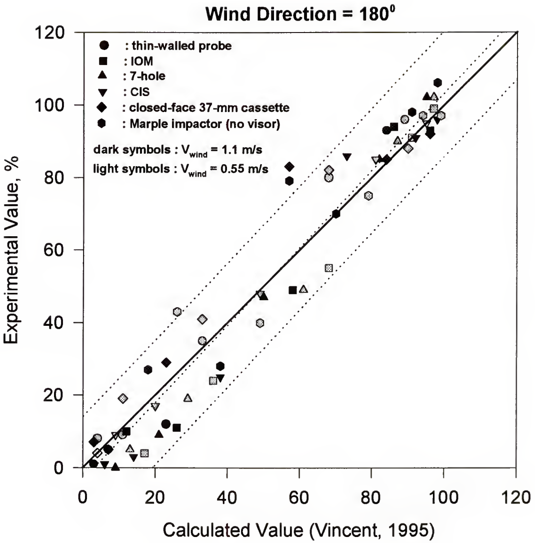

Fig. 3-23. Inlet efficiency comparison between the experimental value and calculated value using the equations developed by Vincent (1995) at 180^0 wind direction. Solid line : one-to-one ratio line. Dotted lines : regression and 95% confidence interval lines.

calculated and measured inlet efficiencies agree fairly well. The difference between the best-fitting regression line and the one-to-one ratio line is less than 5%. The R^2_{corr} value for the regression line is 0.96. The 95% confidence interval lines for all data points are in the range of ± 15%. At inlet efficiency less than 20%, this 15% variation becomes very significant.

Fig. 3-23 shows the comparison between the measured and calculated inlet efficiencies using the equations developed by Vincent and his colleague for $\theta = 180^0$. The calculated and measured inlet efficiencies agree fairly well except at low efficiency values. The difference between the best-fitting regression line and the one-to-one ratio line is less than 5%. The R^2_{corr} value for the regression line is 0.95. The 95% confidence interval lines for all data points are in the range of ± 20%.

CHAPTER 4
CONCLUSIONS

In this study, six inhalable aerosol samplers were tested (as area samplers) using monodisperse solid particles at two wind speeds and their sampling performances compared with the inhalable convention. The RespiCon sampler provided a reasonable match of the inhalable convention (if the manufacture correction factor of 1.5 is not used). However, particle losses inside the RespiCon sampler should be closely monitored (and the unit cleaned) to prevent plugging of the first receiving tube.

The area sampling performance of the IOM, 7-hole, CIS, closed-face 37-mm cassette, and the Prototype Button sampler are all highly dependent on wind orientation, wind speed, and particle size. When comparing the measured sampling efficiency with the inhalable convention, the IOM, 7-hole, and Prototype Button sampler over-sampled large particles (D_a greater than 20 μm) when the wind direction was about 0^0 and under-sampled large particles when the wind direction was 90^0 or greater. The difference between the inhalable convention and the sampler efficiency increased as the particle diameter increased for all tested wind conditions. The closed-face 37-mm cassette and the CIS sampler under-sampled large particles in all three wind directions (0^0, 90^0 , 180^0). Because the wind condition in the indoor working environment varies, if any of the inhalable aerosol samplers (except the RespiCon) is used as area samplers, the sampling performances will not normally provide a good match to the inhalable convention.

The six inhalable aerosol samplers tested can provide a reasonable measurement of aerosol concentration only if all the aerosol is less than ~ 20 μm aerodynamic diameter. The measured sampling performances of the closed-face 37-mm cassette, CIS, and 7-hole sampler, whether used as area or personal samplers, also depend on the stickiness of the sampled particles because internal losses are highly variable for the larger (20 to ~ 100 μm) particles. For fine particle sampling ($D_a < 5$ μm), aerosol type and wind orientation are relatively unimportant, for the normal workplace wind speeds, and all six samplers should perform adequately and equally (±10%).

Particle measurements from the woodworking industry indicate a bimodal particle size distribution with most of the wood-dust (by mass) in the 1 to 1000 μm size range. Measured wood-dust size distributions were highly variable with MMAD ranging from ~ 6 μm to ~ 250 μm and GSD from ~ 2.6 to ~ 6.3.

At low indoor wind speeds ($V_{wind} < 0.3$ m/s), the vertical sampling tube used with the University of Washington impactor, has an inlet efficiency near 100% for particles with D_a less than 10 μm. According to the equation developed in this study and the calculation of Agarwal and Liu[36], the inlet efficiency of a vertical tube could be as high as 80% for particles with D_a of 100 μm at wind speed less than 0.3 m/s. The vertical sampling tube is not significantly different from that used on many standard free-standing impactors, such as the MOUDI (MSP Corp., Minneapolis, MN, U.S.A.) or the Andersen (Andersen Samplers Inc., Atlanta, GA, U.S.A.) impactors. These data show that the sampler inlet bias can greatly distort size distribution measurements for particle size larger than ~ 20 μm when air velocities are greater than ~ 0.5 m/s. This bias or error could be calculated or estimated for the vertical sampling tube from detailed knowledge of the minute-by-minute air velocity and direction data (with respective to the sampler inlet). An impactor inlet sampling criteria needs to be developed to minimize size distribution measurement error for dust measurement in the work environment.

The Marple Personal Cascade (Marple) impactor fitted with the standard visor inlet, in most wind orientations, significantly undersamples particles with aerodynamic diameters greater than 20 µm. When the Marple impactor is used without the visor, the inlet efficiency highly depends on wind speed, wind direction, and particle diameters, and under some conditions may significantly over-sample large particles. An impactor can not provide a true aerosol size distribution if the aerosol entering the impaction stage is not representative of the workplace aerosol.

The comparison between the measured and the calculated inlet efficiency shows that at 0^0 wind direction, the calculated inlet efficiency using the equations developed by Belyaev and Levin (1974)[37] agrees quite well with the experimental value for both the thin-walled probe and the blunt samplers. For blunt samplers, the sampler body diameter was used to replace the inlet diameter for the calculation of the Stokes number. For multi-inlet sampler, such as a 7-hole sampler, an effective inlet diameter was used. For the Marple impactor (without a visor), an effective sampler body diameter was used.

At 0^0 wind direction, the equations developed by Vincent and his colleague underestimate the inlet efficiency when the inlet diameter is close to the sampler body diameter. However, at 90^0 and 180^0 wind directions, the calculated inlet efficiency matches the experimental value fairly well except at low efficiency values.

APPENDIX A
LABORATORY RESULTS OF SIX INHALABLE AEROSOL SAMPLERS

Table A1-1. Measured efficiency and inside loss of a RespiCon sampler.
Wind speed, V_{wind} = 0.55 m/s, sampling flow rate = 3.05 l/min.

		Respirable, %	Thoracic, %	Inhalable, %
D_a = 68 μm	Measured efficiency, %	1.6, 0.1 Avg.=0.8%	2.6, 3.5 Avg.=3%	49.6, 55.7 Avg.=52.7%
	Loss location	Inlet Head	First Nozzle	Second Nozzle
	Inside loss, %	3.5, 0.8 Avg.=2.1%	1.1, 0.0 Avg.=0.5%	0, 0 Avg.=0%
D_a = 41 μm	Measured efficiency, %	0.1, 0.0 Avg.=0.0%	0.1, 0.2 Avg.=0.1%	50.7, 51.9 Avg.=51.3%
	Loss location	Inlet Head	First Nozzle	Second Nozzle
	Inside loss, %	2.3, 1.4 Avg.=1.9%	0, 0 Avg.=0%	1.1, 0.7 Avg.=0.9%
D_a = 21 μm		Respirable, %	Thoracic, %	Inhalable, %
	Measured efficiency, %	0.0, 0.0 Avg.=0.0%	0.1, 0.6 Avg.=0.3%	58.8, 64.0 Avg.=61.4%
	Loss location	Inlet Head	First Nozzle	Second Nozzle
	Inside loss, %	0.9, 1.4 Avg.=1.1%	0.0, 0.0 Avg.=0.0%	0.0, 0.0 Avg.=0.0%
D_a = 10 μm		Respirable, %	Thoracic, %	Inhalable, %
	Measured efficiency, %	0.0, 0.7, 0.4 Avg.=0.3%	35.5, 43, 47.5 Avg.=42%	82.9, 83.5, 88.7 Avg.=85%
	Loss location	Inlet Head	First Nozzle	Second Nozzle
	Inside loss, %	1.0, 1.0, 1.0 Avg.=1.0%	0.9, 1.5, 2.1 Avg.=1.5%	0.4, 0.6, 0.7 Avg.=0.6%
D_a = 5 μm		Respirable, %	Thoracic, %	Inhalable, %
	Measured efficiency, %	32.3, 34.5 Avg. =33.4%	69.7, 70.3 Avg.=70%	78.6, 80.5 Avg.=79.6%
	Loss location	Inlet Head	First Nozzle	Second Nozzle
	Inside loss, %	1.3, 0.9 Avg.=1.1%	17.1, 16 Avg.=16.5%	0.4, 0.4 Avg.=0.4%
D_a = 1.6 μm		Respirable, %	Thoracic, %	Inhalable, %
	Measured efficiency, %	86.1, 77 Avg.=81.6%	93.7, 87 Avg.=90.4%	95.6, 88.5 Avg.=92.1%
	Loss location	Inlet Head	First Nozzle	Second Nozzle
	Inside loss, %	0.1, 0 Avg.= 0%	3.6, 4 Avg.=3.8%	0, 0.1 Avg.=0%

Table A1-2. Measured efficiency and inside loss of a RespiCon sampler.
Wind speed, V_{wind} = 1.1 m/s, sampling flow rate = 3.05 l/min.

		Respirable, %	Thoracic, %	Inhalable, %
D_a = 68 µm	Measured efficiency, %	0.7, 0.4, 0.1 Avg.=0.4%	5.4, 7.4, 2.1 Avg.=5.0%	80.6, 75.5, 71.7 Avg.=76%
	Loss location	Inlet Head	First Nozzle	Second Nozzle
	Inside loss, %	1.1, 1.0, 0.8 Avg.=1.0%	0.1, 0.1, 0.2 Avg.=0.1%	0.2, 0.2, 0.2 Avg.=0.2%
D_a = 41 µm	Measured efficiency, %	0.2, 0.1 Avg.=0.1%	1.3, 1.0 Avg.=1.1%	59.4, 65.1 Avg.=62.2%
	Loss location	Inlet Head	First Nozzle	Second Nozzle
	Inside loss, %	4.9, 7.7 Avg.=6.3%	0, 0 Avg.=0%	2.5, 3.1 Avg.= 2.8%
D_a = 21 µm		Respirable, %	Thoracic, %	Inhalable, %
	Measured efficiency, %	0.2, 0.1 Avg.=0.1%	8.4, 3.7 Avg.=6.1%	54.6, 55.8 Avg.=55.2%
	Loss location	Inlet Head	First Nozzle	Second Nozzle
	Inside loss, %	2.6, 2.8 Avg.=2.7%	0.3, 0 Avg.=0.1%	2.7, 3.4 Avg.=3.0%
D_a = 10 µm		Respirable, %	Thoracic, %	Inhalable, %
	Measured efficiency, %	0, 0 Avg.=0%	38.3, 39.3 Avg.= 38.8%	74.9, 75.4 Avg.=75.1%
	Loss location	Inlet Head	First Nozzle	Second Nozzle
	Inside loss, %	2.2, 2.0 Avg.= 2.1%	0.7, 1.1 Avg.=0.9%	0.5, 0.8 Avg.=0.6%
D_a = 5 µm		Respirable, %	Thoracic, %	Inhalable, %
	Measured efficiency, %	31.3, 35.4 Avg. =33.3%	65.2, 68.6 Avg.=66.9%	76.2, 77 Avg.=76.6%
	Loss location	Inlet Head	First Nozzle	Second Nozzle
	Inside loss, %	1.9, 2.2 Avg.=2%	22.1, 18.4 Avg.=20.3%	0.3, 0.3 Avg.=0.3%
D_a = 1.6 µm		Respirable, %	Thoracic, %	Inhalable, %
	Measured efficiency, %	80.6, 88.8 Avg.=84.7%	90.5, 99.2 Avg.=94.8%	92.1, 100 Avg.=96%
	Loss location	Inlet Head	First Nozzle	Second Nozzle
	Inside loss, %	0.3, 0.3 Avg.=0.3%	4.4, 3.7 Avg.=4.0%	0, 0 Avg.=0%

Table A2-1. Measured efficiency of an IOM sampler at three wind orientations and six particle diameters. *Wind speed, V_{wind} = 0.55 m/s*, sampling flow rate = 2.0 l/min.

	Wind direction, θ	0°	90° (forward)	180°
D_a = 68 μm	Measured efficiency, %	156, 226, 158 Avg.=180%	3.0, 3.2 Avg.=3.1%	3.2, 4.0 Avg.=3.6%
D_a = 41 μm	Measured efficiency, %	120.9, 136.9 Avg.=128.9%	15.4, 18.6 Avg.=17.0%	29.8, 17.4 Avg.=23.6%
D_a = 21 μm	Measured efficiency, %	113, 109 Avg.=111%	40.7, 28.4 Avg.=34.5%	52.8, 56.3 Avg.=54.6%
D_a = 10 μm	Measured efficiency, %	103, 99.6 Avg.=101.3%	85.8, 70.8 Avg.=78%	91.2, 97, 83.4 Avg.=90.5%
D_a = 5 μm	Measured efficiency, %	93, 96, 96, Avg.=95%	91, 94, 91 Avg.=92%	99, 95, 102 Avg.=99%
D_a = 1.6 μm	Measured efficiency, %	99, 100 Avg.=99.5%	---	---

Table A2-2. Measured efficiency of an IOM sampler at three wind orientations and six particle diameters. *Wind speed, V_{wind} = 1.1 m/sec*, sampling flow rate = 2.0 l/min.

	Wind direction, θ	0°	90° (forward)	180°
D_a = 68 μm	Measured efficiency, %	352, 322, 352 Avg.=342%	0.7, 4.3 Avg.=2.5%	9.9, 10.8 Avg.=10.4%
D_a = 41 μm	Measured efficiency, %	239, 234, 225 Avg.= 233%	8.5, 4.0 Avg.= 6%	10.4, 11.5 Avg.= 11%
D_a = 21 μm	Measured efficiency, %	133, 142 Avg.=137%	10, 15 Avg.=12.5%	46.5, 50.9 Avg.=48.7
D_a = 10 μm	Measured efficiency, %	102, 105 Avg.=103.5%	50, 73, 56, 76 Avg.=63.7%	93.7, 95 Avg.=94.3%
D_a = 5 μm	Measured efficiency, %	103, 101, 99.5, 102, 104, 96 Avg.=101%	96, 87, 88. Avg.=90%	93, 101, 90, 88. Avg.=93%
D_a = 1.6 μm	Measured efficiency, %	99, 104 Avg.=101.6%	---	---

Table A3-1. Measured efficiency and inside loss of a 7-hole sampler at three wind orientations and six particle diameters.
Wind speed, V_{wind} = 0.55 m/s, sampling flow rate = 2.0 l/min.

	Wind direction, θ	0°	90° (forward)	180°
D_a = 68 µm	Measured efficiency, %	60.8, 66.1, 61.3 Avg.=62.7%	2.3, 3.7 Avg.=3.0%	4.5, 5.6 Avg.=5.0%
	Inside loss, %	91, 32.2, 49 Avg.=57%	1.9, 1.3 Avg.=1.4%	0.2, 0.0 Avg.=0.1%
	Total efficiency, %	Avg.=119.7%	Avg.=4.4%	Avg.=5.1%
D_a = 41 µm	Measured efficiency, %	105.3, 82 Avg.=93.6%	6.9, 5.4 Avg.=6.1%	21.3, 13 Avg.=17.1%
	Inside loss, %	3.8, 11.5 Avg.=7.6%	0.1, 0.0 Avg.=0.0%	0.6, 2.2 Avg.=1.4%
	Total efficiency, %	Avg.=101.3%	Avg.=6.1%	Avg.=18.5%
D_a = 21 µm	Measured efficiency, %	99.7, 98.8 Avg.=99.3%	15, 28.8, 18.2 Avg.=20.7%	48.4, 49.4 Avg.=48.9%
	Inside loss, %	0.4, 0.6 Avg.=0.5%	---, 0.2, 0.4 Avg.=0.3%	0.2, 0.4 Avg.=0.3%
	Total efficiency, %	Avg.=99.8%	Avg.=21%	Avg.=49.2%
D_a = 10 µm	Measured efficiency, %	99, 100.2 Avg.=99.6%	71.4, 72.1 Avg.=71.7%	86.7, 92.6 Avg.=89.6%
	Inside loss, %	0.4, 0.8 Avg.=0.6%	0.8, 0.8 Avg.=0.8%	0.4, 0.4 Avg.=0.4%
	Total efficiency, %	Avg.=101.2%	Avg.=72.5%	Avg.=90%
D_a = 5 µm	Measured efficiency, %	99, 99, 101 Avg.=99.7%	90.5, 92, 96 Avg.=92.8%	103, 106, 98 Avg.=102%
	Inside loss, %	~0	~0	~0
	Total efficiency, %	Avg.=99.7%	Avg.=92.8%	Avg.=102%
D_a = 1.6 µm	Measured efficiency, %	104, 99 Avg.=101.5%	---	---
	Inside loss, %	0, 0.2 Avg.=0.1%	---	---
	Total efficiency, %	Avg.=101.6%	---	---

Table A3-2. Measured efficiency and inside loss of a 7-hole sampler at three wind orientations and six particle diameters.
Wind speed, V_{wind} = 1.1 m/s, sampling flow rate = 2.0 l/min.

	Wind direction, θ	0°	90° (forward)	180°
D_a = 68 μm	Measured efficiency, %	156, 246, 237, 159, 197, 201 Avg.=199%	2.6, 0.1 Avg.=1.3%	0.4, 0.0 Avg.=0.2%
	Inside loss, %	105, 99, 100, 78, 59, 79 Avg.=87%	0, 0 Avg.=0%	0, 0 Avg.=0%
	Total efficiency, %	Avg.=286%	Avg.=1.3%	Avg.=0.2%
D_a = 41 μm	Measured efficiency, %	183, 164, 165 Avg.= 171%	2.2, 2.6 Avg.= 2.4%	7.3, 8.4 Avg.= 7.8%
	Inside loss, %	16%	1%	1.2%
	Total efficiency, %	Avg.=187%	Avg.=3.4%	Avg.=9.0%
D_a = 21 μm	Measured efficiency, %	129, 132 Avg.=130%	8.8, 15 Avg.=12%	48.3, 44 Avg.=46.1%
	Inside loss, %	2.5, 4.2 Avg.=3.4%	0.4, 0.6 Avg.=0.5%	1, 1.6 Avg.=1.3%
	Total efficiency, %	Avg.=133.4%	Avg.=12.5%	Avg.=47.4%
D_a = 10 μm	Measured efficiency, %	103, 105.6 Avg.=104.3%	53.3, 60.4 Avg.=56.8%	84, 85.3 Avg.=84.6%
	Inside loss, %	~ 0	~ 0	~0
	Total efficiency, %	Avg.= 104.3%	Avg.= 56.8%	Avg.=84.6%
D_a = 5 μm	Measured efficiency, %	103, 104, 96, 102, 101. Avg.=101%	83, 80, 94. Avg.= 86%	102, 103, 102. Avg.=102%
	Inside loss, %	~ 0 %	~ 0 %	~ 0 %
	Total efficiency, %	Avg.=101%	Avg.= 86%	Avg.=102%
D_a = 1.6 μm	Measured efficiency, %	100, 101 Avg.=100.5%	---	---
	Inside loss, %	0.1, 0.1 Avg.=0.1%	---	---
	Total efficiency, %	Avg.=100.6%	---	---

Table A4-1. Measured efficiency and inside loss of a closed-face 37-mm cassette at three wind orientations and six particle diameters.
Wind speed, V_{wind} = 0.55 m/s, sampling flow rate = 2.0 l/min.

	Wind direction, θ	0°	90° (forward)	180°
D_a = 68 μm	Measured efficiency, %	26.2, 4.3 Avg.=15.3%	0.1, 7.0 Avg.=3.5%	3.0, 5.7 Avg.=4.3%
	Inside loss, %	33.7, 56.9 Avg.=45.3%	0.1, 0.4 Avg.=0.2%	0.1, 0.0 Avg.=0%
	Total efficiency, %	Avg.=60.6%	Avg.=3.7%	Avg.=4.3%
D_a = 41 μm	Measured efficiency, %	34.9, 44.1 Avg.=39.5%	1.9, 4.2 Avg.=3.0%	7.5, 9.6 Avg.=8.5%
	Inside loss, %	64.6, 43.8 Avg.=54.2%	1.6, 3.1 Avg.=2.3%	8.3, 11.6 Avg.=10.0%
	Total efficiency, %	Avg.=93.7%	Avg.=5.3%	Avg.=18.5%
D_a = 21 μm	Measured efficiency, %	69.7, 88.8 Avg.=79.2%	19.8, 21.6 Avg.=20.7%	38.5, 33.0 Avg.=35.7%
	Inside loss, %	20.5, 3.5 Avg.=12%	3.3, 8.0 Avg.=5.6%	5.7, 5.7 Avg.=5.7%
	Total efficiency, %	Avg.=91.2%	Avg.=26.3%	Avg.=41.4%
D_a = 10 μm	Measured efficiency, %	97, 99.7 Avg.=98.3%	77.4, 84 Avg.=80.4%	76, 88.1 Avg.=82%
	Inside loss, %	0.5, 0.0 Avg.=0.2%	1.5, 0.0 Avg.=0.7%	0.0, 0.3 Avg.=0.1%
	Total efficiency, %	Avg.=98.5%	Avg.= 81.4%	Avg.=82.1%
D_a = 5 μm	Measured efficiency, %	96, 97, 98 Avg.=97%	97, 94, 85, 93 Avg.=92%	87, 84, 92 Avg.=88%
	Inside loss, %	~0	~0	~0
	Total efficiency, %	Avg.=97%	Avg.=92%	Avg.=88%
D_a = 1.6 μm	Measured efficiency, %	100, 99 Avg.=99.5%	---	---
	Inside loss, %	1.8, 1.0 Avg.=1.4%	---	---
	Total efficiency, %	Avg.=100.9%	---	---

Table A4-2. Measured efficiency and inside loss of a closed-face 37-mm cassette at three wind orientations and six particle diameters.
Wind speed, V_{wind} = 1.1 m/s, sampling flow rate = 2.0 l/min.

	Wind direction, θ	0°	90° (forward)	180°
D_a = 68 μm	Measured efficiency, %	17.1, 20.3 Avg.=18.7%	0.5, 2.5 Avg.=1.5%	2.1, 1.0 Avg.=1.5%
	Inside loss, %	62.5, 101 Avg.=81.7%	0.9, 0.6 Avg.=0.7%	5.0, 6.7 Avg.=5.8%
	Total efficiency, %	Avg.=100%	Avg.=2.2%	Avg.=7.3%
D_a = 41 μm	Measured efficiency, %	28, 35, 39 Avg.= 34%	3.2, 0.6, 1.0 Avg.= 1.6%	2.7, 1.7 Avg.= 2.2%
	Inside loss, %	91, 85, 85 Avg.= 87%	1.9, 0.1, 0.5 Avg.= 0.8%	2.5, 2.7 Avg.= 2.6%
	Total efficiency, %	Avg.=121%	Avg.=2.4%	Avg.=4.8%
D_a = 21 μm	Measured efficiency, %	89, 91, 87 Avg.=89%	15, 11, 11.8 Avg.=12.6%	26, 26.9 Avg.=26.4%
	Inside loss, %	6.1, 7.5, 10.7 Avg.=8.1%	1.4, 1.6, 1.5 Avg.=1.5%	2.3, 3.3 Avg.=2.8%
	Total efficiency, %	Avg.=97.1%	Avg.=14.1%	Avg.=29.2%
D_a = 10 μm	Measured efficiency, %	92, 91 Avg.=91.5%	62, 64 Avg.=63%	83, 82 Avg.=82.5%
	Inside loss, %	0.0, 0.6 Avg.=0.3%	0.8, 1.5 Avg.=1.2%	1.2, 0.2 Avg.=0.7%
	Total efficiency, %	Avg.=91.8%	Avg.=64.2%	Avg.=83.2%
D_a = 5 μm	Measured efficiency, %	95, 105 Avg.=100%	87, 75 Avg.=81%	87, 83 Avg.=85%
	Inside loss, %	0.9, 1.1 Avg.=1%	3.1, 3.5 Avg.=3.3%	0.5, 0 Avg.= 0.2%
	Total efficiency, %	Avg.=101%	Avg.=84.3%	Avg.=85.2%
D_a = 1.6 μm	Measured efficiency, %	95, 96 Avg.=95.5%	95, 93.2 Avg.=94.1%	90.3, 93.5 Avg.=91.9%
	Inside loss, %	1.5, 1.8 Avg.=1.6%	0.4, 0.4 Avg.=0.4%	0.5, 0.5 Avg.=0.5%
	Total efficiency, %	Avg.=97.1%	Avg.=94.5%	Avg.=92.4%

Table A5-1. Measured efficiency and inside loss of a CIS sampler at three wind orientations and six particle diameters.
Wind speed, V_{wind} = 0.55 m/s, sampling flow rate = 3.5 l/min.

	Wind direction, θ	0°	90° (forward)	180°
D_a = 68 μm	Measured efficiency, %	16, 14.1 Avg.=15%	6.7, 2.9 Avg.=4.8%	7.5, 6.3 Avg.=6.9%
	Inside loss, %	50, 65 Avg.=58%	1.5, 0.5 Avg.=1.0%	2.1, 2.0 Avg.=2.0%
	Total efficiency, %	Avg.=73%	Avg.=5.8%	Avg.=8.9%
D_a = 41 μm	Measured efficiency, %	49.3, 51.7 Avg.=50.5%	5.1, 2.9 Avg.=4%	11.4, 8.1 Avg.=9.7%
	Inside loss, %	23.4, 23.9 Avg.=23.6%	6.5, 9.3 Avg.=7.9%	5.5, 8.3 Avg.=6.9%
	Total efficiency, %	Avg.=74.1%	Avg.=11.9%	Avg.=16.6%
D_a = 21 μm	Measured efficiency, %	89, 87, 88.4 Avg.=88.1%	43.5, 44.6 Avg.=44%	41.4, 41.9 Avg.=41.6%
	Inside loss, %	0.9, 2.1, 0.6 Avg.=1.2%	13.5, 13.3 Avg.=13.4%	6.6, 6.1 Avg.=6.3%
	Total efficiency, %	Avg.=89.3%	Avg. = 57.4%	Avg.=47.9%
D_a = 10 μm	Measured efficiency, %	92.8, 94.5 Avg.=93.6%	75.4, 75.3 Avg.=75.3%	80.3, 80.9 Avg.=80.6%
	Inside loss, %	2.7, 2.5 Avg.=2.6%	7.1, 6.0 Avg.=6.5%	4.6, 4.0 Avg.=4.3%
	Total efficiency, %	Avg.=96.2%	Avg.=81.8%	Avg.=84.9%
D_a = 5 μm	Measured efficiency, %	103, 100, 96 Avg.=99.7%	86, 89, 78, Avg.=84.3%	99.5, 91, 93 Avg.=94.6%
	Inside loss, %	0.3, 0.4, 0.4 Avg.=0.4%	0.7, 0.9, 1.0 Avg.=0.9%	0.4, 0.6, 0.9 Avg.=0.6%
	Total efficiency, %	Avg.=100.1%	Avg.=85.2%	Avg.=95.2%
D_a = 1.6 μm	Measured efficiency, %	99.7, 97 Avg.= 98.4%	---	---
	Inside loss, %	0.1, 0.3 Avg.=0.2%	---	---
	Total efficiency, %	Avg.=98.6%	---	---

Table A5-2. Measured efficiency and inside loss of a CIS sampler at three wind orientations and six particle diameters.
Wind speed, V_{wind} *= 1.1 m/s,* sampling flow rate, Q = 3.5 l/min.

	Wind direction, θ	0°	90° (forward)	180°
D_a = 68 μm	Measured efficiency, %	47.8, 32.3 Avg.=40%	1.0, 1.7 Avg.=1.3%	0.4, 1.1 Avg.=0.7%
	Inside loss, %	54.7, 68.0 Avg.=61.3%	1.3, 2.3 Avg.=1.8%	0.9, 0.4 Avg.=0.6%
	Total efficiency, %	Avg.=101.3%	Avg.=3.1%	Avg.=1.3%
D_a = 41 μm	Measured efficiency, %	56, 75, 51 Avg.= 61%	0.3, 0.9, 0.9 Avg.= 0.7%	1.9, 1.9 Avg.= 1.9%
	Inside loss, %	54, 30, 43 Avg.= 42%	1.3, 1.1, 1.0 Avg.= 1.1%	0.9, 1.3 Avg.= 1.1%
	Total efficiency, %	Avg.=103%	Avg.=1.8%	Avg.=3.0%
D_a = 21 μm	Measured efficiency, %	79, 77 Avg.=78%	7.3, 8.4 Avg.=7.8%	13.8, 13.7 Avg.=13.7%
	Inside loss, %	18.1, 15.1 Avg.=16.6%	8.6, 9.5 Avg.=9%	10.3, 11.7 Avg.=11%
	Total efficiency, %	Avg.=94.6%	Avg.=16.9%	Avg.=24.8%
D_a = 10 μm	Measured efficiency, %	89.4, 86.8 Avg.=88.1%	63; 66.4, 64.8 Avg.=64.7%	78, 82.8 Avg.=80.4%
	Inside loss, %	5.9, 8.7 Avg.=7.3%	5, 3.7, 3.6 Avg.=4.1%	4.6, 5.7 Avg.= 5.1%
	Total efficiency, %	Avg.=95.4%	Avg.=68.8%	Avg.=85.5%
D_a = 5 μm	Measured efficiency, %	95, 98, 97, 88 Avg.=94.5%	80, 83, 80.7 Avg.= 81.2%	94, 93, 83, 86 Avg.=89%
	Inside loss, %	0.7, 0.6, 1.4, 0.5 Avg.=0.8%	0.6, 0.3, 1.3, Avg.=0.7%	0.5, 0.7, 0.8, 5.9 Avg=2%
	Total efficiency, %	Avg.=95.3%	Avg.=82%	Avg.=91%
D_a = 1.6 μm	Measured efficiency, %	97.7, 96.6 Avg.=97.2%	96.2, 95.5 Avg.=95.9%	95.4, 96.3 Avg.=95.9%
	Inside loss, %	0, 0 Avg.=0%	1.2, 1.2 Avg.=1.2%	0, 0 Avg.=0%
	Total efficiency, %	Avg.=97.2%	Avg.=97.1%	Avg.=95.9%

Table A6-1. Measured efficiency and inside loss of a Prototype Button Sampler at three wind orientations and six particle diameters.
Wind Speed = 0.55 m/s, sampling flow rate = 2.0 l/min.

	Wind direction, θ	0°	90° (forward)	180°
D_a = 68 µm	Measured efficiency, %	122, 88, 106 Avg.=105%	10.7, 6.0 Avg.=8.3%	2.7, 1.2 Avg.=2.0%
	Loss on gasket	11, 0.1, 0.3 Avg.=3.8%	0.4, 0.2 Avg.=0.3%	0.6, 0.2 Avg.=0.4%
	Total efficiency, %	Avg.=108.8%	Avg.=8.6%	Avg.=2.4%
D_a = 41 µm	Measured efficiency, %	117.4, 135.3 Avg.=126.3%	7.6, 17.5 Avg.=12.6%	11.3, 9.5 Avg.=10.4%
	Loss on gasket	8.9, 7.1 Avg.=8%	0.0, 0.4 Avg.=0.2%	1.6, 0.7 Avg.=1.1%
	Total efficiency, %	Avg.=134.3%	Avg.=12.8%	Avg.=11.5%
D_a = 21 µm	Measured efficiency, %	66.3, 84.3 Avg.=75.3%	19.1, 26.7 Avg.=22.9%	15.6, 21.5 Avg.=18.6%
	Loss on gasket	2.2, 2.7 Avg.=2.4%	0.1, 0.2 Avg.=0.1%	0.7, 0.6 Avg.=0.6%
	Total efficiency, %	Avg.=77.7%	Avg.=23%	Avg.=19.2%
D_a = 10 µm	Measured efficiency, %	91.7, 94.8 Avg.=93.2%	61.1, 58 Avg.=59.6%	79.3, 83.2 Avg.=81.2%
	Loss on gasket	2.2, 1.0 Avg.=1.6%	0.9, 0 Avg.=0.4%	1.6, 0.3 Avg.=1.0%
	Total efficiency, %	Avg.=94.8%	Avg.=60%	Avg.=82.2%
D_a = 5 µm	Measured efficiency, %	86, 86, 84, 85, 87, 92 Avg.=87%	80, 84, 79, 76 Avg.=80%	85.3, 77, 83, Avg.=81.8%
	Loss on gasket	0, 1, 2.9, 0.6, 0.5, 1.8 Avg.=1.1%	~ 0	0.4, 0, 0 Avg.=0.1%
	Total efficiency, %	Avg.=88%	Avg.=80%	Avg.=81.9%
D_a = 1.6 µm	Measured efficiency, %	98.3, 95 Avg.=96.6%	---	---
	Loss on gasket	0.3, 0.5 Avg.=0.4%	---	---
	Total efficiency, %	Avg.=97%	---	---

Table A6-2. Measured efficiency and inside loss of a Prototype Button Sampler at three wind orientations and six particle diameters.
Wind speed, V_{wind} = 1.1 m/s, Sampling flow rate, Q = 2.0 l/min.

	Wind direction, θ	0°	90° (forward)	180°
D_a = 68 μm	Measured efficiency, %	150, 135 Avg.=142%	7.4, 3.6 Avg.=5.5%	3.9, 1.8 Avg.=2.8%
	Loss on gasket	26.5, 37.4 Avg.=32%	3.5, 3.2 Avg.=3.3%	0.3, 0.2 Avg.=0.2%
	Total efficiency, %	Avg.=174%	Avg.=8.8%	Avg.=3.0%
D_a = 41 μm	Measured efficiency, %	166, 182, 172 Avg.= 174%	28, 22 Avg.= 25%	2.4, 2.4 Avg.=2.4%
	Loss on gasket	11.4, 22.5, 20 Avg=18%	2, 0.6 Avg.=1.3%	0.3, 0.7 Avg.=0.5%
	Total efficiency, %	Avg.=192%	26.3%	2.9%
D_a = 21 μm	Measured efficiency, %	130, 121 Avg.=125%	31.4, 33.2 Avg.=32.3%	33.6, 34.5 Avg.=34%
	Loss on gasket	7.5, 6 Avg.=6.8%	1.1, 1.2 Avg.=1.1%	2, 2.5 Avg.=2.2%
	Total efficiency, %	Avg.=132%	Avg.=33.4%	Avg.=36.2%
D_a = 10 μm	Measured efficiency, %	86, 94, 85 Avg.=88%	45.4, 50.2 Avg.=47.8	67, 69.7 Avg.=68.3%
	Loss on gasket	2.3, 3, 2 Avg.=2.4%	1.6, 2.6 Avg.=2.1%	3.0%
	Total efficiency, %	Avg.=90.4%	Avg.= 49.0%	Avg.=71.3%
D_a = 5 μm	Measured efficiency, %	86, 92, 82. Avg.=87%	60. 63.4, 56, 69. Avg.=62%	86, 96 Avg.=91%
	Loss on gasket	0, 1, 3.5. Avg.= 1.5%	1.9, 1.3, 0, 0.6 Avg.=0.9%	0, 1 Avg.=0.5%
	Total efficiency, %	Avg.=87%	Avg.=63%	Avg.=91%
D_a = 1.6 μm	Measured efficiency, %	98.5, 97.6 Avg.=98%	---	---
	Loss on gasket	0.2, 0.2 Avg.=0.2%	---	---
	Total efficiency, %	Avg.=98.2%	---	---

Table A7. Effect of wind orientation on the aspiration efficiency of an IOM sampler. Wind speed, V_{wind} = 1.1 m/sec, sampling flow rate = 2 .0 l/min, particle diameter, D_a = 21 µm.

Inlet efficiency, %	0°	30°	60°	90°
	133, 142 Avg.=137%	127, 124 Avg.=125%	89, 77, 75 Avg.= 80%	10, 15 Avg.=12.5%
	120°	150°	180°	---
	10.2, 13.3 Avg.= 11.7%	45.4, 43.3 Avg.= 44.3%	46.5, 50.9 Avg.= 48.7%	---

APPENDIX B
PARTICLE SIZE DISTRIBUTION MEASURED IN THE WOODWORKING INDUSTRY

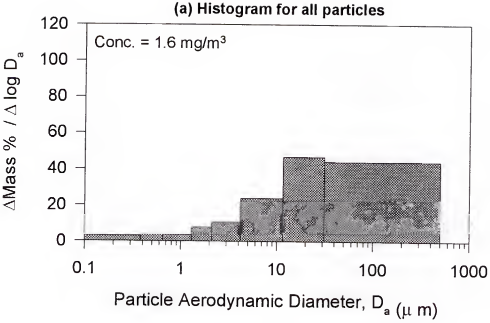
(a) Histogram for all particles

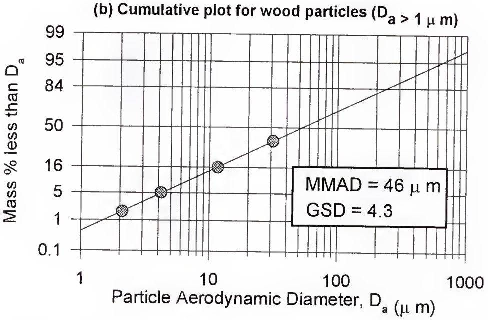
(b) Cumulative plot for wood particles ($D_a > 1\ \mu m$)

Fig. B1-1. Particle size distribution measurement using a University of Washington impactor. Wind speed = 0.3 m/s.

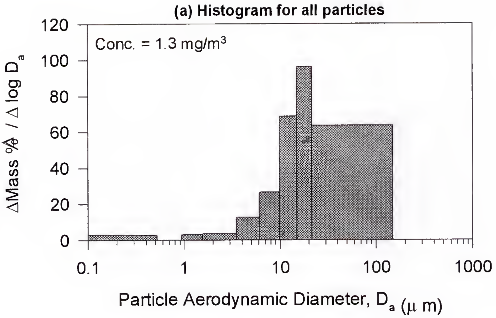

(a) Histogram for all particles

(b) Cumulative plot for wood particles (D_a > 1 μm)

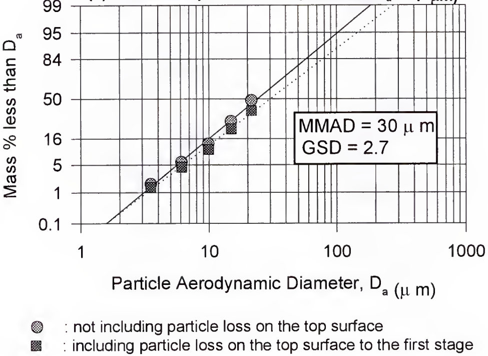

Fig. B1-2. Particle size distribution measurement using a Marple Personal Cascade impactor. Wind speed = 0.3 m/s.

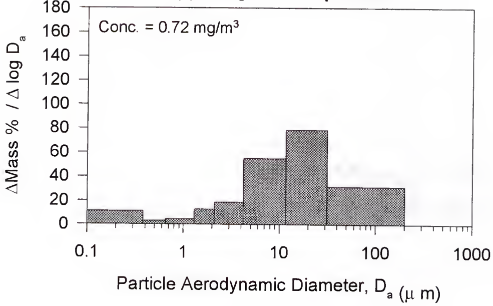

(a) Histogram for all particles

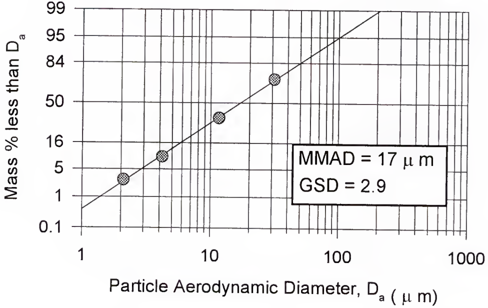

(b) Cumulative plot for wood particles ($D_a > 1\ \mu m$)

Fig. B2-1. Particle size distribution measurement using a University of Washington impactor. Wind speed = 0.3 m/s.

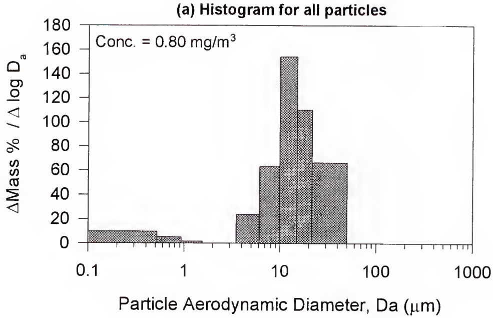
(a) Histogram for all particles

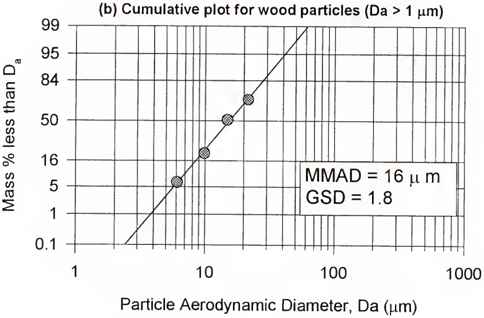
(b) Cumulative plot for wood particles (Da > 1 μm)

Fig. B2-2. Particle size distribution measurement using a Marple Personal Cascade impactor. Wind speed = 0.3 m/s.

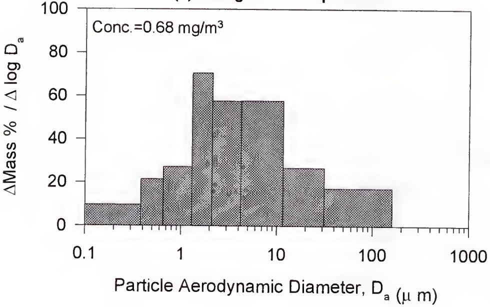
(a) Histogram for all particles

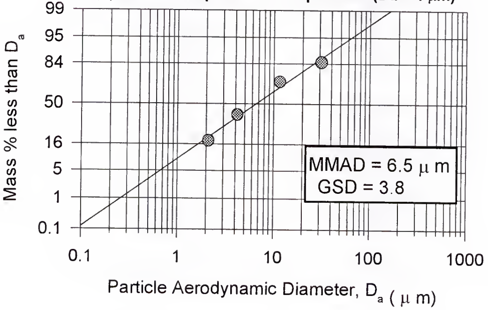
(b) Cumulative plot for wood particles (Da > 1 μm)

Fig. B3-1. Particle size distribution measurement using a University of Washington impactor. Wind speed < 0.2 m/s.

(a) Histogram for all particles

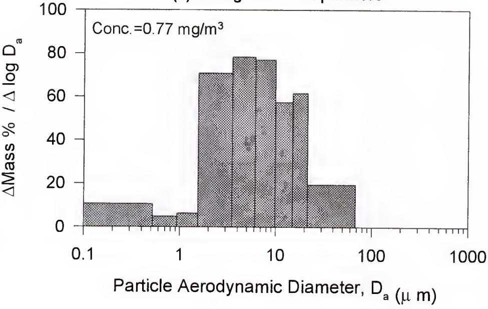

(b) Cumulative plot for wood particles ($D_a > 1$ μ m)

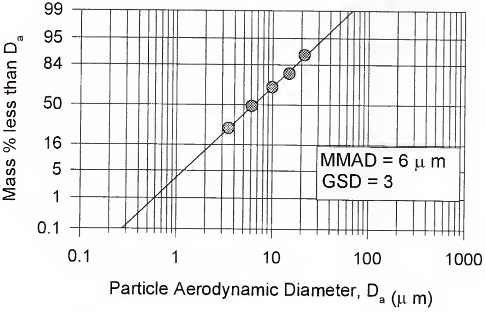

Fig. B3-2. Particle size distribution measurement using a Marple Personal Cascade impactor. Wind speed < 0.2 m/s.

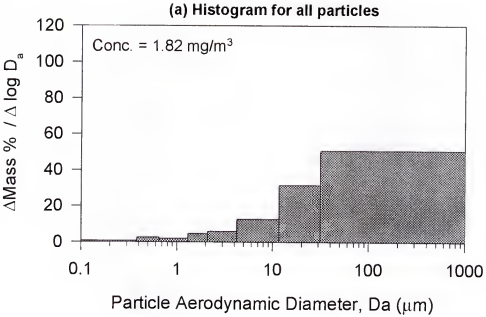

(a) Histogram for all particles

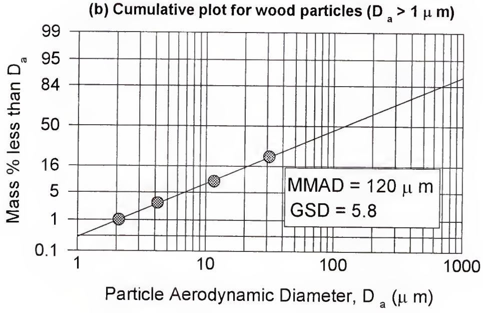

(b) Cumulative plot for wood particles ($D_a > 1\ \mu m$)

Fig. B4-1. Particle size distribution measurement using a University of Washington impactor. Wind speed < 0.2 m/s.

(a) Histogram for all particles

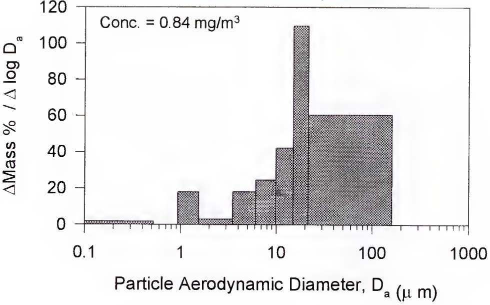

(b) Cumulative plot for wood particles (D$_a$ > 1 μ m)

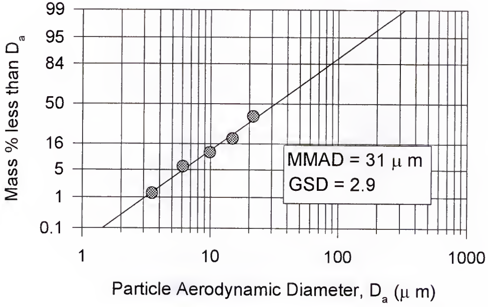

Fig. B4-2. Particle size distribution measurement using a Marple Personal Cascade impactor. Wind speed < 0.2 m/s.

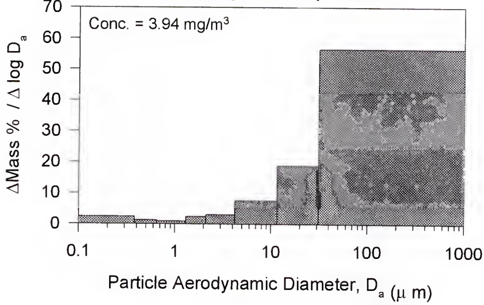

(a) Histogram for all particles

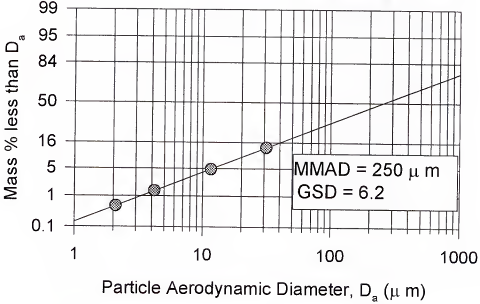

(b) Cumulative plot for wood particles ($D_a > 1$ μ m)

Fig. B5-1. Particle size distributions measured using a University of Washington impactor. Wind speed = 0.2 m/s.

(a) Histogram for all particles

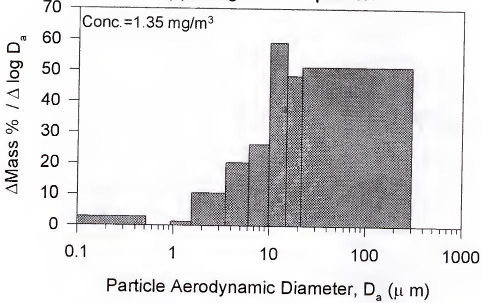

(b) Cumulative plot for wood particles ($D_a > 1$ μ m)

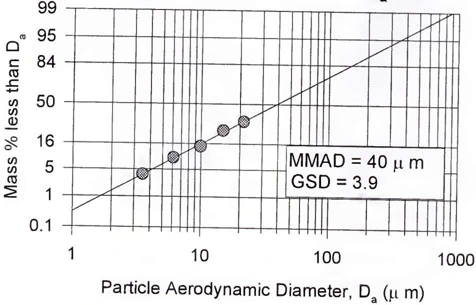

Fig. B5-2. Particle size distribution measurement using a Marple Personal Cascade impactor. Wind speed = 0.2 m/s.

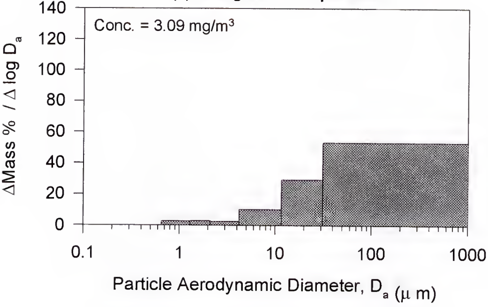

(a) Histogram for all particles

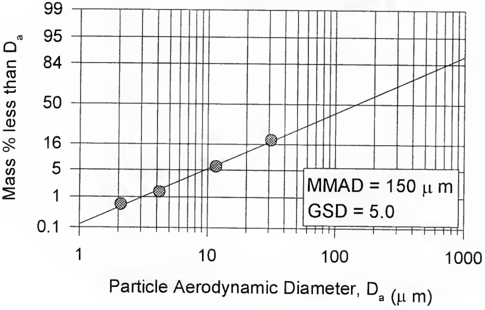

(b) Cumulative plot for wood particles ($D_a > 1$ μ m)

Fig. B6-1. Particle size distribution measurement using a University of Washington impactor. Wind speed < 0.2 m/s.

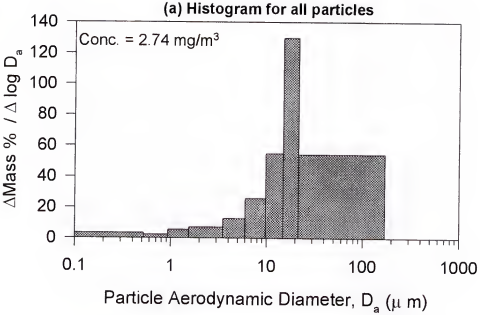
(a) Histogram for all particles

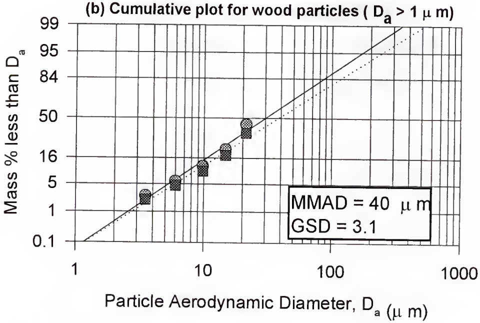
(b) Cumulative plot for wood particles ($D_a > 1$ μ m)

● : not including particle loss on the top surface

▨ : including particle loss on the top surface to the first stage

Fig. B6-2. Particle size distribution measurement using a Marple Personal Cascade impactor. Wind speed < 0.2 m/s.

(a) Histogram for all particles

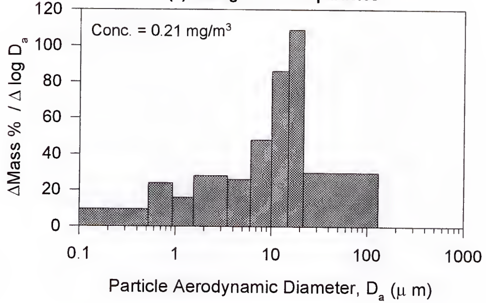

(b) Cumulative plot for wood particles (D_a > 1 μ m)

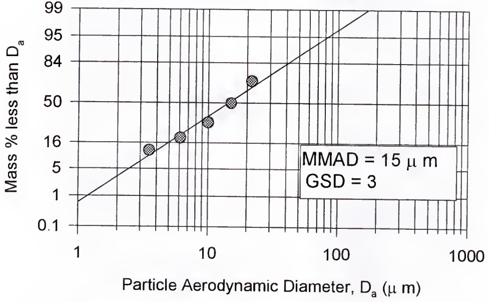

Fig. B7. Particle size distribution measurement using a Marple Personal Cascade impactor. Wind speed = 0.6 m/s.

(a) Histogram for all particles

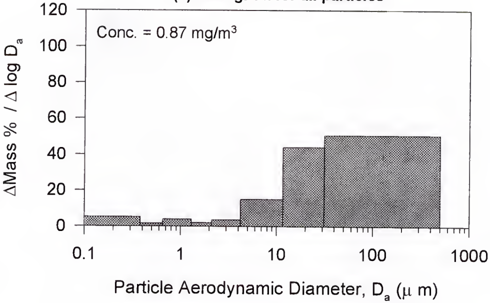

(b) Cumulative plot for wood particles (D_a > 1 μ m)

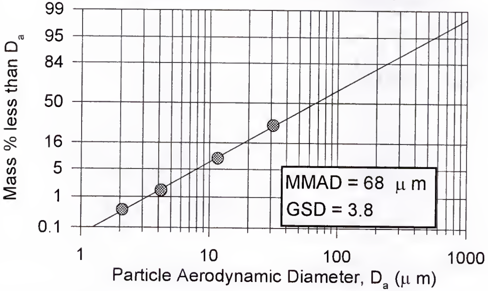

Fig. B8-1. Particle size distribution measurement using a University of Washington impactor. Wind speed < 0.2 m/s.

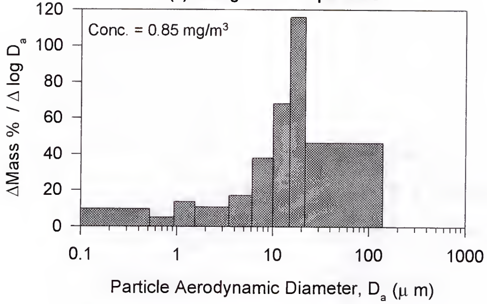

(a) Histogram for all particles

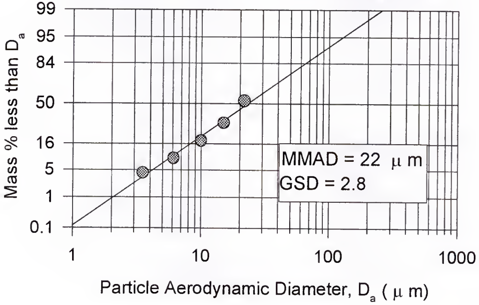

(b) Cumulative plot for wood particles (D_a > 1 μ m)

Fig. B8-2. Particle size distribution measurement using a Marple Personal Cascade impactor. Wind speed < 0.2 m/s.

(a) Histogram for all particles

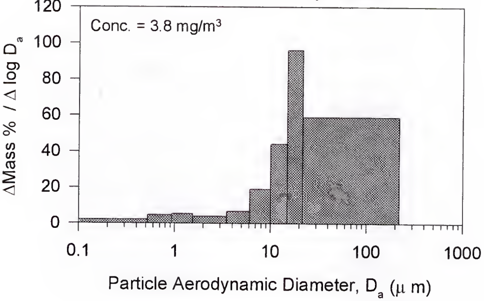

(b) Cumulative plot for wood particles (D_a > 1 μ m)

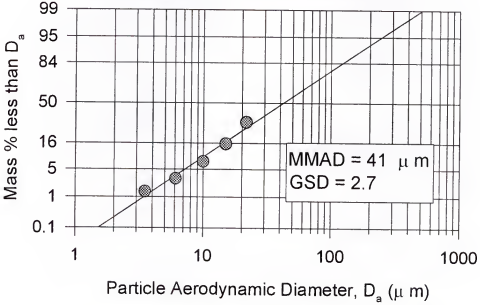

Fig. B9. Particle size distribution measurement using a Marple Personal Cascade impactor. Wind speed < 0.2 m/s.

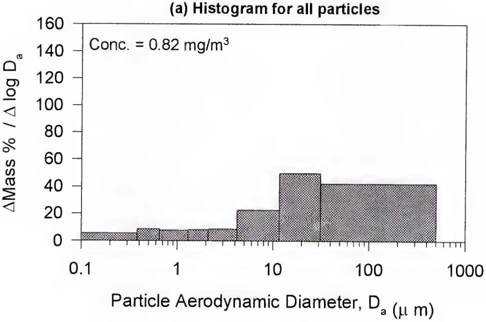

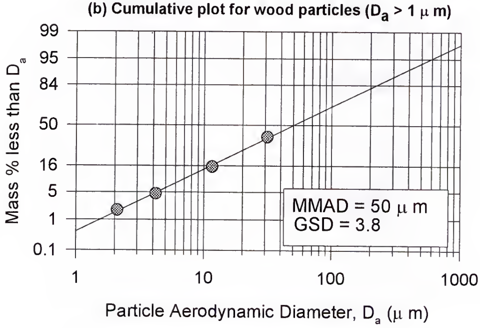

Fig. B10-1. Particle size distribution measurement using a University of Washington impactor. Wind speed = 0.3 m/s.

(a) Histogram for all particles

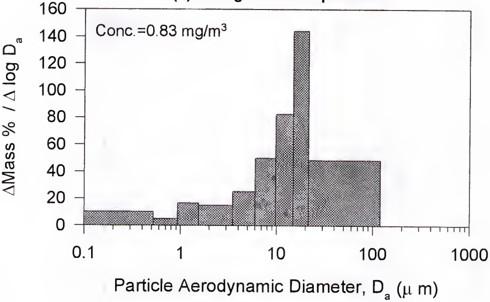

(b) Cumulative plot for wood particles (D_a > 1 μ m)

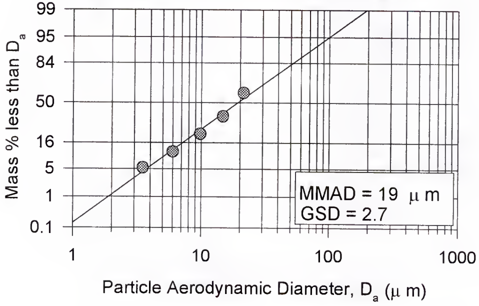

Fig. B10-2. Particle size distribution measurement using a Marple Personal Cascade impactor. Wind speed = 0.3 m/s.

(a) Histogram for all particles

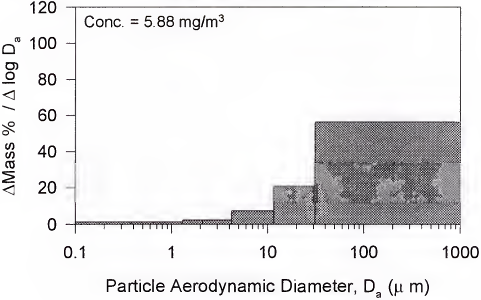

(b) Cumulative plot for wood particles (D_a > 1 μ m)

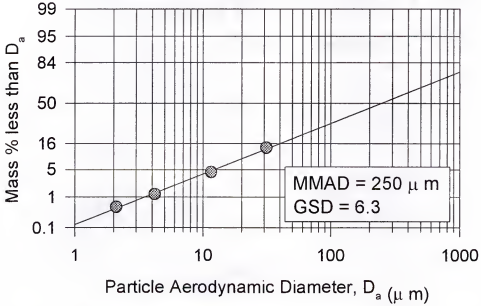

Fig. B11-1. Particle size distribution measurement using a University of Washington impactor. Wind speed < 0.2 m/s.

(a) Histogram for all particles

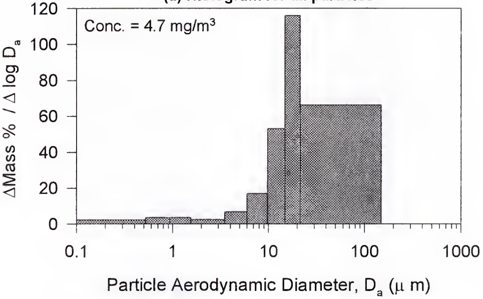

(b) Cumulative plot for wood particles ($D_a > 1$ μ m)

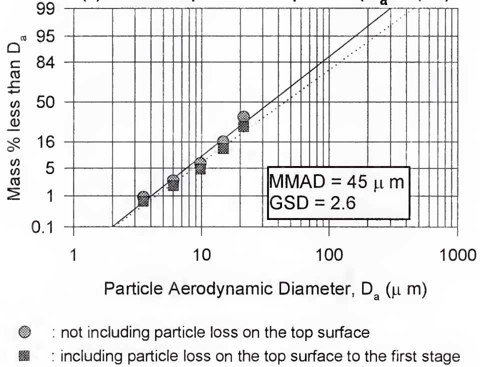

Fig. B11-2. Particle size distribution measurement using a Marple Personal Cascade impactor. Wind speed < 0.2 m/s.

(a) Histogram for all particles

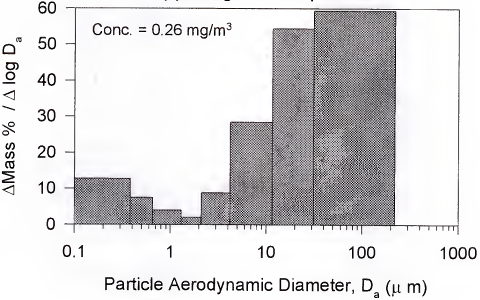

(b) Cumulative plot for wood particles (D_a > 1 μ m)

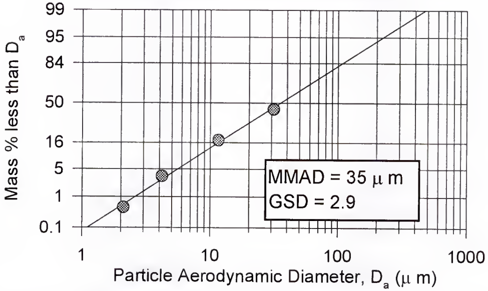

Fig. B12. Particle size distribution measurement using a University of Washington impactor. Wind speed < 0.2 m/s.

(a) Histogram for all particles

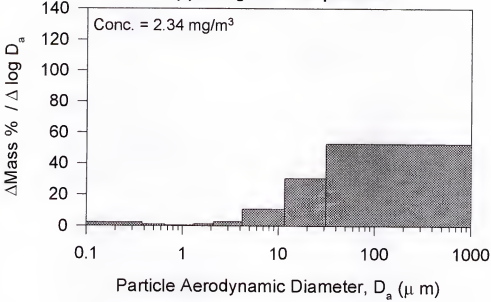

(b) Cumulative plot for wood particles (D_a > 1 μ m)

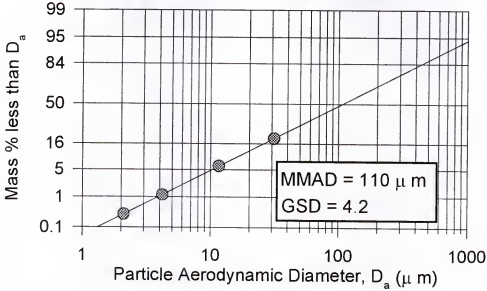

Fig. B13-1. Particle size distribution measurement using a University of Washington impactor. Wind speed < 0.2 m/s.

(a) Histogram for all particles

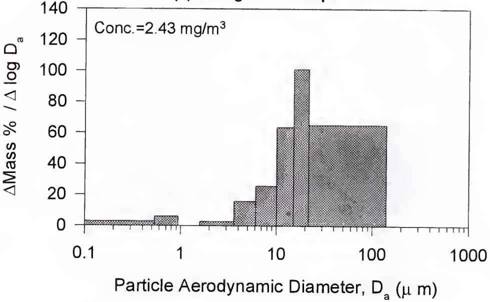

(b) Cumulative plot for wood particles ($D_a > 1$ μ m)

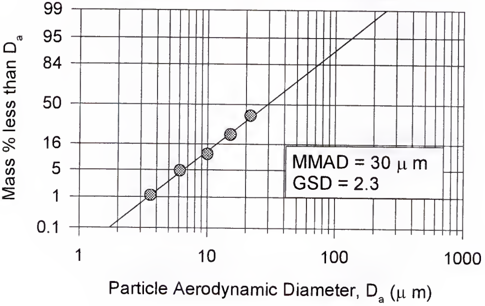

Fig. B13-2. Particle size distribution measurement using a Marple Personal Cascade impactor. Wind speed < 0.2 m/s.

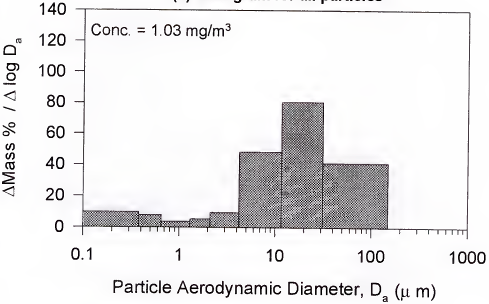

(a) Histogram for all particles

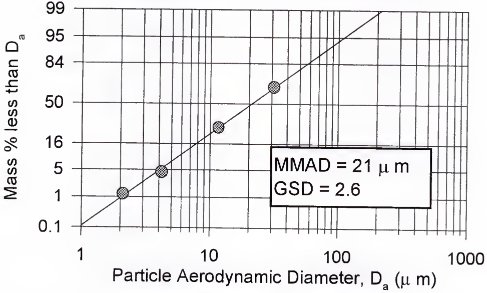

(b) Cumulative plot for wood particles ($D_a > 1$ μ m)

Fig. B14-1. Particle size distribution measurement using a University of Washington impactor. Wind speed < 0.2 m/s.

(a) Histogram for all particles

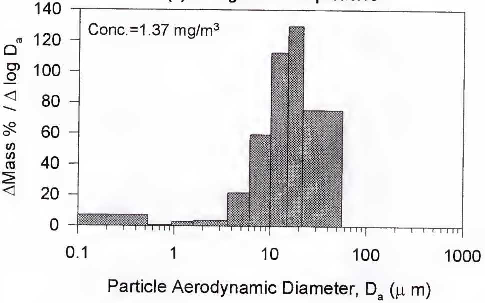

(b) Cumulative plot for wood particles (D_a > 1 μ m)

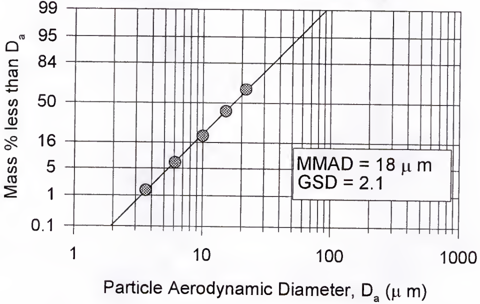

Fig. B14-2. Particle size distribution measurement using a Marple Personal Cascade impactor. Wind speed < 0.2 m/s.

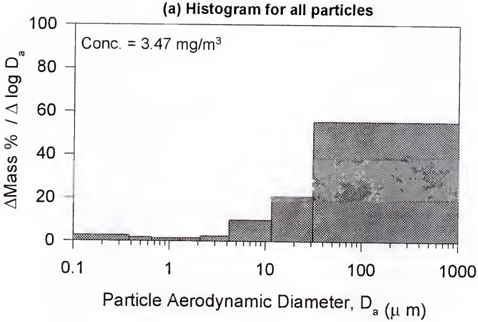

(a) Histogram for all particles

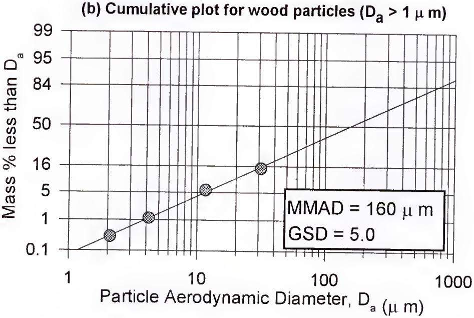

(b) Cumulative plot for wood particles (D_a > 1 μ m)

Fig. B15-1. Particle size distribution measurement using a University of Washington impactor. Wind speed < 0.2 m/s.

(a) Histogram for all particles

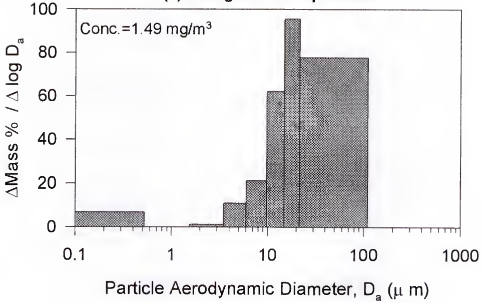

(b) Cumulative plot for wood particles ($D_a > 1$ μ m)

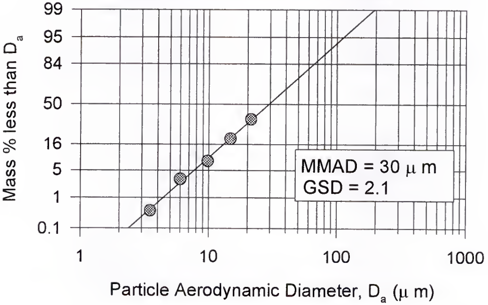

Fig. B15-2. Particle size distribution measurement using a Marple Personal Cascade impactor. Wind speed < 0.2 m/s.

APPENDIX C
INLET EFFICIENCIES OF TWO IMPACTORS AND ONE THIN-WALLED PROBE

Table C1-1. Inlet efficiency and inside loss of a Marple Personal Cascade impactor **(with a visor)** at three wind orientations and six particle diameters.
Wind speed, V_{wind} *= 0.55 m/s*, sampling flow rate = 2.0 l/min.

	Wind direction,θ	0°	90° (forward)	180°
D_a = 68 μm	First-stage outlet efficiency, %	7.1, 11.8 Avg.=9.4%	10.2, 10.4 Avg.=10.3%	6.4, 4.4 Avg.=5.4%
	Loss on first stage, %	0.7, 1.5 Avg.=1.1%	3.3, 5.4 Avg.=4%	1.1, 0.2 Avg.=1.1%
	Loss inside the cap, %	0, 0 Avg.=0%	0.0, 0.7 Avg.=0.3%	0.2, 0.0 Avg.=0.1%
	Inlet efficiency, %	Avg.=10.5%	Avg.=15.0%	Avg.=6.1%
D_a = 41 μm	First-stage outlet efficiency, %	9.9, 9.0 Avg.=9.4%	10.0, 5.1 Avg.= 7.8%	20.5, 9.2 Avg.=15.3%
	Loss on first stage, %	5.1, 5.5 Avg.=5.3%	3.8, 4.8 Avg.=4.3%	9.8, 6.8 Avg.=8.3%
	Loss inside the cap, %	1.0, 0.4 Avg.=0.7%	1.5, 3.6 Avg.=2.5%	0.4, 0.2 Avg.=0.3%
	Inlet efficiency, %	Avg.=15.4%	Avg.=14.4%	Avg.=23.4%
D_a = 21 μm	First-stage outlet efficiency, %	33.9, 32.5 Avg.=33.2%	29.8, 29.7 Avg.=29.7%	33.6, 35.3 Avg.=34.4%
	Loss on first stage, %	11.1, 9.9 Avg.=10.9%	7.2, 5.5 Avg.=6.3%	11.3, 13.1 Avg.=12.2%
	Loss inside the cap, %	5.3, 0.9 Avg.=3.1%	7.9, 6.7 Avg.=7.3%	1.6, 0.5 Avg.=1.0%
	Inlet efficiency, %	Avg.=46.8%	Avg.=43.4%	Avg.=47.7%
D_a = 10 μm	First-stage outlet efficiency, %	83.2, 73.5 Avg.=78.3%	80.9, 84.1 Avg.=82.5%	81.2, 79.7 Avg.=80.4%
	Loss on first stage, %	6.9, 9.0 Avg.=8%	4.9, 5.1 Avg.=5.0%	6.3, 6.6 Avg.=6.5%
	Loss inside the cap, %	1.0, 0.5 Avg.=0.7%	0.5, 2.5 Avg.=1.5%	0.5, 0.0 Avg.=0.2%
	Inlet efficiency, %	Avg.=87%	Avg.=89%	Avg.=87.1%

	Wind direction, θ	0°	90° (forward)	180°
$D_a = 5\ \mu m$	First-stage outlet efficiency, %	92, 96, 94 Avg.=94%	102, 103 Avg.=102.5%	98, 93.5 Avg.=95.7%
	Loss on first stage, %	2.2, 2.2, 1.8 Avg.=2.1%	2.3, 2.3 Avg.=2.3%	1.7, 2.6 Avg.=2.1%
	Loss inside the cap, %	0.4, 0.1, 0.4 Avg.=0.3%	0.5, 0.3 Avg.=0.4%	0, 0 Avg.= 0%
	Inlet efficiency, %	Avg.=96.4%	Avg.=105.2%	Avg.=97.8%
$D_a = 1.6\ \mu m$	First-stage outlet efficiency, %	98, 95 Avg.= 96.5%	---	---
	Loss on first stage, %	0.1, 0.4 Avg.=0.2%	---	---
	Loss inside the cap, %	0, 0 Avg.=0%	---	---
	Inlet efficiency, %	96.7%	---	---

Table C1-2. Inlet efficiency and inside loss of a Marple Personal Cascade impactor **(with a visor)** at three wind orientation and six particle diameters.
Wind speed, V_{wind} = 1.1 m/s, sampling flow rate = 2.0 l/min.

	Wind direction, θ	0°	90° (forward)	180°
D_a = 68 μm	First-stage outlet efficiency, %	8.3, 1.9, 1.7 Avg.=4.0%	17.3, 26.8 Avg.=22%	16.9, 14.9 Avg.=15.9%
	Loss on first stage, %	6.3, 1.6, 0.1 Avg.=2.7%	7.8, 12.6 Avg.=10.2%	13.0, 8.3 Avg.=10.6%
	Loss inside the cap, %	0.0, 0.1, 0.0 Avg.=0%	1.4, 0.0 Avg.=0.7%	0.1, 0.2 Avg.=0.1%
	Inlet efficiency, %	Avg.= 6.7%	Avg.=33%	Avg.=26.7%
D_a = 41 μm	First-stage outlet efficiency, %	12%, 15% Avg. = 13%	13.6, 14.6 Avg. = 14.1%	13%, 13.7% Avg.=13.3%
	Loss on first stage, %	7.7%, 18% Avg.=12%	10.2, 14 Avg.=12%	12%, 10% Avg. = 11%
	Loss inside the cap, %	2.3, 2 Avg.=2.1%	10.1, 17.3 Avg.=13.7%	1.2%, 1% Avg. =1.1%
	Inlet efficiency, %	Avg.= 27.1%	Avg.=39.8%	Avg.=25.4%
D_a = 21 μm	First-stage outlet efficiency, %	37, 36 Avg.=36.5%	23.1, 9.1 Avg.=16.1%	35.1, 26 Avg.=30.6%
	Loss on first stage, %	12.7, 11.1 Avg.=11.9%	7.8, 4.7 Avg.=6.2%	11.8, 7.1 Avg.=9.4%
	Loss inside the cap, %	6.2, 5.0 Avg.=5.6%	21.9, 32.9 Avg.=27.4%	1.1, 2.4 Avg.=1.8%
	Inlet efficiency, %	Avg.=54%	Avg.=49.5%	Avg.=42%
D_a = 10 μm	First-stage outlet efficiency, %	77, 93, 78 Avg.=82.6%	72.3, 60.6 Avg.=66.5%	79.1, 76.8 Avg.=78%
	Loss on first stage, %	6.9, 8.7, 8.6 Avg.=8.1%	6.0, 6.0 Avg.=6.0%	8.1, 5.3 Avg.=6.7%
	Loss inside the cap, %	4.1, 4.2, 2.5 Avg.=3.6%	3.1, 3.9 Avg.=3.5	0.5, 0.3 Avg.=0.4%
	Inlet efficiency, %	Avg.=94.3%	Avg.=76%	Avg.=85%

	Wind direction,θ	0°	90° (forward)	180°
D_a = 5 μm	First-stage outlet efficiency, %	102, 96.5 Avg.=99.2%	95.5, 97 Avg.= 96.2%	96, 99 Avg.=97.5%
	Loss on first stage, %	1.8, 1.5 Avg.=1.1%	2.0, 2.4 Avg.=2.2%	3.1, 2.8 Avg.=3%
	Loss inside the cap, %	0.3, 0.5 Avg.=0.4%	1.0, 1.5 Avg.=1.2	0, 0 Avg.=0 %
	Inlet efficiency, %	Avg.=100.7 %	Avg.=99.6%	Avg.=100%
D_a = 1.6 μm	First-stage outlet efficiency, %	95, 94 Avg.=94.5%	---	---
	Loss on first stage, %	0.4, 0.7 Avg.=0.5%	---	---
	Loss inside the cap, %	0, 0 Avg.=0%	---	---
	Inlet efficiency, %	Avg.=95%	---	---

Table C2-1. Inlet efficiency and inside loss of a Marple Personal Cascade impactor **(without a visor)** at three wind orientations and six particle diameters.
Wind speed, V_{wind} = 0.55 m/s, sampling flow rate = 2.0 l/min.

	Wind direction, θ	0°	90° (forward)	180°
D_a = 68 µm	First-stage outlet efficiency, %	279, 183 Avg.=231%	6.1, 8.2 Avg.=7.1%	28.5, 23.6 Avg.=26%
	Loss on first stage, %	103, 67 Avg.=85%	4.0, 3.2 Avg.=3.6%	12.4, 20.8 Avg.=16.6%
	Loss inside the cap, %	0, 4.7 Avg.=2.3%	0.1, 0.6 Avg.=0.3%	0.0, 0.0 Avg.=0%
	Inlet efficiency, %	Avg.=318%	Avg.=11%	Avg.=42.6%
D_a = 41 µm	First-stage outlet efficiency, %	101.5, 121.8 Avg.=112%	9.9, 19, 14 Avg.=17.6%	25.5, 23.8 Avg.=24.6%
	Loss on first stage, %	69, 69.8 Avg.=69.4%	6.1, 8.5, 5.4 Avg.=6.7%	15.3, 15.1 Avg.=15.2%
	Loss inside the cap, %	3.4, 4.3 Avg.=3.8%	0.5, 1.1, 0.1 Avg.=0.6%	0.0, 0.1 Avg.=0.0%
	Inlet efficiency, %	Avg.=185%	Avg.=21.5%	Avg.=40.3%
D_a = 21 µm	First-stage outlet efficiency, %	106, 120 Avg.=113%	29.9, 28.3 Avg.=29.1%	58.3, 57.7 Avg.=58%
	Loss on first stage, %	37.6, 44.4 Avg.=41%	7.5, 7.8 Avg.=7.6%	18.3, 16.2 Avg.=17.2%
	Loss inside the cap, %	1.2, 3.0 Avg.=2.1%	9.1, 12.4 Avg.=10.7%	0.0, 0.0 Avg.=0.0%
	Inlet efficiency, %	Avg.=156%	Avg.=47.5%	Avg.=75.2%
D_a = 10 µm	First-stage outlet efficiency, %	102, 106 Avg.=104%	82.5, 83.6 Avg.=83%	89.4, 88.3 Avg.=88.8%
	Loss on first stage, %	9.3, 12.4 Avg.=10.8%	5.7, 5.0 Avg.=5.3%	7.8, 8.6 Avg.=8.2%
	Loss inside the cap, %	0.1, 0.7 Avg.=0.4%	0.4, 0.5 Avg.=0.4%	0.1, 0.0 Avg.=0%
	Inlet efficiency, %	Avg.=115.2 %	Avg.=88.8%	Avg.=97.1%

	Wind direction,θ	0°	90° (forward)	180°
D_a = 5 μm	First-stage outlet efficiency, %	94.6, 100.4 Avg.=97.5%	94, 95 Avg.=94.5%	93, 98 Avg.=95.5%
	Loss on first stage, %	1.6, 2.0 Avg.=1.8%	1.6, 1.9 Avg.=1.7%	1.3, 1.7 Avg.=1.5%
	Loss inside the cap, %	0, 0 Avg.=0 %	0.3, 0.1 Avg.=0.2%	0, 0 Avg.=0 %
	Inlet efficiency, %	Avg.=99.3%	Avg.=96.4%	Avg.=97%
D_a = 1.6 μm	First-stage outlet efficiency, %	102, 98 Avg.=100%	---	---
	Loss on first stage, %	0.8, 0.7 Avg.=0.7%	---	---
	Loss inside the cap, %	0, 0.1 Avg.=0%	---	---
	Inlet efficiency, %	Avg.=100.7 %	---	---

Table C2-2. Inlet efficiency and inside loss of a Marple Personal Cascade impactor **(without a visor)** at three wind orientations and six particle diameters.
Wind speed, $V_{wind} = 1.1$ *m/s*, sampling flow rate = 2.0 l/min.

	Wind direction, θ	0°	90° (forward)	180°
D_a = 68 µm	First-stage outlet efficiency, %	458, 565, 484 Avg.=502%	6.5, 11.5 Avg.=9%	22.1, 18 Avg.=20%
	Loss on first stage, %	260, 205, 289 Avg.=2581%	1.6, 3.5 Avg.=2.5%	7.9, 5.0 Avg.=6.5%
	Loss inside the cap, %	2.6, 1.4, 0.2 Avg.=1.4%	1.3, 1.8 Avg.=1.5%	0.1, 0.0 Avg.=0.0%
	Inlet efficiency, %	Avg.=755%	Avg.=13.1%	Avg.=26.7%
D_a = 41 µm	First-stage outlet efficiency, %	150%, 182% Avg. = 166%	6.2, 5.3 Avg. = 5.7%	18%, 17.6% Avg.=17.8%
	Loss on first stage, %	160%, 169% Avg.=164%	2.1, 4.0 Avg.=3%	11%, 7.7% Avg. =9.4%
	Loss inside the cap, %	25, 30 Avg.=27%	0, 0.8 Avg.=0.4%	0.6%, 0% Avg. =0.3%
	Inlet efficiency, %	Avg.=357%	Avg.=9.1%	Avg.=27.5%
D_a = 21 µm	First-stage outlet efficiency, %	133, 128 Avg.=130.5%	32.7, 24.8 Avg.=28.7%	53.2, 57.3 Avg.=55.3%
	Loss on first stage, %	65.7, 49 Avg.=57.4%	10.5, 9.9 Avg.=10.2%	13.7, 14 Avg.=13.8%
	Loss inside the cap, %	18.1, 7 Avg.=12.6%	17.8, 6.4 Avg.=12.1%	1, 0.3 Avg.=0.6%
	Inlet efficiency, %	Avg.=200.4%	Avg.=51%	Avg.=69.8%
D_a = 10 µm	First-stage outlet efficiency, %	116, 111 Avg.=113%	79.3, 72.2 Avg.=75.7%	86.3, 97 Avg.=91.6%
	Loss on first stage, %	9.4, 11.7 Avg.=10.5%	6.0, 6.7 Avg.=6.3%	6.2, 5.1 Avg.=5.6%
	Loss inside the cap, %	0.8, 0.9 Avg.=0.8%	2.6, 1.5 Avg.=2.0%	0.8, 0.0 Avg.=0.4%
	Inlet efficiency, %	Avg.=124.3%	Avg.=84.1%	Avg.=97.7%

	Wind direction,θ	0°	90° (forward)	180°
D_a = 5 µm	First-stage outlet efficiency, %	109, 112, 108, 112. Avg=110.2%	101.5, 93 Avg.=97.2%	100, 106 Avg.=103%
	Loss on first stage, %	2.1, 1.7, 3.5, 3. Avg.=2.6%	2.0, 1.8 Avg.=1.9%	4.9, 0.7 Avg.=2.87%
	Loss inside the cap, %	0, 0.1, 0.3, 0.2. Avg.=0.1%	1.2, 0.3 Avg.=0.7%	0, 0 Avg.=0%
	Inlet efficiency, %	Avg.=113%	Avg.=99.9%	Avg.=106%
D_a = 1.6 µm	First-stage outlet efficiency, %	96, 100 Avg.=98%	---	---
	Loss on first stage, %	0.7, 0.3 Avg.=0.5%	---	---
	Loss inside the cap, %	0.1, 0 Avg.=0%	---	---
	Inlet efficiency, %	Avg.= 98.5%	---	---

Table C3-1. Effect of wind orientation on the inlet efficiency of a Marple Personal Cascade impactor (**with a visor**). $D_a = 68$ µm, $V_{wind} = 1.1$ m/s.

	0°	45°	90°	135°	180°
First-stage outlet efficiency, %	8.3, 1.9, 1.7 Avg.=4.0%	117, 98 Avg.=108%	17.3, 26.8 Avg.=22%	59, 62.8 Avg.=61%	16.9, 14.9 Avg.=15.9%
Loss on first stage	6.3, 1.6, 0.1 Avg.=2.7%	63.7, 30 Avg.=47%	7.8, 12.6 Avg.=10%	47, 47.8 Avg.=47.4%	13.0, 8.3 Avg.=10.6%
Loss inside the cap	0.0, 0.1, 0.0 Avg.=0%	1.0, 27 Avg.=14%	1.4, 0.0 Avg.=0.7%	0, 0 Avg.=0%	0.1, 0.2 Avg.=0.1%
Inlet efficiency, %	Avg.= 6.7%	Avg.=168%	Avg.=33%	Avg.=108%	Avg.=26.7%

Table C3-2. Effect of wind orientation on the inlet efficiency of a Marple Personal Cascade impactor (**without a visor**). $D_a = 68$ µm, $V_{wind} = 1.1$ m/s.

	0°	90°	135°	180°
First-stage outlet efficiency, %	458, 565, 484 Avg.=502%	6.5, 11.5 Avg.=9%	3.3%	22.1, 18 Avg.=20%
Loss on first stage	260, 205, 289 Avg.=2581%	1.6, 3.5 Avg.=2.5%	2.1%	7.9, 5.0 Avg.=6.5%
Loss inside the cap	2.6, 1.4, 0.2 Avg.=1.4%	1.3, 1.8 Avg.=1.5%	0.1%	0.1, 0.0 Avg.=0.0%
Inlet efficiency, %	Avg.=755%	Avg.=13.1%	5.5%	Avg.=26.7%

Table C4-1. Inlet efficiency of a University of Washington (U-W) impactor. *Wind speed, V_{wind} = 0.55 m/s*, sampling flow rate = 15 l/min.

Particle Diameter	D_a = 68 μm	D_a = 41 μm	D_a = 21 μm
Efficiency, %	47.4, 45.1 Avg.=46%	74.4, 74.8 Avg.=75%	88.5, 89.5 Avg.=89%
Particle Diameter	D_a = 10 μm	D_a = 5 μm	D_a =1.6 μm
Efficiency, %	96.8, 98.7 Avg.=98%	96, 104, 103, 101 Avg.=101%	99.5, 96 Avg.=98%

Table C4-2. Inlet efficiency of a University of Washington (U-W) impactor. *Wind speed, V_{wind} = 1.1 m/s*, sampling flow rate = 15 l/min.

Particle Diameter	D_a =68 μm	D_a =41 μm	D_a =21 μm
Efficiency, %	11.6, 7.4 Avg.=9%	20.7, 15.7, 22, 18 Avg.=19%	63, 52, 58, 62 Avg.=59%
Particle Diameter	D_a =10 μm	D_a = 5 μm	D_a =1.6 μm
Efficiency, %	91, 90.5 Avg.=91%	97, 97 Avg.=97%	95.5, 100 Avg.=98%

Table C5-1. Inlet efficiency of a thin-walled probe (D_i = 6.8 mm).
Wind speed, V_{wind} = 0.55 m/s, Sampling flow rate = 2.0 l/min.

	Wind direction, θ	0°	90° (forward)	180°
D_a = 68 μm	Inlet efficiency, %	66, 67 Avg.=66.5%	8.8, 3.7 Avg.=6.2%	10.7, 6.1 Avg.=8.4%
D_a = 41 μm	Inlet efficiency, %	82.3, 74.0 Avg.=78.1%	24.1, 31.3 Avg.=27.7%	10.5, 8.1 Avg.=9.3%
D_a = 21 μm	Inlet efficiency, %	95.4, 102 Avg.=98.7%	61.9, 56.3 Avg.=59.1%	34.5, 34.6 Avg.=34.5%
D_a = 10 μm	Inlet efficiency, %	93.8, 101 Avg.=97.4%	92.2, 85.3 Avg.=88..8%	80.3, 80.3 Avg.=80.3%
D_a = 5 μm	Inlet efficiency, %	102, 100 Avg.=101%	103, 87, 94.5 Avg.=95%	102, 97, 87.5 Avg.=95.5%
D_a = 1.6 μm	Inlet efficiency, %	100, 99.3 Avg.=99.6%	---	---

Table C5-2. Inlet efficiency of a thin-walled probe (D_i = 6.8 mm).
Wind speed, V_{wind} = 1.1 m/s, sampling flow rate = 2.0 l/min.

	Wind direction, θ	0°	90° (forward)	180°
D_a = 68 µm	Inlet efficiency, %	109, 106 Avg.=107.5 %	13, 9.0 Avg.=11%	0.9, 1.9 Avg.=1.4%
D_a = 41 µm	Inlet efficiency, %	105, 104 Avg.=104.5 %	7.4, 12.6 Avg.=10%	4.8, 5.5 Avg.=5.1%
D_a = 21 µm	Inlet efficiency, %	105%	29.2, 20.7 Avg.=24.9%	9.7, 14.9 Avg.=12.3%
D_a = 10 µm	Inlet efficiency, %	103, 101 Avg.=102%	77.8, 73.7 Avg.= 75.7%	77.2, 81.2 Avg.=79.2%
D_a = 5 µm	Inlet efficiency, %	102, 99 Avg.=100.5 %	96, 94 Avg.=95%	93, 92.5 Avg.=92.7%
D_a = 1.6 µm	Inlet efficiency, %	102, 97 Avg.=99.5%	---	---

APPENDIX D

COMPARISON BETWEEN THE MEASURED AND THE CALCULATED INLET EFFICIENCY

Table D1-1. Comparison between the measured and the calculated inlet efficiency using the equations developed by Belyaev and Levin (1974) for a thin-walled probe ($D_i = 6.8$ mm, $Q_i = 2.0$ l/min).
Wind speed, V_w = 0.55 m/s, wind direction, $\theta = 0^0$.

D_a (μm)	68	41	21	10	5	1.6
Calculated value	69%	78%	90%	97%	99%	100%
Experimental value	67%	78%	99%	97%	101%	100%

Table D1-2. Comparison between the measured and the calculated inlet efficiency using the equations developed by Belyaev and Levin (1974) for a thin-walled probe ($D_i = 6.8$ mm, $Q_i = 2.0$ l/min).
Wind speed, V_w = 1.1 m/s, wind direction, $\theta = 0^0$.

D_a (μm)	68	41	21	10	5	1.6
Calculated value	117%	114%	107%	102%	101%	100%
Experimental value	108%	105%	105%	102%	101%	100%

Table D2-1. Comparison between the measured and the calculated inlet efficiency using the equations developed by Belyaev and Levin (1974) for a CIS sampler (D_b = 10 mm, D_i = 8.5 mm, Q_i = 3.5 l/min).
Wind speed, V_w = 0.55 m/s, wind direction, $\theta = 0^0$.

D_a (µm)	68	41	21	10	5	1.6
Calculated value	65%	76%	90%	97%	99%	100%
Experimental value	73%	74%	89%	96%	100%	99%

Table D2-2. Comparison between the measured and the calculated inlet efficiency using the equations developed by Belyaev and Levin (1974) for a CIS sampler (D_b = 10 mm, D_i = 8.5 mm, Q_i = 3.5 l/min).
Wind speed, V_w = 1.1 m/s, wind direction, $\theta = 0^0$.

D_a (µm)	68	41	21	10	5	1.6
Calculated value	106%	104%	102%	101%	100%	100%
Experimental value	101%	103%	95%	95%	95%	97%

Table D3-1. Comparison between the measured and the calculated inlet efficiency using the equations developed by Belyaev and Levin (1974) for an IOM sampler (D_b = 34 mm, D_i = 15 mm, Q_i = 2.0 l/min).
Wind speed, V_w = 0.55 m/s, wind direction, $\theta = 0^0$.

D_a (µm)	68	41	21	10	5	1.6
Calculated value	164%	130%	109%	102%	101%	100%
Experimental value	180%	129%	111%	101%	95%	100%

Table D3-2. Comparison between the measured and the calculated inlet efficiency using the equations developed by Belyaev and Levin (1974) for an IOM sampler (D_b = 34 mm, D_i = 15 mm, Q_i = 2.0 l/min).
Wind speed, V_w = 1.1 m/s, wind direction, $\theta = 0^0$.

D_a (µm)	68	41	21	10	5	1.6
Calculated value	336%	227%	141%	110%	103%	100%
Experimental value	342%	233%	137%	104%	101%	102%

Table D4-1. Comparison between the measured and the calculated inlet efficiency using the equations developed by Belyaev and Levin (1974) for a 7-hole sampler ($D_b = 34$ mm, $D_i = 13$ mm, $Q_i = 2.0$ l/min).
Wind speed, $V_w = 0.55$ m/s, wind direction, $\theta = 0^0$.

D_a (µm)	68	41	21	10	5	1.6
Calculated value	140%	119%	106%	101%	100%	100%
Experimental value	120%	101%	100%	101%	100%	102%

Table D4-2. Comparison between the measured and the calculated inlet efficiency using the equations developed by Belyaev and Levin (1974) for a 7-hole sampler ($D_b = 34$ mm, $D_i = 13$ mm, $Q_i = 2.0$ l/min).
Wind speed, $V_w = 1.1$ m/s, wind direction, $\theta = 0^0$.

D_a (µm)	68	41	21	10	5	1.6
Calculated value	270%	190%	129%	107%	102%	100%
Experimental value	286%	187%	133%	104%	101%	101%

Table D5-1. Comparison between the measured and the calculated inlet efficiency using the equations developed by Belyaev and Levin (1974) for a closed-face 37-mm sassette (D_b = 40 mm, D_i = 4.5 mm, Q_i = 2.0 l/min).
Wind speed, V_w = 0.55 m/s, wind direction, $\theta = 0^0$.

D_a (μm)	68	41	21	10	5	1.6
Calculated value	66%	82%	94%	99%	100%	100%
Experimental value	61%	94%	91%	99%	97%	101%

Table D5-2. Comparison between the measured and the calculated inlet efficiency using the equations developed by Belyaev and Levin (1974) for a closed-face 37-mm sassette (D_b = 40 mm, D_i = 4.5 mm, Q_i = 2.0 l/min).
Wind speed, V_w = 1.1 m/s, wind direction, $\theta = 0^0$.

D_a (μm)	68	41	21	10	5	1.6
Calculated value	73%	85%	95%	99%	100%	100%
Experimental value	100%	121%	97%	92%	101%	97%

Table D6-1. Comparison between the measured and the calculated inlet efficiency using the equations developed by Belyaev and Levin (1974) for a Marple Personal Cascade impactor (without a visor), (D_b = 45 mm, D_i = 25 mm, Q_i = 2.0 l/min).
Wind speed, V_w = 0.55 m/s, wind direction, $\theta = 0^0$.

D_a (μm)	68	41	21	10	5	1.6
Calculated value	285%	182%	124%	106%	101%	100%
Experimental value	318%	185%	156%	115%	99%	101%

Table D6-2. Comparison between the measured and the calculated inlet efficiency using the equations developed by Belyaev and Levin (1974) for a Marple Personal Cascade impactor (without a visor), (D_b = 45 mm, D_i = 25 mm, Q_i = 2.0 l/min).
Wind speed, V_w = 1.1 m/s, wind direction, $\theta = 0^0$.

D_a (μm)	68	41	21	10	5	1.6
Calculated value	733%	413%	196%	123%	106%	101%
Experimental value	755%	357%	200%	124%	113%	99%

Table D7-1. Comparison between the measured and the calculated inlet efficiency using the equations developed by Vincent and his colleague for a thin-walled probe ($D_i = 6.8$ mm, $Q_i = 2.0$ l/min).

Wind speed, V_w = 0.55 m/s, wind direction, $\theta = 0^0$.

D_a (μm)	68	41	21	10	5	1.6
Calculated value	72%	77%	87%	96%	99%	100%
Experimental value	67%	78%	99%	97%	101%	100%

Table D7-2. Comparison between the measured and the calculated inlet efficiency using the equations developed by Vincent and his colleague for a thin-walled probe ($D_i = 6.8$ mm, $Q_i = 2.0$ l/min).

Wind speed, V_w = 1.1 m/s, wind direction, $\theta = 0^0$.

D_a (μm)	68	41	21	10	5	1.6
Calculated value	114%	112%	107%	103%	101%	100%
Experimental value	108%	105%	105%	102%	101%	100%

Table D8-1. Comparison between the measured and the calculated inlet efficiency using the equations developed by Vincent and his colleague for a CIS sampler (D_b = 10 mm, D_i = 8.5 mm, Q_i = 3.5 l/min).

Wind speed, V_w = 0.55 m/s, wind direction, $\theta = 0^0$.

D_a (μm)	68	41	21	10	5	1.6
Calculated value	64%	71%	85%	95%	99%	99%
Experimental value	73%	74%	89%	96%	100%	99%

Table D8-2. Comparison between the measured and the calculated inlet efficiency using the equations developed by Vincent and his colleague for a CIS sampler (D_b = 10 mm, D_i = 8.5 mm, Q_i = 3.5 l/min).

Wind speed, V_w = 1.1 m/s, wind direction, $\theta = 0^0$.

D_a (μm)	68	41	21	10	5	1.6
Calculated value	98%	97%	98%	99%	100%	100%
Experimental value	101%	103%	95%	95%	95%	97%

Table D9-1. Comparison between the measured and the calculated inlet efficiency using the equations developed by Vincent and his colleague for an IOM sampler ($D_b = 34$ mm, $D_i = 15$ mm, $Q_i = 2.0$ l/min).
Wind speed, V_w = 0.55 m/s, wind direction, $\theta = 0^0$.

D_a (µm)	68	41	21	10	5	1.6
Calculated value	130%	113%	104%	101%	100%	100%
Experimental value	180%	129%	111%	101%	95%	100%

Table D9-2. Comparison between the measured and the calculated inlet efficiency using the equations developed by Vincent and his colleague for an IOM sampler ($D_b = 34$ mm, $D_i = 15$ mm, $Q_i = 2.0$ l/min).
Wind speed, V_w = 1.1 m/s, wind direction, $\theta = 0^0$.

D_a (µm)	68	41	21	10	5	1.6
Calculated value	247%	170%	122%	105%	101%	100%
Experimental value	342%	233%	137%	104%	101%	102%

Table D10-1. Comparison between the measured and the calculated inlet efficiency using the equations developed by Vincent and his colleague for a 7-hole sampler (D_b = 34 mm, D_i = 13 mm, Q_i = 2.0 l/min).
Wind speed, V_w = 0.55 m/s, wind direction, $\theta = 0^0$.

D_a (µm)	68	41	21	10	5	1.6
Calculated value	111%	103%	101%	100%	100%	100%
Experimental value	120%	101%	100%	101%	100%	102%

Table D10-2. Comparison between the measured and the calculated inlet efficiency using the equations developed by Vincent and his colleague for a 7-hole sampler (D_b = 34 mm, D_i = 13 mm, Q_i = 2.0 l/min).
Wind speed, V_w = 1.1 m/s, wind direction, $\theta = 0^0$.

D_a (µm)	68	41	21	10	5	1.6
Calculated value	201%	148%	115%	104%	101%	100%
Experimental value	286%	187%	133%	104%	101%	101%

Table D11-1. Comparison between the measured and the calculated inlet efficiency using the equations developed by Vincent and his colleague for a closed-face 37-mm sassette (D_b = 40 mm, D_i = 4.5 mm, Q_i = 2.0 l/min).
Wind speed, V_w = 0.55 m/s, wind direction, $\theta = 0^0$.

D_a (μm)	68	41	21	10	5	1.6
Calculated value	34%	51%	78%	94%	98%	100%
Experimental value	61%	94%	91%	99%	97%	101%

Table D11-2. Comparison between the measured and the calculated inlet efficiency using the equations developed by Vincent and his colleague for a closed-face 37-mm sassette (D_b = 40 mm, D_i = 4.5 mm, Q_i = 2.0 l/min).
Wind speed, V_w = 1.1 m/s, wind direction, $\theta = 0^0$.

D_a (μm)	68	41	21	10	5	1.6
Calculated value	44%	53%	74%	92%	98%	100%
Experimental value	100%	121%	97%	92%	101%	97%

Table D12-1. Comparison between the measured and the calculated inlet efficiency using the equations developed by Vincent and his colleague for a Marple Personal Cascade impactor (without a visor), ($D_b = 45$ mm, $D_i = 25$ mm, $Q_i = 2.0$ l/min).
Wind speed, $V_w = 0.55$ m/s, wind direction, $\theta = 0^0$.

D_a (μm)	68	41	21	10	5	1.6
Calculated value	205%	144%	112%	103%	101%	100%
Experimental value	318%	185%	156%	115%	99%	101%

Table D12-2. Comparison between the measured and the calculated inlet efficiency using the equations developed by Vincent and his colleague for a Marple Personal Cascade impactor (without a visor), ($D_b = 45$ mm, $D_i = 25$ mm, $Q_i = 2.0$ l/min).
Wind speed, $V_w = 1.1$ m/s, wind direction, $\theta = 0^0$.

D_a (μm)	68	41	21	10	5	1.6
Calculated value	447%	244%	140%	109%	102%	100%
Experimental value	755%	357%	200%	124%	113%	99%

Table D13-1. Comparison between the measured and the calculated inlet efficiency using the equations developed by Vincent and his colleague for a thin-walled probe ($D_i = 6.8$ mm, $Q_i = 2.0$ l/min).
Wind speed, V_w = 0.55 m/s, wind direction, $\theta = 90^0$.

D_a (μm)	68	41	21	10	5
Calculated value	11%	26%	57%	85%	96%
Experimental value	6%	28%	59%	89%	95%

Table D13-2. Comparison between the measured and the calculated inlet efficiency using the equations developed by Vincent and his colleague for a thin-walled probe ($D_i = 6.8$ mm, $Q_i = 2.0$ l/min).
Wind speed, V_w = 1.1 m/s, wind direction, $\theta = 90^0$.

D_a (μm)	68	41	21	10	5
Calculated value	4%	11%	32%	67%	89%
Experimental value	11%	10%	25%	76%	95%

Table D14-1. Comparison between the measured and the calculated inlet efficiency using the equations developed by Vincent and his colleague for a CIS sampler (D_b = 30 mm D_i = 8.5 mm, Q_i = 3.5 l/min).
Wind speed, V_w = 0.55 m/s, wind direction, θ = 90^0.

D_a (µm)	68	41	21	10	5
Calculated value	8%	20%	48%	80%	94%
Experimental value	6%	12%	57%	82%	85%

Table D14-2. Comparison between the measured and the calculated inlet efficiency using the equations developed by Vincent and his colleague for a CIS sampler (D_b = 30 mm, D_i = 8.5 mm, Q_i = 3.5 l/min).
Wind speed, V_w = 1.1 m/s, wind direction, θ = 90^0.

D_a (µm)	68	41	21	10	5	1.6
Calculated value	3%	8%	25%	59%	85%	98%
Experimental value	3%	2%	17%	69%	82%	97%

Table D15-1. Comparison between the measured and the calculated inlet efficiency using the equations developed by Vincent and his colleague for an IOM sampler (D_b = 26 mm, D_i = 15 mm, Q_i = 2.0 l/min).
Wind speed, V_w = 0.55 m/s, wind direction, $\theta = 90^0$.

D_a (µm)	68	41	21	10	5
Calculated value	9%	21%	50%	82%	95%
Experimental value	3%	17%	35%	78%	92%

Table D15-2. Comparison between the measured and the calculated inlet efficiency using the equations developed by Vincent and his colleague for an IOM sampler (D_b = 26 mm, D_i = 15 mm, Q_i = 2.0 l/min).
Wind speed, V_w = 1.1 m/s, wind direction, $\theta = 90^0$.

D_a (µm)	68	41	21	10	5
Calculated value	3%	9%	26%	61%	86%
Experimental value	3%	6%	13%	64%	90%

Table D16-1. Comparison between the measured and the calculated inlet efficiency using the equations developed by Vincent and his colleague for a 7-hole sampler (D_b = 28 mm, D_i = 10 mm, Q_i = 2.0 l/min).
Wind speed, V_w = 0.55 m/s, wind direction, $\theta = 90^0$.

D_a (µm)	68	41	21	10	5
Calculated value	5%	14%	38%	73%	91%
Experimental value	4%	6%	21%	73%	93%

Table D16-2. Comparison between the measured and the calculated inlet efficiency using the equations developed by Vincent and his colleague for a 7-hole sampler (D_b = 28 mm, D_i = 10 mm, Q_i = 2.0 l/min).
Wind speed, V_w = 1.1 m/s, wind direction, $\theta = 90^0$.

D_a (µm)	68	41	21	10	5
Calculated value	2%	5%	18%	49%	79%
Experimental value	1%	3%	13%	57%	86%

Table D17-1. Comparison between the measured and the calculated inlet efficiency using the equations developed by Vincent and his colleague for a closed-face 37-mm sassette (D_b = 37 mm, D_i = 4.5 mm, Q_i = 2.0 l/min).
Wind speed, V_w = 0.55 m/s, wind direction, $\theta = 90^0$.

D_a (µm)	68	41	21	10	5
Calculated value	4%	11%	32%	67%	89%
Experimental value	4%	5%	26%	81%	92%

Table D17-2. Comparison between the measured and the calculated inlet efficiency using the equations developed by Vincent and his colleague for a closed-face 37-mm sassette (D_b = 37 mm, D_i = 4.5 mm, Q_i = 2.0 l/min).
Wind speed, V_w = 1.1 m/s, wind direction, $\theta = 90^0$.

D_a (µm)	68	41	21	10	5	1.6
Calculated value	2%	4%	14%	42%	74%	97%
Experimental value	2%	2%	14%	65%	84%	95%

Table D18-1. Comparison between the measured and the calculated inlet efficiency using the equations developed by Vincent and his colleague for a Marple Personal Cascade impactor (without a visor), (D_b = 32 mm, D_i = 25 mm, Q_i = 2.0 l/min).
Wind speed, V_w = 0.55 m/s, wind direction, $\theta = 90^0$.

D_a (μm)	68	41	21	10	5
Calculated value	10%	24%	54%	84%	95%
Experimental value	11%	22%	48%	89%	96%

Table D18-2. Comparison between the measured and the calculated inlet efficiency using the equations developed by Vincent and his colleague for a Marple Personal Cascade impactor (without a visor), (D_b = 32 mm, D_i = 25 mm, Q_i = 2.0 l/min).
Wind speed, V_w = 1.1 m/s, wind direction, $\theta = 90^0$.

D_a (μm)	68	41	21	10	5
Calculated value	4%	10%	29%	65%	88%
Experimental value	13%	9%	51%	84%	100%

Table D19-1. Comparison between the measured and the calculated inlet efficiency using the equations developed by Vincent and his colleague for a thin-walled probe ($D_b = 9.5$ mm, $D_i = 6.8$ mm, $Q_i = 2.0$ l/min).
Wind speed, V_w = 0.55 m/s, wind direction, $\theta = 180^0$.

D_a (μm)	68	41	21	10	5
Calculated value	4%	11%	33%	68%	89%
Experimental value	8%	9%	35%	80%	96%

Table D19-2. Comparison between the measured and the calculated inlet efficiency using the equations developed by Vincent and his colleague for a thin-walled probe ($D_b = 9.5$ mm, $D_i = 6.8$ mm, $Q_i = 2.0$ l/min).
Wind speed, V_w = 1.1 m/s, wind direction, $\theta = 180^0$.

D_a (μm)	68	41	21	10	5
Calculated value	3%	7%	23%	57%	84%
Experimental value	1%	5%	12%	79%	93%

Table D20-1. Comparison between the measured and the calculated inlet efficiency using the equations developed by Vincent and his colleague for a CIS sampler (D_b = 47 mm D_i = 8.5 mm, Q_i = 3.5 l/min).
Wind speed, V_w = 0.55 m/s, wind direction, θ = 180°.

D_a (µm)	68	41	21	10	5
Calculated value	9%	20%	49%	81%	95%
Experimental value	9%	17%	48%	85%	95%

Table D20-2. Comparison between the measured and the calculated inlet efficiency using the equations developed by Vincent and his colleague for a CIS sampler (D_b = 47 mm, D_i = 8.5 mm, Q_i = 3.5 l/min).
Wind speed, V_w = 1.1 m/s, wind direction, θ = 180°.

D_a (µm)	68	41	21	10	5	1.6
Calculated value	6%	14%	38%	73%	92%	98%
Experimental value	1%	3%	25%	86%	91%	96%

Table D21-1. Comparison between the measured and the calculated inlet efficiency using the equations developed by Vincent and his colleague for an IOM sampler (D_b = 34 mm, D_i = 15 mm, Q_i = 2.0 l/min).
Wind speed, V_w = 0.55 m/s, wind direction, θ = 180°.

D_a (µm)	68	41	21	10	5
Calculated value	17%	36%	68%	91%	97%
Experimental value	4%	24%	55%	91%	99%

Table D21-2. Comparison between the measured and the calculated inlet efficiency using the equations developed by Vincent and his colleague for an IOM sampler (D_b = 34 mm, D_i = 15 mm, Q_i = 2.0 l/min).
Wind speed, V_w = 1.1 m/s, wind direction, θ = 180°.

D_a (µm)	68	41	21	10	5
Calculated value	12%	26%	58%	86%	96%
Experimental value	10%	11%	49%	94%	93%

Table D22-1. Comparison between the measured and the calculated inlet efficiency using the equations developed by Vincent and his colleague for a 7-hole sampler (D_b = 34 mm, D_i = 10 mm, Q_i = 2.0 l/min).
Wind speed, V_w = 0.55 m/s, wind direction, θ = 180^0.

D_a (μm)	68	41	21	10	5
Calculated value	13%	29%	61%	87%	97%
Experimental value	5%	19%	49%	90%	102%

Table D22-2. Comparison between the measured and the calculated inlet efficiency using the equations developed by Vincent and his colleague for a 7-hole sampler (D_b = 34 mm, D_i = 10 mm, Q_i = 2.0 l/min).
Wind speed, V_w = 1.1 m/s, wind direction, θ = 180^0.

D_a (μm)	68	41	21	10	5
Calculated value	9%	21%	50%	82%	95%
Experimental value	0%	9%	47%	85%	102%

Table D23-1. Comparison between the measured and the calculated inlet efficiency using the equations developed by Vincent and his colleague for a closed-face 37-mm sassette (D_b = 40 mm, D_i = 4.5 mm, Q_i = 2.0 l/min).
Wind speed, V_w = 0.55 m/s, wind direction, θ = 180°.

D_a (μm)	68	41	21	10	5
Calculated value	4%	11%	33%	68%	90%
Experimental value	4%	19%	41%	82%	88%

Table D23-2. Comparison between the measured and the calculated inlet efficiency using the equations developed by Vincent and his colleague for a closed-face 37-mm sassette (D_b = 40 mm, D_i = 4.5 mm, Q_i = 2.0 l/min).
Wind speed, V_w = 1.1 m/s, wind direction, θ = 180°.

D_a (μm)	68	41	21	10	5	1.6
Calculated value	3%	7%	23%	57%	84%	96%
Experimental value	7%	5%	29%	83%	85%	92%

Table D24-1. Comparison between the measured and the calculated inlet efficiency using the equations developed by Vincent and his colleague for a Marple Personal Cascade impactor (without a visor), (D_b = 45 mm, D_i = 25 mm, Q_i = 2.0 l/min).
Wind speed, V_w = 0.55 m/s, wind direction, $\theta = 180^0$.

D_a (μm)	68	41	21	10	5
Calculated value	31%	55%	82%	95%	99%
Experimental value	43%	40%	75%	97%	97%

Table D24-2. Comparison between the measured and the calculated inlet efficiency using the equations developed by Vincent and his colleague for a Marple Personal Cascade impactor (without a visor), (D_b = 45 mm, D_i = 25 mm, Q_i = 2.0 l/min).
Wind speed, V_w = 1.1 m/s, wind direction, $\theta = 180^0$.

D_a (μm)	68	41	21	10	5
Calculated value	22%	43%	75%	93%	98%
Experimental value	27%	28%	70%	98%	106%

REFERENCES

1. Whitehead, L. W. Health Effects of Wood Dust - Relevance for an Occupational Standard. *Am. Ind. Hyg. Assoc. J.* **1982**, 43, 674.

2. Jahnke, J. A. Source Sampling for Particulate Pollutants - Student Manual. U.S. Environmental Protection Agency, NC, 1995.

3. Vincent, J. H. and Mark, D. Applications of Blunt Sampler Theory to the Definition and Measurement of Inhalable Dust. *Ann. Occup. Hyg.* **1982**, 26, 3.

4. Armbruster, L. and Breuer, H. Investigations into Defining Inhalable Dust. *Ann. Occup. Hyg.* **1982**, 26, 21.

5. American Conference of Govermental Industrial Hygienists (ACGIH). Threshold Limit Values for Chemical Substances and Physical Agents and Biological Exposure Indices. ACGIH, Cincinnati, OH, 1998.

6. International Organization for Standardization (ISO). Air Quality - Particle Size Fraction Definition for Health-Related Sampling (ISO CD7708). Geneva : ISO, 1992.

7. Comité Européen de Normalisation (CEN). Workplace Atomosphere : Size Fraction Definitions for Measurement of Airborne Particles in the Workplace (CEN Standard EN 481). Brussels : CEN, 1992.

8. Vincent, J. H. *Aerosol Science for Industrial Hygienists.* New York : Elsevier, 1995, p. 211.

9. Kenny, L.C., Aitken, R., Chalmers, C., Fabriés, J.F., Gonzalez-Fernandez, E., Kromhout, H., Lidén, G., Mark, D., Riediger, G., and Prodi, V. A Collaborative European Study of Personal Inhalable Aerosol Sampler Performance. *Ann. Occup. Hyg.* **1997**, 41(2), 135.

10. American Industrial Hygiene Association (AIHA) : Particle Size-Selective Aerosol Sampling in the Workplace. VA : AIHA, 1996.

11. Mark, D. and Vincent, J.H. A New Personal Sampler for Airborne Total Dust in Workplaces. *Ann. Occup. Hyg.* **1986**, 30(1), 89.

12. Tsai, P.J., Vincent, J.H., Wahl, G.A., and Maldonado, G. Worker Exposures to Inhalable and Total Aerosol during Nickel Alloy Production. *Ann. Occup. Hyg.* **1996**, 40(6), 651.

13. Wilsey, P.W., Vincent, J.H., Bishop, M.J., Brosseau, L.M., and Greaves, I.A. Exposures to Inhalable and Total Oil Mist Aerosol by Metal Maching Shop Workers. *Am. Ind. Hyg. Assoc. J.* **1996**, 57, 1149.

14. Spear, T.M., Werner M.A., Bootland, J., Harbour, A., Murray, E.P., Rossi, R., and Vincent, J.H. Comparison of Methods for Personal Sampling of Inhalable and Total Lead and Cadmium-Containing Aerosols in a Primary Lead Smelter. *Am. Ind. Hyg. Assoc. J.* **1997**, 58, 893.

15. Werner, M.A., Spear, T.M., and Vincent, J.H. Investigation into the Impact of Introducing Workplace Aerosol Sandards Based on the Inhalable Fraction. *Analyst.* **1996**, 121, 1207.

16. Marple, V.A., Rubow, K.L. and Behm, S.M. A Microorifice Uniform Deposit Impactor (MOUDI) : Description, Calibration, and Use. *Aerosol Sci. and Technol.* **1991,** 14, 434.

17. Willeke, K. and Baron, P. A. *Aerosol Measurement.* New York : Van Nostrand Reinhold, 1993, p. 212.

18. Vanderpool, R.W. and Lundgren, R.W. Design and Calibration of an In-Stack Low-Pressure Impactor. *Aerosol Sci. and Technol.* **1990,** 12(2), 215.

19. Lundgren, D. A., Harris, F. S., Marlow, W. H., Lippmann, M., Clark, W. E., and Durham, M. D. Aerosol Measurement. Florida : University of Florida, 1976, p. 92.

20. Marple, V.A. A Fundamental Study of Inertial Impactors. PhD Dissertation, Mechanical Engineering Department, University of Minnesota, Minneapolis, MN, 1970.

21. Lundgren, D.A. An Aerosol Sampler for Determination of Particle Concentration as a Function of Size and Time. *JAPC.* **1967**, 17, 225.

22. Berglund, R.N. and Liu, B.Y.H. Generation of Monodisperse Aerosol Standards. *Environ. Sci. Technol.* **1973**, 7, 147.

23. Li, S.N. and Lundgren, D.A. Effect of Clean Air Core Geometry on Fine Particle Contamination and Calibration of a Virtual Impactor. *Aerosol Sci. and Technol.* **1997**, 27, 625.

24. Stöber, W. and Flachsbart, H. An Evaluation of Nebulized Ammonium Fluorescein as a Laboratory Aerosol. *Atmospheric Environment.* **1973**, 7, 737.

25. Hinds, W.C. *Aerosol Technology*. New York : John Wiley and Sons, 1982, p. 49.

26. Health and Safety Executive, *MDHS* - Methods for the Determination of Hazardous Substances. **1997**, 1, 1.

27. NIOSH (National Institute for Occupational Safety and Health) Manual of Analytical Methods (NMAM), 4th ed., August 15, 1994.

28. Baldwin, E.J. and Maynard, A.D. A Survey of Wind Speeds in Indoor Workplaces. *Ann. Occup. Hyg.* **1998**, 42(5), 303.

29. Loo, B.W. and Cork, C.P. Development of High Efficiency Virtual Impactors. *Aerosol Science and Technol.* **1988**, 9, 167.

30. Moore, L.L., Dube, D.J., and Burk, T. Improved Sampling and Recovery of Wood Dust Using MSA Respirable Dust Cassettes. *Am. Ind. Hyg. Assoc. J.* **1990**, 51, A475.

31. Burkhart, J. E., McCawley, M. A., and Wheeler, R. W. Particle Size Distributions in Underground Coal Mines. *Am. Ind. Hyg. Assoc. J.* **1987**, 48(2), 122.

32. Whitehead, L. W., Freund, T., and Hahn, L. L. Suspended dust concentrations and size distributions, and qualitative analysis of inorganic particles, from woodworking operations. *Am. Ind. Hyg. Assoc. J.* **1981**, 42(6), 461.

33. Bullock, W.H. and Laird, L.T. A Pilot Study of the Particle Size Distribution of Dust in the Paper and Wood Products. *Am. Ind. Hyg. Assoc. J.* **1994**, 55(9), 836.

34. Rubow, K.L., Marple, V.A., Olin, J., and McCawley, M.A. A Personal Casscade Impactor: Design, Evaluation and Calibration. *Am. Ind. Hyg. Assoc. J.* **1987**, 48(6), 532.

35. Okazaki, K., Wiener, R.W., and Willeke, K. Non-Isoaxial Aerosol Sampling : Mechanisms Controling the Overall Sampling Efficiency. *Environ. Sci. Technol.* **1987**, 2, 183.

36. Agarwal, J.K. and Liu, B.Y.H. A criterion for accurate aerosol sampling in calm air. *Am. Ind. Hyg. Assoc. J.* **1980**, 41(3), 191.

37. Belyaev, S.P. and Levin, L.M. Techniques for Collection of Representative Aerosol Samples. *J. Aerosol Sci.* **1974**, 5, 325.

38. Vincent, J.H. Recent Advances in Aspiration Theory for Thin-walled and Blunt Aerosol Sampling Probes. *J. Aerosol Sci.* **1987**, 18(5), 487.

39. Tsai, P-J and Vincent, J. H. Impaction Model for the Aspiration Efficiencies of Aerosol Samplers at Large Angles with Respect to the Wind. *J. Aerosol Sci.* **1993**, 24(7), 919.

40. Tsai, P-J, Vincent, J. H., Mark, D., and Maldonado, G. Impaction Model for the Aspiration Efficiencies of Aerosol Samplers in Moving Air under Orientation-Averaged Conditions. *Aerosol Science and Technol.* **1995**, 22, 271.

BIOGRAPHICAL SKETCH

Shou-Nan Li was born in Taiwan on February 2, 1968. He received his bachelor's degree from National Cheng-Kung University in July of 1990. After two years compulsory military services in Taiwan, he came to the United States and began studying at the University of Florida in August of 1993. He received his master's degree in May 1996 and his doctorate in 1999.

During his study in the University of Florida, he got married and now has two sons, Bryce and Eric. He deeply appreciates the help and support of all his friends and professors at the University of Florida.

I certify that I have read this study and that in my opinion it conforms to acceptable standards of scholarly presentation and is fully adequate, in scope and quality, as a dissertation for the degree of Doctor of Philosophy.

Dale A Lundgren

Dale A. Lundgren, Chairman
Professor of Environmental
Engineering Sciences

I certify that I have read this study and that in my opinion it conforms to acceptable standards of scholarly presentation and is fully adequate, in scope and quality, as a dissertation for the degree of Doctor of Philosophy.

Jean M. Andino
Assistant Professor of Environmental
Engineering Sciences

I certify that I have read this study and that in my opinion it conforms to acceptable standards of scholarly presentation and is fully adequate, in scope and quality, as a dissertation for the degree of Doctor of Philosophy.

Paul A. Chadik
Assistant Professor of Environmental
Engineering Sciences

I certify that I have read this study and that in my opinion it conforms to acceptable standards of scholarly presentation and is fully adequate, in scope and quality, as a dissertation for the degree of Doctor of Philosophy.

H. Anson Moye

H. Anson Moye
Professor of Food Science and
Human Nutrition

I certify that I have read this study and that in my opinion it conforms to acceptable standards of scholarly presentation and is fully adequate, in scope and quality, as a dissertation for the degree of Doctor of Philosophy.

Chang-Yu Wu

Chang-Yu Wu
Assistant Professor of Environmental
Engineering Sciences

This dissertation was submitted to the Graduate Faculty of the College of Engineering and to the Graduate School and was accepted as partial fulfillment of the requirements for the degree of Doctor of Philosophy.

May 1999

Winfred M. Phillips
Dean, College of Engineering

M. J. Ohanian
Dean, Graduate School